SEISMIC ASSESSMENT OF THE MULTI STOREY STRUCTURAL BUILDING MODEL IN ACCORDANCE WITH EURO CODE 8 AND NEW MALAYSIAN ANNEX GUIDELINES

SYED MUHAMMAD BILAL HAIDER

MASTERS OF ENGINEERING SCIENCE

FACULTY OF ENGINEERING AND GREEN TECHNOLOGY
UNIVERSITI TUNKU ABDUL RAHMAN
OCTOBER 2019

SEISMIC ASSESSMENT OF THE MULTI STOREY STRUCTURAL BUILDING MODEL IN ACCORDANCE WITH EURO CODE 8 AND NEW MALAYSIAN ANNEX GUIDELINES

By

SYED MUHAMMAD BILAL HAIDER

A thesis submitted to the Department of Environmental Engineering,
Faculty of Engineering and Green Technology,
Universiti Tunku Abdul Rahman,
in partial fulfilment of the requirements for the degree of
Masters of Engineering Science
October 2019

ABSTRACT

SEISMIC ASSESSMENT OF THE MULTI STOREY STRUCTURAL BUILDING MODEL IN ACCORDANCE WITH EURO CODE 8 AND NEW MALAYSIAN ANNEX GUIDELINES

Syed Muhammad Bilal Haider

Multiple Earthquakes that occur during short seismic intervals affect the inelastic behavior of the structures. Sequential ground motions against the single earthquake event cause the building structure to face loss in stiffness and its strength. Although, numerous research studies had been conducted in this research area but still significant limitations exist such as use of traditional design procedure which usually considers single seismic excitation; and selecting a seismic excitation data based on earthquake events occurred at another place and time. Therefore, it is important to study the effects of successive ground motions on the framed structures. The objective of this study is to overcome the aforementioned limitations through testing a two storey reinforced concrete (RC) building structural model scaled down to 1/10 ratio through a similitude technique Buckingham Pi theorem. The scaled model is examined using a shaking table. Thereafter, the experimental model results are validated with simulated results using ETABS software. The test framed specimen is subjected to sequential five artificial and four real-time earthquake motions. Dynamic response history analysis has been conducted to investigate the observed response and crack pattern; maximum displacement; residual displacement; residual interstorey drift ratio, serviceability limit state, ultimate

limit state, acceleration response, interstorey drift ratio and storey drift ratio. The results of the study concluded that the framed model highlighted the structural strength against its ductility, which is justified through the model ability to resist the multiple ground motions in low seismicity region (i.e. Malaysia) under extreme PGAs' up to 0.82g. Displacement parameters showed that real-time successive ground motions had not severely affected the RC model, as the maximum PGA in sequential motion was 0.34g. However, artificially produced seismic motions show that the intense PGAs (i.e. 0.25g to 0.82g) cause the framed structure to displace each storey twice in correlation with vary first artificial seismic vibration. Therefore, traditional seismic design Euro code 8 (EC8) is required to reconsider the traditional design procedure and damage limitation criteria for multiple ground motions.

ACKNOWLEDGEMENT

First of all, I acknowledge my supervisor, Prof. Dr. Zafarullah Nizamani, for his persistent encouragement, kind guidance and careful monitoring. He has always been there for my moral, financial and psychological support. I am thankful to my co-supervisor, Prof. Dr. Chun Chieh Yip, for guiding me about the earthquake engineering aspect of this research. I can never forget Dean of FEGT, Prof. Dr. Yap Vooi Voon whose smiling face has always been keeping my morale high throughout the course of this research. I extend my deepest gratitude to UTAR where I have been provided excellent working environment, without any bureaucratic or financial obstacles.

The authors acknowledge the financial support through UTAR-RF grant no. IPSR/RMC/UTARRF/2016-C1/Z1 provided by Universiti Tunku Abdul Rahman (UTAR), Perak, Malaysia.

APPROVAL SHEET

This thesis entitled **"SEISMIC ASSESSMENT OF THE MULTI STOREY STRUCTURAL BUILDING MODEL IN ACCORDANCE WITH EURO CODE 8 AND NEW MALAYSIAN ANNEX GUIDELINES"** was prepared by SYED MUHAMMAD BILAL HAIDER and submitted as partial fulfillment of the requirements for the degree of Masters of Engineering Science at Universiti Tunku Abdul Rahman.

Approved by:

_____

(Dr. Zafarullah Nizamani) Date: 30-12-2019
Assistant Professor/Supervisor
Department of Environmental Engineering
Faculty of Engineering and Green Technology
Universiti Tunku Abdul Rahman

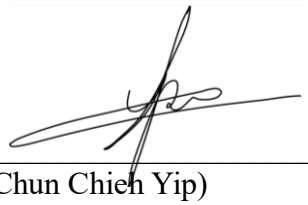

_____

(Dr. Chun Chieh Yip) Date: 30-12-2019
Assistant Professor/Co-supervisor
Department of Civil Engineering
Lee Kong Chian Faculty of Engineering & Science
Universiti Tunku Abdul Rahman

FACULTY OF ENGINEERING AND GREEN TECHNOLOGY

UNIVERSITI TUNKU ABDUL RAHMAN

Date: 30th December 2019

SUBMISSION OF FINAL YEAR PROJECT /DISSERTATION/THESIS

It is hereby certified that **SYED MUHAMMAD BILAL HAIDER** (ID No: 17AGM05340) has completed this thesis entitled **"SEISMIC ASSESSMENT OF THE MULTI STOREY STRUCTURAL BUILDING MODEL IN ACCORDANCE WITH EURO CODE 8 AND NEW MALAYSIAN ANNEX GUIDELINES"** under the supervision of **Dr. Zafarullah Nizamani** (Supervisor) from the department of Environmental Engineering, Faculty of Engineering and Green Technology and **Dr. Chun Chieh Yip** (Co-Supervisor) department of Civil Engineering, Lee Kong Chian Faculty of Engineering & Science at Universiti Tunku Abdul Rahman.

I understand that University will upload softcopy of my final year project / dissertation/ thesis* in pdf format into UTAR Institutional Repository, which may be made accessible to UTAR community and public.

Yours truly,

_____

(*Syed Muhammad Bilal Haider*)

DECLARATION

I, Syed Muhammad Bilal Haider, hereby declare that this dissertation is based on my original work except for citations and quotations which have been duly acknowledged. I also declare that it has not been previously and concurrently submitted for any other degree or award at UTAR or other institutions.

Signature: 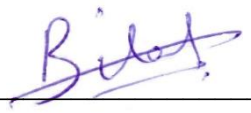

Name: Syed Muhammad Bilal Haider

Registration No: 17AGM05340

Date: 30-12-2019

DEDICATION

I dedicate this thesis to my family, and friends from UTAR, Malaysia and NED-UET, Pakistan. Without their intellectual, kind and sincere support, I would never be able to complete this work.

TABLE OF CONTENTS

LIST OF TABLES

LIST OF FIGURES

DEFINITIONS

Artificial ground motion: Ground motions which has a uniform harmonic wave produced on shaking table with the help of two input parameters, frequency and displacement is termed as artificial ground motion.

Interstorey drift ratio (IDR): It is the maximum relative displacement between two consecutive stories divided by the storey height.

Real time ground motion: These ground motions are recorded at the location where earthquake occurs. Stations are placed to measure motions of the ground during earthquake.

Test 1, 2, 3, 4, and 5: Artificial ground motions which are applied sequentially in experimental and simulated model, represents with Test 1 to 5.

LIST OF SYMBOLS

c	Damping ratio
d	Maximum displacement, mm
d_e	Maximum elastic displacement, mm
d_y	Yield displacement, mm
E	Modulus of elasticity, MPa
f_{cu}	Compressive strength, N/mm^2
f_D	Damping force vector, KN
f_I	Inertial force vector, KN
f_S	Restoring force vector, KN
f_t	Splitting strength, N/mm^2
F_e	Maximum force response of linear elastic system, KN
F_u	Yield force of the system, KN
g	Spectral acceleration, m/s^2
k	Stiffness, KN/mm
l	Length, mm
m	Mass, kg
M_w	Moment magnitude
PGA	Peak ground acceleration, m/s^2 or gal
P_{DLR}	Probability of exceedance, %
$p(t)$	External applied, KN
q	Behaviour factor
S	Dimensional scale factor
S_a	Acceleration scale factor

S_D	Soil classification *D*
S_E	Scale factor
T_{DLR}	Reference return period, years
t	Time, sec
V	Shear Force, KN
v	Velocity, m/s
V_{max}	Maximum shear force, KN
x	Displacement, mm
π	Non-dimensional parameter Pi
δ_{max}	Maximum displacement, mm
Ω	Frequency, Hz
ρ	Density, kg/m^3
σ	Stress, KN
$\dot{x}$	Velocity, m/s
$\ddot{x}$	Acceleration, m/s^2
μ	Ductility

LIST OF ABBREVIATIONS

ACI318	American Concrete Institute 318
BS8110	British Standard 8110
DCL	Ductility Class Low
DCM	Ductility Class Medium
DCH	Ductility Class High
EC	Eurocode
ETABS	Extended Three Dimensional Analysis of Building System
FEMA	Federal Emergency Management Agency
IEM	Institution of Engineers Malaysia
IRIS	Incorporated Research Institutions for Seismology
IDR	Interstorey Drift Ratio
LVDT	Linear Variable Displacement Transformer
ML	Mammoth Lake
MDOF	Multiple Degree Of Freedom
MMD	Malaysian Metrological Department
POA	Pushover Analysis
PEER	Pacific Earthquake Engineering Research Center
RC	Reinforced Concrete
RSA	Response Spectrum accelerations
SLS	Serviceability Limit State
SDOF	Single Degree Of Freedom
THA	Time History Analysis
UBBL	Uniform Building By-Laws

ULS	Ultimate Limit State
UBC-97	Uniform Building Code 1997

LIST OF APPENDICES

CHAPTER 1

INTRODUCTION

1.1 Overview

Earth plate moves over the hard rocky surface of earth core called mental. Due to the movement of these plates, very strong forces generate. The movement of such plates is termed as Plate tectonic. The earth crust is made up of seven major tectonic plates. These tectonic plates are continuously in motion that's why they hold strong potential energy. When such potential energy become enormous, it transforms into kinetic energy due to motion of plates and form a ground motion vibration known as earthquake. The boundaries of these plates overlaps at the most sensitive locations from where ground motion starts. Seismic magnitude and duration vary from location to location of overlapped tectonic plates. Seismic waves forms when volcano erupted and disturb the earth surface by transporting the energy through waves or vibrations to cause damage to structures (Gill et al., 2015).

In last 15 years, earthquakes and tremors have been experienced much more frequently in Malaysia. These earthquake tremors in Malaysia are mainly originated from local earthquakes, and distant earthquakes from Sumatera with the two major sources of Sunda Arc subduction fault zone source offshore of Sumatra and Sumatran strike-slip fault source (Qianyi, 2016) . Regional

earthquake zone extends from outside geographical boundaries to within the state boundaries. In Peninsular Malaysia, there were a series of weak earthquakes in Bukit Tinggi from year 2007 to year 2009 which were attributed by the Bukit Tinggi fault. This fault line is located across the Univrsiti Tunku Abdul Rahman, Kampar campus. As for the local earthquakes in Sarawak and Sabah, the faults were identified at Tubau and Kelawit, and Mensaban, Perancangan, Lahad Datu, Keningau, Danum, Binuang, Tabin and Beluran respectively (Qianyi, 2016).

1.2 Problem Background

In the past, one of the most significant regional disaster 2004 Indian Ocean Earthquake with a magnitude of Mw 9.1 brought devastating impact through tsunami and killed 68 Malaysian citizens (Lye et al., 2009). Such massive earthquake had disturbed the movement of tectonic plates and deformed the core of Sunda land. After the catastrophic event, the disturbed peninsular plate was shifted to the west-southwest and become close to the epicentre (Sumatra subduction zone) which indicated that inactive fault lines are going to be reactivated in near future and may cause strong excitation in West Malaysia (Marto & Kasim, 2013). Since thereafter, the number of seismic motions has increased in Malaysia because of the Philippines and Sumatra Andaman plates movements (Majid et al., 2014). In year 2015, local earthquake Ranau with 6.0 M_w vibrated Sabah, Malaysia and lasted for 30 second. It was the strongest local earthquake since 1976 earthquake at Lahad Datu, Sabah (Tongkul, 2015). According to Malaysian Metrological Department (MMD) annual report 2016,

a total of 274 local earthquakes (less than 5.0 on the Richter scale) were detected in Ranau, Lahad Datu, Kudat, Sandakan, Semporna and Tawau in Sabah and in Temenggor in Perak. MMD received reports from the public that tremors can be felt for 13 local earthquakes with magnitude 2.3 to 4.0 on the Richter scale, mostly in the Ranau, Sabah (MMD, 2016). In MMD annual report 2017, A total of 200 local earthquakes (less than 5.0 on the Richter scale) was detected in 16 areas in Sabah. Ranau recorded the highest number of 88, followed by Semporna, 45 and Lahad Datu, 33. The highest magnitude incident occurred on 26th March 2017 in Lahad Datu, Sabah at 9.30am with a 4.2 magnitude earthquake (MMD, 2017). In 2018, 5.2 M_w earthquake hit Sabah, three years after Ranau earthquake 2015 (Yusa, 2018). Lastly, the recent earthquake recorded in Sabah was 4.5 M_w (Earthquake track, 2019).

1.3 Previous work and limitation of existing studies

The past reports have stated that most of the buildings in Peninsula Malaysia have gone through concrete deterioration due to seismic ground movements from the far field (Adiyanto & Majid, 2014a). Usually, first seismic ground motions are followed by another seismic events within few hours and may continue for days. In such conditions, the buildings have experienced minor to moderate damages (Adiyanto & Majid, 2014a). Many previous researches have proved that repeated seismic excitations affects the strength of the building and it requires to rehabilitate the building after each seismic motion (Amadio et al., 2003). Furthermore, repeated seismic motions induced 1.3 to 1.4 times

increment in the maximum storey ductility demand as compared with single seismic excitation (Faisal et al., 2013).

In all past research studies, researchers used real-time ground motion events which are recorded in far field countries. To assess the actual behaviour of local structure, regional ground motions from near and far field requires to take into account. Malaysia, which lies in low seismicity region (Sooria et al., 2012), has not being vibrated with sequential ground motions with PGAs' ranging between 0.25g to 0.82g. Therefore, in order to assess a building model with such intensive ground motions, artificially produced intensive harmonic waves can be produced and used to assess the RC structures in Malaysia. Moreover, it has been observed in Malaysia that all the past studies had focused on analyzing the structure using simulation only and no experimental work had been performed to investigate the RC framed structures in Malaysia. As far as author's knowledge, this is the first time a framed structure is tested on a shaking table considering a real structure with conditions prevailing in Malaysia.

1.4 Problem Motivation

In 2018, Institutions of Engineers, Malaysia invited public comments for preparing an Annex to EC8. This work was conducted to determine the ductility class of structures. Thus, this study is conducted keeping in view the new annex requirements for Malaysia as required by Eurocode EC8.

1.5 Problem Statement

In the current scenario, the provisions recommended by FEMA 368 and Eurocode EC8 overlook the repetition of seismic vibration in the analysis (Adiyanto & Majid, 2014a; Moustafa & Takewaki, 2011). Therefore, current design procedure of Eurocode required to reconsider its structural design building code that is based on a single earthquake vibration (Hatzigeorgiou, 2010; Hatzigeorgiou & Beskos, 2009)

1.6 Problem Description

Most of the Malaysian building structures are designed only for gravity and wind load combination. Less than 1% are designed considering the earthquake loads in the design load combination (Sooria et al., 2012). The reason is that, most of the countries including Malaysia in South East Asia had implemented British Standard BS8110 (British Standard, 1997), a code that did not include any condition for earthquakes (Megawati et al., 2004). Even though, Eurocode which has design procedures for earthquake resistant structures but, still, it has limitation of designing the building model for single seismic excitation. Additionally, the damage limitation criteria in Eurocode are also based on single ground motion. In such case, the models design on Eurocode does respond differently on multiple ground motions particularly the damages being observed after each ground motions and the displacements of each storey.

1.7 Aims and Research Objectives

The aim of the present research is to investigate the dynamic behaviour of low-rise reinforced concrete building model particularly for Malaysia. Three objectives are set to achieve the research aim:

- To evaluate the building response of the two storey small scale RC building model.

- To determine the displacements response with five artificial and four real-time sequential ground motions.

- To calculate the damage limitation set by EC8 for the full scale reinforced concrete building model.

1.8 Research Scope

The study is focused on an institutional building of Block 'N', Universit Tunku Abdul Rahman (UTAR), Kampar, Perak. The study uses the Nonlinear Dynamic Time History Analyses. Building design guideline Euro code EC2 and EC8 are selected. The building structure with Ductility Class Low (DCL) as recommended by EC8 is used for low seismic zones. In total, nine ground motions have been used, out of which, five ground motion data has been generated on shaking table before assessing the test framed building model.

Remaining four real-time ground motions of Mammoth Lake are taken from database of Pacific Earthquake Engineering Research Center (PEER).

1.9 Limitation of Study

In Universiti Tunku Abdul Rahman, Malaysia, shaking table has not performed the real-time seismic excitations but harmonic motions are able to simulate desired ‘g’ values and uniform patterns of signal. Ground motion acceleration ranges from 0.25g to 0.82g (limitation in Shaking table). Shaking table motion is unidirectional moving along the Z-axis as shown in Figure 3.3.

1.10 Significance of the study

A study is required to examine the effects of repeated earthquakes on three-dimensional reinforced concrete building structural model using a shaking table. In this study, an RC two storey building model is tested under a series of five ground motions produced on a shaking table. The test is performed to have an added experimental data and thereafter, formed a complete documentation on results of test framed specimen during successive ground motions. The study has particularly focused on Malaysian RC structures with Ductility Class Low (DCL). This study reconsider the traditional design code EC8 (European Standard, 2011) in accordance with Malaysia National Annex to MS EN 1998-1:2015 (Department of Standards Malaysia, 2017) for multiple excitations. The study shall help the design engineers to draw a serviceable, reliable, safe and seismic resistant buildings which can play a comprehensive role during ground motion vibrations in Malaysia. The results of the study create a bench mark for

low-rise RC building structures and may be consider as a reference to design a building model for multiple seismic excitations.

1.11 Research Methodology

The research work can be divided into the following six phases:

Phase I: Scaled down the structural model with the help of dimensional analysis tool (Buckingham Pi Theorem).

Phase II: Validate the Concrete Mix design.

Phase III: Construct a two storey 1/10 scaled Reinforced concrete building model

Phase IV: Analyzing the model with different input frequencies, displacement and gravitational acceleration.

Phase V: Signal Processing of the data recorded by LVDT and Accelerometer

Phase VI: Validate the Scaled up experimental building model results with prototype simulated model drawn in ETABS software.

1.12 Assumptions

As the small scale model covers a small part of the prototype full scale model as shown in Figure 3.2 and Figure 3.3, it is assumed that continuous span, multiple columns and beams of prototype full scale model which are not considered in small scale model, does not affect the results of this study.

1.13 Summary

In this chapter, effect of local regional and far field earthquakes had been discussed. The causes which disturbed the Malaysian fault lines were identified. Furthermore, the reconsideration of building design code Eurocode EC8 for multiple ground motions was focused in this chapter. Problem Statement identified the importance of this current study. Aims and objectives elaborate the focus of study and acknowledge the significance of the current research.

1.14 Organization of Thesis

This thesis is divided into five main chapters: Introduction (Chapter 1), Literature Review (Chapter 2), Methodology (Chapter 3), Result and Discussion (Chapter 4), and Conclusion and Recommendation (Chapter 5). Introductory note and concluding remark are provided in each chapter to highlight the importance as well as to summarize the chapter systematically.

Chapter 1 introduces the background study pertaining to the present research. Problem statement, research aims, and objectives are formulated. Last but not least, the scope and limitation of the study is outlined.

Chapter 2 provides a literature review on the topics relevant to the present research. This chapter begins with the historic earthquakes occurred in near or far field of Malaysia. Design guideline of Eurocode enlightens with different ductility classes. Moreover, seismic ground motions applied on three dimensional framed structures are also studied. Multiple ground motions

effecting the behavior of test specimen are discussed. Small scale RC building model tested on shaking table are reviewed. Similitude theory was discussed and lastly, method of signal processing is studied.

Chapter 3 highlights the dimensional analysis tool named as Buckingham Pi Theorem, a similitude law, which deals with scaling factor to scale up or down the results. Moreover, concrete mix design has been used to check 30MPa (30/37) compressive strength of cylindrical specimen which later would use in pouring and casting of building model. Additionally, an RC two storey building model has been tested on shaking table with five incremental ground motion excitations ranging from 0.25g to 0.82g. Later on, signal processing is used for the data recorded by Accelerometer and Linear Variable Displacement Transformer (LVDT).

Chapter 4 comprises of the discussion on results accompanied by critical discussion. The building response after each seismic ground motion has been recorded and presented. Results of displacement response have been scaled up with the help of Buckingham Pi theorem. The results are validated with commercial software ETABS. In the end, damage limitation set by EC8 has been calculated for all artificial and real-time ground motions.

Chapter 5 presents the conclusions drawn from the present study and provides a list of recommendations for further improvement.

CHAPTER 2

LITERATURE REVIEW

This chapter provides a review on the historical earthquake events occurred in Malaysia. General outline of Eurocode 2 and ductility classes stated in EC8 are also discussed. In addition to that, important aspects of dynamic behaviour of building model under nonlinear time history analysis are also discussed. Scaling of building with the support of similitude law is discussed. Lastly, techniques used in signal processing of data recorded by contact sensors are reported concisely.

2.1 History of earthquakes

Earthquake had been recorded from last few centuries. The most catastrophic and destructive earthquake was occurred in Shaanxi, China on 23rd January 1556 with a magnitude of around 8 in Richter scale. Such deadliest earthquake caused 830,000 fatalities (EN, 2019). The strongest earthquake recorded in the history of mankind was The Great Chilean Earthquake 1960 with a moment magnitude of 9.5 M_w. Such massive seismic motion not only shook the cities of Chile but also affected the Pacific Ocean by triggering the destructive Tsunami. Approximately 1,655 killed, 3,000 injured, 2,000,000 homeless, and $550 million damage in southern Chile; tsunami caused 61 deaths, $75 million damage in Hawaii; 138 deaths and $50 million damage in Japan; 32 dead and

missing in the Philippines; and $500,000 damage to the west coast of the United States (USGS, 1960). Similarly, the Indian ocean earthquake that is also the deadliest earthquake, occurred in year 2004. Such largest earthquake struck off the west coast of northern Sumatra, Indonesia with a magnitude of 9.1 M_w and IX on the Mercalli intensity scale. It was the third largest recorded earthquake and had the longest duration which lasted as long as ten minutes. Such natural disaster caused more than 227,000 deaths in total, and over 165,000 in Indonesia, making it as the deadliest earthquake occurred in the 21st century (Mercycorps, 2018).

2.1.1 South East Asia earthquake events

In Sumatran subduction zone, four strong earthquakes had been recorded since last 300 years. In 19th century, two earthquake occurred with 8.75 and 8.4

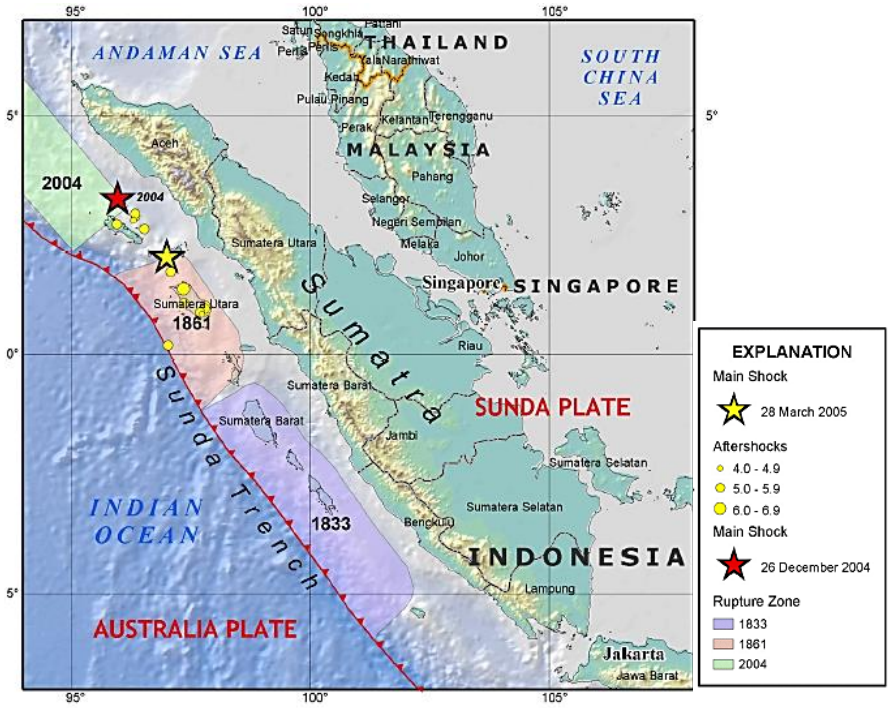

Figure 2.1: Four Main Shocks and Rupture Zones observed at Sumatra (Balendra & Li, 2008)

Moment magnitude in year 1833 and 1861 respectively (Newcomb & McCann, 1987). The remaining two ground motions recorded recently; Aceh earthquake 2004 and Nias earthquake 2005 with a moment magnitude of M_w 9.3 and 8.7 respectively. The epicenter of all four earthquakes are shown in Figure 2.1. According to the historians, Aceh earthquake 2004 is the fourth largest earthquake in the world since 1900 and is the largest since the 1964 Prince William Sound, Alaska earthquake. In total, more than 283,100 people were killed, 14,100 are still listed as missing. 1,126,900 were displaced by the earthquake and subsequent tsunami in 10 countries in South Asia and East Africa. The earthquake was felt (IX) at Banda Aceh, (VIII) at Meulaboh and (IV) at Medan, Sumatra and (III-V) in parts of Bangladesh, India, Malaysia, Maldives, Myanmar, Singapore, Sri Lanka and Thailand on the Mercalli

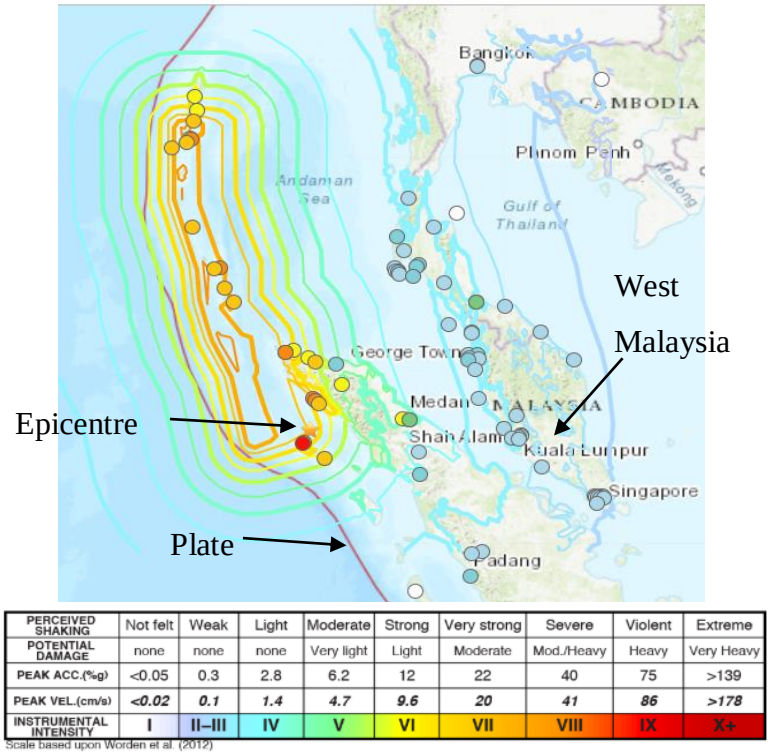

PERCEIVED SHAKING	Not felt	Weak	Light	Moderate	Strong	Very strong	Severe	Violent	Extreme
POTENTIAL DAMAGE	none	none	none	Very light	Light	Moderate	Mod./Heavy	Heavy	Very Heavy
PEAK ACC.(%g)	<0.05	0.3	2.8	6.2	12	22	40	75	>139
PEAK VEL.(cm/s)	*<0.02*	*0.1*	*1.4*	*4.7*	*9.6*	*20*	*41*	*86*	*>178*
INSTRUMENTAL INTENSITY	I	II–III	IV	V	VI	VII	VIII	IX	X+

Scale based upon Worden et al. (2012)

Figure 2.2: Shake Map Intensities of Aceh Earthquake 2004 (USGS, 2004)

intensity scale. The tsunami caused more casualties than any other in recorded history and was recorded nearly world-wide on tide gauges in the Indian, Pacific and Atlantic Oceans as shown in Figure 2.2 (USGS, 2004).

2.1.2 Origin of seismic activities in Malaysia

There are two seismic active plates surrounding Peninsular Malaysia. In west, Sunda Subduction Trench is located between Indo-Australian and Eurasian Plates. Moreover, Philippines Subduction Trench is situated in east between Eurasian and Philippine Plates. These are active plate boundaries and often causes Malaysia to face ground motion vibrations across the far-field sources (Abas et al., 2017). Sumatran subduction zone and Sumatran strike slip fault are the origins of earthquakes as shown in Figure 2.3. Particularly for Malaysia, Leyu et al., (1985) had recorded the earthquake intensities.

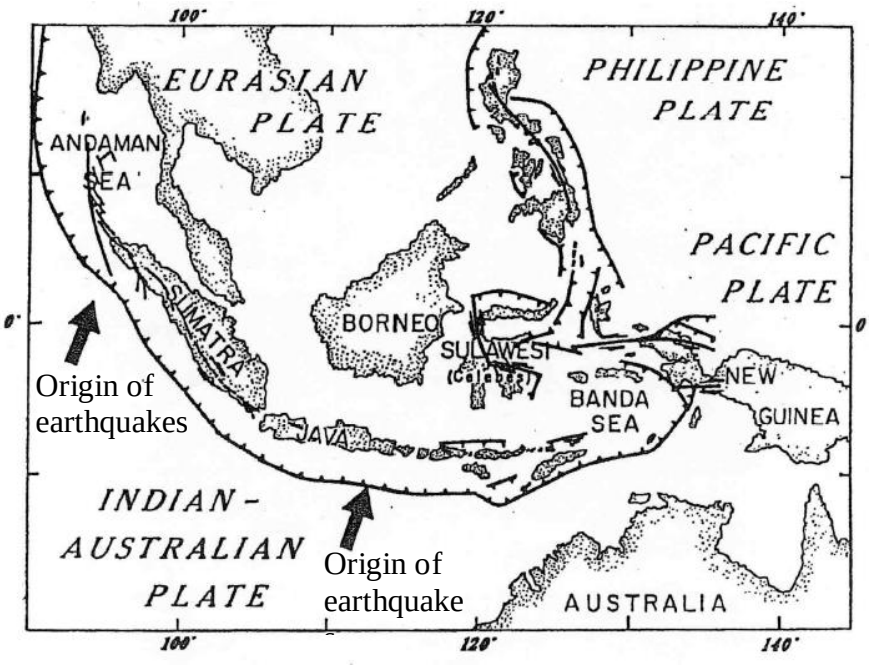

Figure 2.3: Origin of Sumatran Fault Line and Subduction Zone (Newcomb & McCann, 1987)

2.1.3 Multiple earthquake activities in Malaysia

The tectonic movements in recent years had showed the stability of earth crust in Southeast Asian region particularly for Malaysia. As shown in Figure 2.4, the 2004 Indian ocean earthquake was followed by multiple aftershocks from year 2005 onwards (Majid et al., 2014). According to Incorporated Research Institutions for Seismology (IRIS) database, Peninsular observed maximum magnitude up to 4.6Mw from year 1978 to 2006. In between 2007 to 2009, MMD had recorded 30 local earthquakes within Peninsular Malaysia (Latiff & Khalil, 2016). These earthquake, with magnitude of less than 4.3 M_w, were originated from fault lines such as Bukit Tinggi (Pahang), Kuala Pilah (Negri Sembilan), Jerantut (Pahang) and Manjung (Perak). As indicated by Malaysian Metrological Department (MMD), country experienced 4.2 Mw of earthquake during year 2007 till 2010. Ranau earthquake having 6.0 Mw strike Sabah in year 2015 which cause 18 fatalities in East Malaysia (Tongkul, 2015).

Aforementioned earthquakes discussion showed that after the occurrence of Indian Ocean earthquake 2004, the inactive fault lines have activated. Such fault lines can create destruction in West Malaysia from local near field earthquake, mostly at Bukit Tinggi fault (Marto & Kasim, 2013; Nizamani et al., 2018).

2.1.3.1 Bukit Tinggi fault line

Bukit Tinggi is a fault line passes across the Kampar, Perak. In 2009, Bukit Tinggi area had seven low level of earthquakes which subsequently believed to

be recurrence of Bukit Tinggi Fault system due to Southern Sumatra Earthquake (Abas et al., 2017). The event between 2007-09, Bukit Tinggi earthquakes instigated the local authorities to take action against the possible dangers and risk. Thus, these local events indicated that Malaysia is not a risk free zone. Moreover, existed fault maps were observed to be outdated with the current seismic levels. Abas et al., (2017) believed that these activated fault lines will increase the level of local ground motions in Malaysia. Moreover, Sumatra-Andaman Earthquake 2004, Nias Earthquake 2005 and Bengkulu Earthquake 2007 are the major cause of fault line reactivation in West Malaysia.

2.1.3.2 Seismic activities in East Malaysia

In last two decades, East Malaysia had witnessed an increase in low to moderate seismic activities due to active fault lines (Herayani & Adnan, 2017). In 2015, the earthquake occurred in Ranau, East Malaysia with moment magnitude (M_w) of 5.9 caused serious damage to many infrastructures. Malaymail, (2015) said that it was the second powerful quake to hit Sabah after the 1976 earthquake measuring 6.2 on the Richter scale that occurred near Lahad Datu.

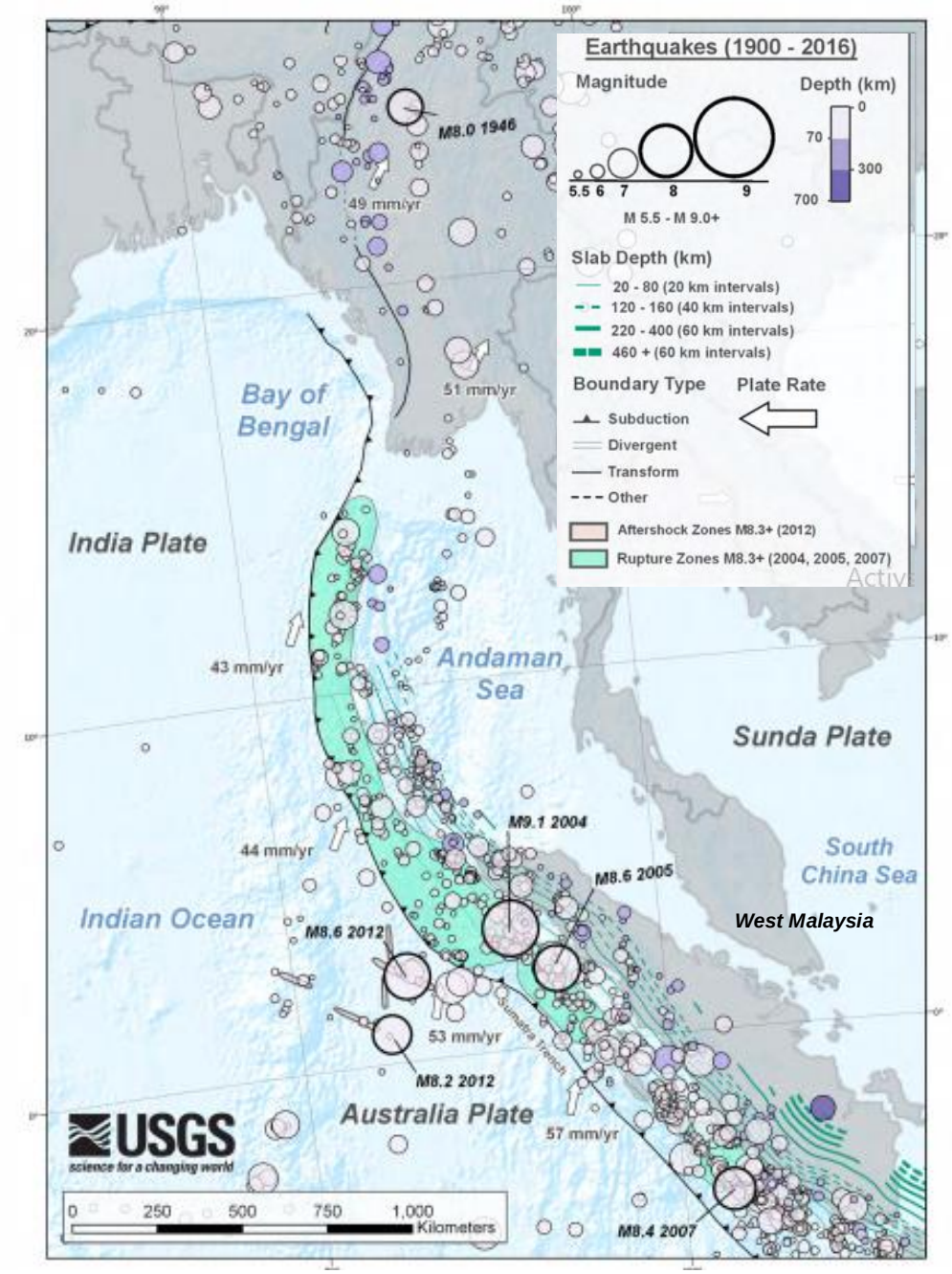

Figure 2.4: Map of Tectonic Summary Region (USGS, 2016)

2.2 Peak ground acceleration

Peak Ground Accelerations or PGA is the maximum ground acceleration emitted in an earthquake event. There are two types of earthquake events that is local and far field. The PGA predicted for the far field earthquakes in Malaysia was found to be 80-100 gal in Kuala Lumpur for 500 years return period (Adnan et al., 2006). Moreover, 40-120 gal (Petersen et al., 2004); and 1-191gals (Manafizad et al., 2016) was predicted as shown in Table 2.1.

A study generated Response Spectrum accelerations (RSA) based on the input parameters such as PGA from far field earthquake, the strong motion data and soil data of each borehole (Majid et al., 2007). They also stated that most of Northern Peninsular Malaysia had Soil classification 'S_D', which is stiff soil. Most of the soils were categorized in 'S_D', with the highest RSA at Penang Island with 'S_c' of 0.76 g (Majid et al., 2007). Ipoh (including Kampar) and Alor Star had soil class 'S_E' (soft soil) with acceleration of 0.31g and 0.47g respectively, as shown in Table 2.1. Here, the PGA values categories as far field and regional earthquakes which concludes that Malaysia is vulnerable to far field ground motions. The unit 1 g is equals to 981gal.

Table 2.1: Comparison between far field and local PGAs'

Type	PGA	Description
Far field	80-100 gal	(Adnan et al., 2006)
	1-191gals	(Manafizad et al., 2016)
	40-120 gal	(Petersen et al., 2004)
	0.76g	Penang Island (T. Majid et al., 2007)
	0.31g	Ipoh (T. Majid et al., 2007)
	0.47g	Alor Star (T. Majid et al., 2007)

Local	0.08g	Notional design PGA on rock sites for Peninsular Malaysia and Sarawak (Department of standards Malaysia, 2017)
	0.14g	Notional design PGA on rock sites for Sabah (Department of standards Malaysia, 2017)

2.3 General outline of Eurocodes

Eurocode provide the basis for structural design. The provisions recommended by code are the standard rules set by European Union. Supplementary documents named National Annex specified several clauses to be adapted by each country based on their social and economic condition.

The Malaysia National Annex of Eurocode is prepared by the Institution of Engineers Malaysia (IEM), a technical committee on code of practice for design of concrete structures. IEM basically provides the nationally determined parameters (NDP) such as Reference return period (T_{DLR}). Here, T_{DLR} refers to the seismic action for the damage limitation requirement (or, equivalently, reference probability of exceedance in 10 years, P_{DLR}) that is 2%.

2.3.1 Outline of Eurocode EC2 and EC8

Eurocode 2, "Design of concrete Structures" is considered to design plain, reinforced and pre-stressed concrete structures. EN 1992-1-1 (General rules and rules for buildings) complies with the principles and requirements for the safety and serviceability of structures. Eurocode 2 has two main stages that are involved in design of RC structure such as Serviceability Limit State (SLS) and

Ultimate Limit State (ULS). These two states correspond to the strength and stability of a structure under design loads.

Many of the Eurocode rules are based on the same theory as the British Standards, however, there are clauses that are structured in a slightly different way in Euro code. Table 2.2 shows a comparison between BS code and EC code in terms of their material properties, partial safety factor, yield strength, load equations and return period.

Table 2.2: Difference between BS code and EC codes (Ajis, 2012; British Standard, 2008)

BS 8110 code and UK National Annex	EC2 and EC8 codes
BS 8110 uses 28 days concrete cube strength, f_{cu}	In EC2, the formula is based on the design of cylindrical concrete strength 28 days, f_{ck}
In BS 8110, f_{cu} should not be taken as greater than 40 N/mm^2	There is no limit on the concrete strength in EC2
Yield strength for reinforcement is 460N/mm^2	Yield strength for reinforcement is 500N/mm^2
Partial safety factor for reinforcing steel in BS8110 is 1.05	EC2 uses a value of 1.15
BS8110 have different values of partial safety factor for bending, shear and bond	EC2 adopt partial safety factor for concrete of about 1.5

BS8110 does not includes any provision to check the stress level in reinforced concrete	EC2 includes the provision to check the stress level in reinforced concrete
Equation of Ultimate design load (W) is, $W = 1.4G_k + 1.6Q_k$ Where, G_k and Q_k are dead load and imposed load.	In EC2, the equation is: $W = 1.35\ G_k + 1.5\ Q_k$ Here, 1.35 and 1.5 are partial safety factors.
UK decisions for the Nationally Determined Parameters described in BS EN 1998-1:2004 for T_{NCR} is 2500 years	In EC8, reference return period T_{NCR} of seismic action for the no-collapse requirement is 475 years
Threshold of low seismicity is $a_g \leq 2.0 m/s^2$ (For T_{NCR} = 2500years)	$a_g \leq 0.78 m/s^2$ or $a_g S \leq 0.98 m/s^2$

MS EN 1998: "Design of Structures for Earthquake Resistance", provides guideline of design and execution of buildings and civil engineering works in seismic regions. The purpose of EC8 code is to ensure that in the event of earthquakes, human lives are protected; damage is limited; and structures important for civil protection remain operational. The provisions set by EC8 aims to construct a building model by fulfilling the performance requirement, seismic actions and analytical procedures and rules, which would benefit the building model after constructing it (EN1998-1, Clause 1.1.2, Appendix D). For low-rise buildings, design procedures comply with Eurocode 8 along with supplementary document know as Malaysia National Annex.

Earthquake motions are the major cause of the structural damage, which can be accepted in such a way that building model get adequate ductility by achieving the inelastic energy dissipation without losing structural stability. Conceptually, two idealized conditions that is equal displacement approximation and equal energy approximation had been proposed considering the relationship between behaviour factor 'q' and ductility 'μ' as shown in Figure 2.5 (a) and (b). Here, equation (2.1) and (2.2) represents equal displacement approximation and equal energy approximation (Lu et al., 2001).

$$\mu = q \tag{2.1}$$

$$\mu = \frac{1}{2}(q^2 + 1) \tag{2.2}$$

The building model had long natural period and would belong to equal displacement category. However, the building model with average natural period would fall in equal energy approximation (Lu et al., 2001).

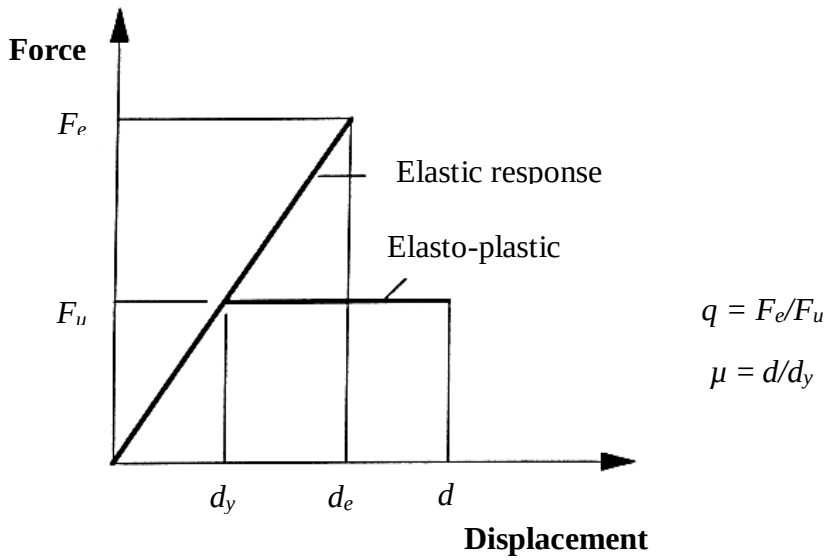

Figure 2.5 (a): Behavior factor and ductility terms (Hatzigeorgiou & Beskos, 2009; Lu et al., 2001)

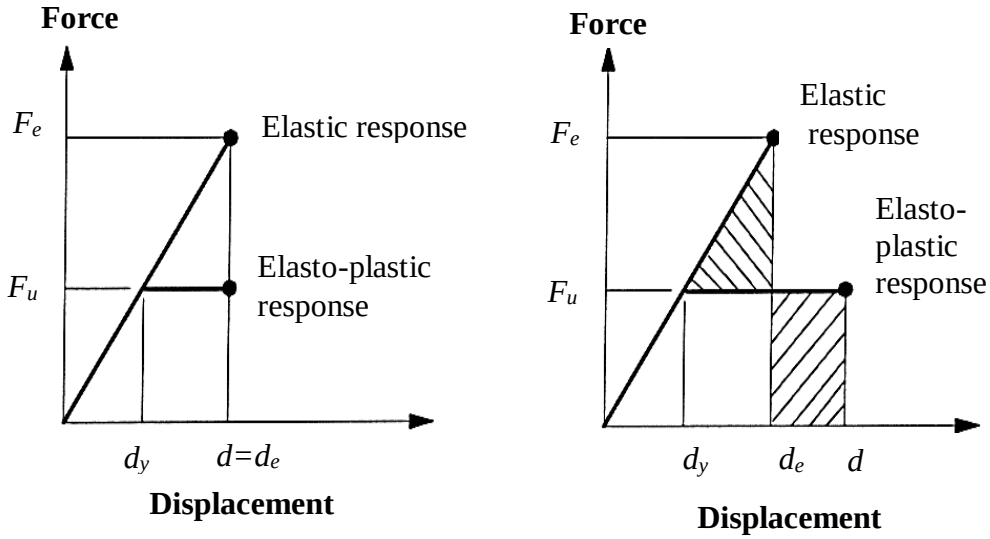

Figure 2.5 (b) Equal displacement approximation (Left) and Equal energy approximation (Right) (Hatzigeorgiou & Beskos, 2009; Lu et al., 2001)

Where,

F_e = Maximum force response of linear elastic system

F_u = Yield force of the system

d_y = Yield displacement

d_e = Maximum elastic displacement

d = Maximum displacement

2.3.1.1 Classification of ductility classes

EC8 provides different classes of ductility (DC) for reinforced concrete buildings. Each class provides different ranges of behavior factor from 1 to 6. EC8 suggested three ductility classes that is Ductility Class Low (DCL), Ductility Class Medium (DCM) and Ductility Class High (DCH).

In DCL, no hysteretic ductility is intended and the resistance to earthquake loading is achieved through strength of the structure rather than ductility (Elghazouli, 2009). Building model seismic design does not depend on the dissipation of energy. It focuses on elastic response of the building model. Standard concrete design to EC2 should be carried out. However, only additional requirement for ductile reinforcement should be selected from Class B or C as mentioned in Table C.1, Annex C of EC2. The behavior factor is considered to be less than equal to 1.5 (Elghazouli, 2009). The dimensioning and detailing of the framed structure is designed according to EC2 without earthquake resistance. EC8 has suggested to design building model on DCL for low seismic areas such as Malaysia, which is defined by Clause 3.2.1(4) of EC8 Part 1, Appendix D. EC8 (Clause 3.2.1 (4)) recommended that for such low seismic regions, maximum limit for peak ground acceleration (PGA) would be 0.1g (Panagiotakos & Fardis, 2004).

In DCM and DCH, the building model is designed for energy dissipation and its ductility. The behavior factor 'q' for DCM ranges from $1.5 < q \leq 4$. However, the limit for DCH is $4< q \leq 6$ (Faisal et al., 2013). These two ductility classes aim to control inelastic behaviour of building model through structural specifications and relative size of members. Moreover, inelastic deformations demand in the framed structure would be accommodated through detailing of plastic hinges region. In both the classes, Ultimate Limit State (ULS) and damage limitation are required to verify the member strength against the forces and resistances provided through ground motions (Panagiotakos & Fardis,

2004). Most importantly, building model design on DCM and DCH should follow strong column and weak beam rule to avoid the occurrence of soft storey.

Malaysia have low seismicity that is why few studies focusing on DCL are discussed. A two storey office building was redesign to DCL (EC8) and analysed through nonlinear time history analysis. Behavior factor 1.0 and 1.5 had incremental cost of about 270% and 72% as compared to current practice code BS8110. Moreover, frames designed based on higher behaviour factor tend to experienced higher interstorey drift ratio due to lower strength provided even had the same size of section for all elements (Adiyanto & Majid, 2014b).

Three storey six RC building models were designed on DCL and DCM, respectively. Pushover Analysis was conducted to assess the ductility of RC structure. The framed model design on EC8 (DCM) had greater ductility about an average of 20% as compared to model design on EC2 (DCL) (Zahid et al., 2013).

A study investigated the performance of six storey reinforced concrete building models by focusing on its ductility classes based on Eurocode EC8 (Rodrigues & Elawady, 2019). To dissipate the seismic energy, which could damage the frame structure, the building famed had been design on ductility of DCL, DCM and DCH by considering seismic zones from low to high. The building model had been examined by pushover analysis. Their study showed that DCL building model was considered to be more economical as compared to other ductility classes in low seismic zone (Rodrigues & Elawady, 2019).

A reinforced concrete building having four, eight and twelve storey regular framed structures were designed on three different ductility classes DCL, DCM and DCH with a PGA of 0.2g and 0.4g respectively. Member collapse preventions performance level had been examined through nonlinear time history analysis. Damage limitation check was also considered for member collapse prevention. They concluded that the limitation set by EC8 for the application of DCL to low seismic zone were not supporting the results based on safety and performance grounds. However, the results were fully justified on the basis of cost effective and design of building model (Panagiotakos & Fardis, 2004). Aforementioned study was comprehensive but DCL designed building model under extreme multiple seismic ground motions required to take into account for further assessment.

2.4 Dynamic behavior of Structures under seismic motions

Dynamic analysis occurs in two steps. Firstly, find the natural frequencies and mode shapes without the presence of the external loads. Later, utilized these dynamic properties to get the response of earthquake. Earthquakes usually forms nonlinearity in the building response but mostly the seismic design procedures follow the linear analysis. The nonlinear analysis is introduced in the design procedures by modifying the linear analysis method (Elghazouli, 2009).

2.4.1 Linear dynamic behavior of SDOF system

In linear dynamic analysis, a structure can be expressed with three properties that is stiffness (*k*), mass (*m*) and damping (*c*). Here, SDOF stands for single degree of freedom. Stiffness is defined as the constant of proportionality between displacement and force. When the structure is displaced from its rest position, a restoring force will oscillate the structure around its mean position. In addition, structure will dissipate the energy and contain variety of mechanism, which are grouped together known as damping (Elghazouli, 2009).

2.4.1.1 Equation of motion of Linear SDOF system

In SDOF system, the deformation defined with single displacement. Contrary, real structures have many degree of freedom but, SDOF system consider to be the most popular in the structural modelling (Elghazouli, 2009).

Figure 2.6 describes the SDOF system, which is subjected to external forces with respect to time period. The forces *F(t)* cause to move the mass '*m*' with a displacement '*x*'. The movement of mass generates the restoring force as shown in right side of Figure 2.6.

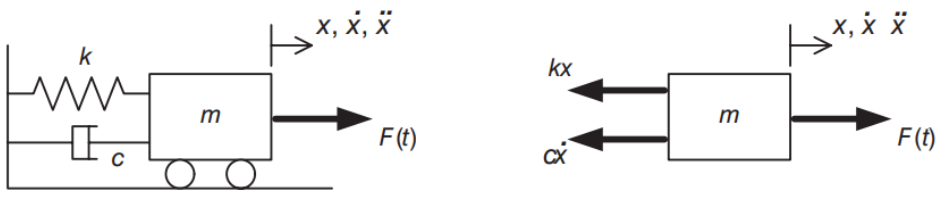

Figure 2.6: Dynamic forces on a mass-spring-damper system (Elghazouli, 2009)

According to Newton's law, Resultant force = mass × acceleration. Therefore, it can be represented by equation of motion as shown in equation (2.3) as:

$$m\ddot{x} + c\dot{x} + kx = F(t) \tag{2.3}$$

Where, $\dot{x}$ represents velocity, $\ddot{x}$ shows acceleration and c is damping coefficient. Here, dot represents the differentiation with respect to time (Elghazouli, 2009). During earthquakes, the forces are not applied directly to the building structure. However, the ground under the structure moves with horizontal time varying motion as shown in Figure 2.7.

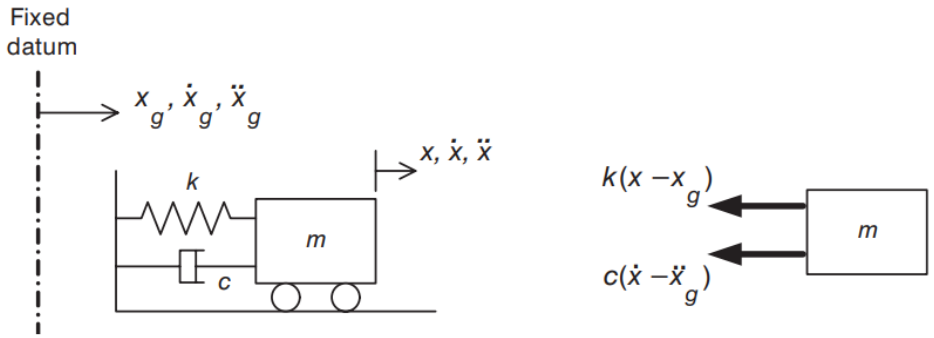

Figure 2.7: Mass-spring-damper system subjected to base motion (Elghazouli, 2009)

According to Newton law, equation of motions is represented in equation (2.4) if there is no external force applied (Elghazouli, 2009),

$$-k(x-x_g) - c(\dot{x}-\dot{x}_g) = m\,\ddot{x}$$

$$m\ddot{x} + c(\dot{x}-\dot{x_g}) + k(x-x_g) = 0 \quad (2.4)$$

Substitute the relative displacement between the mass and the ground with $y = x - x_g$. The equation (2.4) can be expressed as shown in equation (2.5),

$$m\ddot{y} + c\dot{y} + ky = -m\ddot{x}_g \quad (2.5)$$

Equation (2.5) shows that the seismic ground motion results in a similar equation of motion to an applied force (Elghazouli, 2009).

SDOF system allowed to explore the horizontal inelastic displacement demands to assess and rehabilitate the new or existing building structures. A study calculated the inelastic displacement ratio for SDOF structures under multiple repeated ground motions (Hatzigeorgiou & Beskos, 2009). Nonlinear time history analysis was conducted based on equation (2.5). Study revealed that time period of structural model for SDOF system is inversely proportional to inelastic displacement ratio. They found that inelastic displacement ratio increased by more than 100% in multiple ground motions with respect to single earthquake motion (Hatzigeorgiou & Beskos, 2009). The elastic and inelastic flexible system recognized the maximum relative displacement identical to maximum ground displacement in repeated and single seismic event.

A study had been conducted to calculate peak ductility demands of inelastic SDOF systems under real and artificially produced mainshock and aftershock sequential ground motions (Katsuichiro & Colin, 2012). For real

mainshock–aftershock sequences, they observed aftershock had less than 10% incremental effect as compared to mainshock on peak ductility demand. However, in artificially produced mainshock–aftershock sequences, significant incremental effect of aftershock had been observed on peak ductility demand of about 40-60%. The significant increase appears to be caused by the use of some inadequate assumptions on aftershock productivity.

A study determined the ductility demand spectra for single degree of freedom (SDOF) systems under multiple near and far field seismic ground motions (Hatzigeorgiou, 2010). Due to lack in recorded sequential real ground motions, only artificial seismic ground motions had been used in the current study. These artificial ground motions were produced via a rational and random combination of real single seismic events. The principles of performance-based seismic design stated that moderate seismic ground motions would not make damages in the structure. However, they highlighted the fact that multiple small seismic ground motions could lead the framed structure to higher ductility demands and damage levels with the design earthquake. Their study concluded that considering traditional 'design earthquake' is inadequate for sequential seismic ground motions. It underestimated the ductility demands and structural damage.

A study focused on the effect of bidirectional ground motion with single, double and triple artificial repeated earthquakes on the maximum story ductility demands of three-dimensional inelastic concrete frames (Faisal et al., 2013). In total, six RC building model with different height and behavior factor had been

examined. Results clearly showed that low-rise three storey building model with behaviour factor less than equal to '2' get negligible amount of storey ductility demand under repeated ground motions. Moreover, six, twelve and eighteen storey building model got maximum story ductility demands in the bottom storey irrespective of behaviour factor under multiple ground motions (i-e Ground Motion GM Case 2 and GM Case 3) as shown in Figure 2.8. They concluded that maximum story ductility demand increase about 40% in the repeated earthquakes (i-e GM Case 2 and GM Case 3) as compared to single ground motion (i-e GM Case 1).

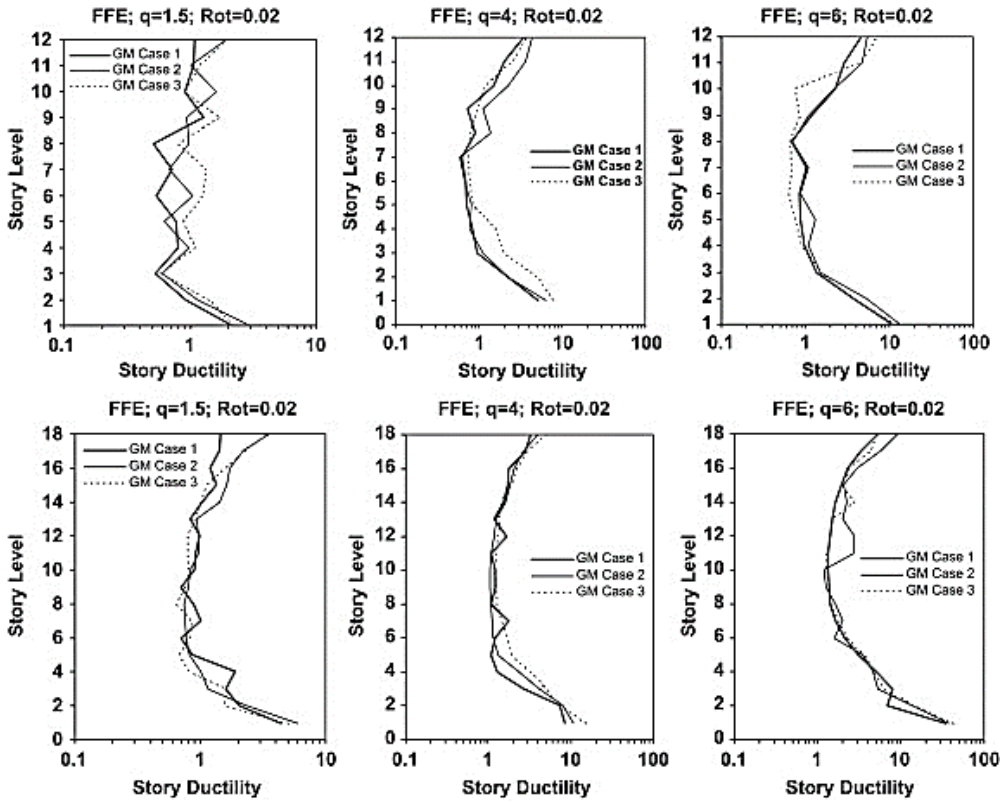

Figure 2.8: Story ductility demands of 12- and 18-story inelastic concrete frames (Faisal et al., 2013)

2.4.2 Dynamic behavior of MDOF system

The real structures which are represented by SDOF shows the real deformation behavior and may need to define with more than one degree of freedom. The complex deformation cannot be presented by considering single coordinate displacement of the real structure. Therefore, response of the real structure can be described well with Multiple degree of freedom (MDOF) system (Fardis et al., 2015).

The dynamic condition in the SDOF system considers to be in equilibrium. Restoring force, damping force, and inertial force in respective degree of freedom equals to the externally applied forces which can be expressed in equation (2.6) as (Fardis et al., 2015),

$$f_I + f_D + f_S = p(t) \tag{2.6}$$

Where, f_I represents inertial force vector, f_D shows damping force vector, f_S is restoring force vector and $p(t)$ represents external applied force with respect to time.

Assume that there is no ground motion, which suggested that displacement 'u', velocity '$\dot{u}$' and acceleration '$\ddot{u}$' are same. Here, vector of restoring force can be expressed in equation (2.7) as (Fardis et al., 2015):

$$f_s = k\,u \tag{2.7}$$

Damping force vector depends on damping matrix ‘c’ which is given in equation (2.8):

$$f_D = c\,\dot{u} \tag{2.8}$$

Finally, the inertial force can be expressed in matrix form in equation (2.9):

$$f_I = m\,\ddot{u} \tag{2.9}$$

Substitute the values from equation (2.7), (2.8), and (2.9) in equation (2.6),

$$m\,\ddot{u} + c\,\dot{u} + k\,u = p \tag{2.10}$$

Equation (2.10) represents the complete dynamic equilibrium of the system. Here, the dependence of time and applied forces has not been considered in the current system (Fardis et al., 2015).

Now, consider that base is not fixed and it is in motion as for seismic action. To calculate the restoring and damping forces, relative displacement and relative velocities need to be considered. Similarly, relative acceleration requires to be considered for inertial forces. Hence, the system having fixed points at base with same motions can be expressed by equation (2.11), (2.12) and (2.13) as (Fardis et al., 2015),

$$u = u^t - \imath\, u_g \tag{2.11}$$

$$\dot{u} = \dot{u}^t - \imath\, \dot{u}_g \tag{2.12}$$

$$\ddot{u} = \ddot{u}^t - \imath\, \ddot{u}_g \tag{2.13}$$

where, 'ı' represents the influence vector resulting in the displacement of the masses due to the unit ground displacement. Considering equation (2.10) for equation of motion in MDOF system as,

$$m\,\ddot{u} + c\dot{u} + ku = p - m\,\imath\,\ddot{u}_g \tag{2.14}$$

Equation (2.14) represents the basic equation for MDOF system similar to equation (2.5) of SDOF system (Fardis et al., 2015).

2.4.3 Non-linear analysis system

The aforementioned equations are based on linear elastic system. However, the structures facing the ground motions usually moves to inelastic range and cause the structure to deform. Here, restoring force and deformation has non-linear relation.

2.4.3.1 Nonlinear Structural system for MDOF system

The equation (2.7) shows restoring force in linear elastic system, which is considered to be invalid for nonlinear inelastic system. Therefore, the equation should be modified for a general relationship among force and deformation.

Thus, the equation (2.14) for inelastic structure is modified in equation (2.15) as (Fardis et al., 2015):

$$m\,\ddot{u} + c\dot{u} + f_s = -m\,\iota\,\ddot{u}_g \qquad (2.15)$$

For MDOF system, the above equation can only be solved through integration method of differential equation termed as non-linear time history analysis (Fardis et al., 2015).

2.4.3.1.1 Assessment of building model on shaking table

The test conducted on shaking table shows the real behaviour of MDOF system. A 1/20 scaled model of shear wall high-rise building had been examined on shaking table as shown in Figure 2.9 (Zhu et al., 2005). Nonlinear time history analysis was conducted under a series of multiple ground motions. Cracks, failure pattern and interstorey drift had been highlighted in their study. The study found out that intense shear wall failure was observed in higher level of floors. However, there was no structural failure recorded. Interstorey drift of shear wall in upper floors exceeded the limit set by the code which showed that necessary steps should be taken into account in structural designing. The architectural openings with a particular size and shape located in longitudinal direction weakened the shear wall to resist against horizontal forces. Moreover, higher floors had lower compressive strength caused the premature shear wall failure.

Figure 2.9: 1/20 scaled model of shear wall high-rise building (Zhu et al., 2005)

Five reinforced concrete framed structures were assessed on shaking table (Rizwan et al., 2018). Each model had two storey and scaled to 1:3. Figure 2.10 shows the reinforcement specification of each structural element. The model was design on UBC-97 and ACI318 guidelines. Northridge 1994 acceleration time history had been used to examined the framed structure. The study revealed that joint between beam and column was the major concern, which lower down the strength of frame structure.

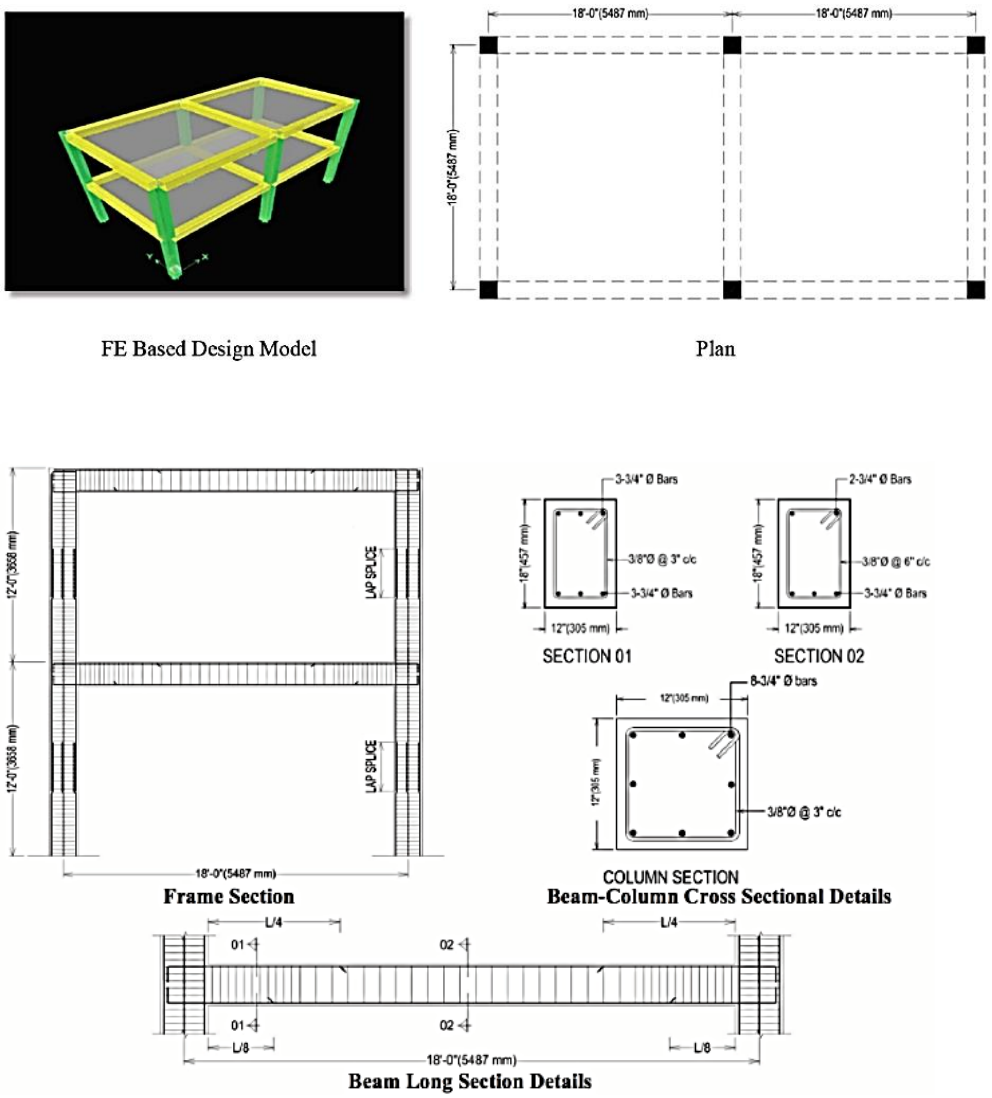

Figure 2.10: Plan and reinforcement details of RC model (Rizwan et al., 2018)

A shaking table test was performed to verify the conversion methods for acceleration and displacement data (Heuisoo et al., 2019). A small scaled 10 storey building model was attached with contact sensor accelerometers and high-speed image recorder to collect the data under strong ground motions. In this study, data recorded by accelerometers were validated with high speed images. Thereafter, three different methods were used to correct and convert acceleration into velocity and displacement. Study revealed that cosine Fourier

transform and baseline correction is the most suitable method to process the data. The converted displacement obtained from such method was close to data recorded by shaking table. Used of zero padding and baseline correction technique makes cosine Fourier transform methodology very effective.

A study aims to investigate the seismic behaviour of the asymmetric SMART 2013 RC building structure, considering torsional effect and material nonlinearity (Lim et al., 2018). The model was scaled to 1:4 and examined on Shaking table. Results showed that the difference in the X directional absolute maximum displacement between the asymmetric and symmetric structures was up to 15%. While the difference in the Y directional absolute maximum displacement was up to 31%. Thus, a larger seismic response should be considered in the seismic design of an asymmetric structure compared to a symmetric structure with similar design conditions.

An experimental study had been conducted on four RC two storey residential building models as shown in Figure 2.11 (Bahadir & Balik, 2018). The experimental models were scaled to 1/6 and placed at different angle on Shaking table to examined the structural behaviour. Multiple ground motions were applied until the structural failure occur. The results showed that each model had a soft storey that is 1st storey which was completely destroyed at the end of each test. Column beam and column base were the most critical joints where plastic hinges produced in each test.

Figure 2.11: Constructing RC model (Bahadir & Balik, 2018)

A four storey full scaled RC building model was studied to assess the adequacy of using the residual drift to estimate the damage sustained by the building subjected to ground motions on Shaking table (Dai et al., 2017). The seismic performance assessment of this tested building was performed with the peak roof drift calculated from the residual deformation. Their findings indicated that the approach could be used to infer probabilistically the peak drift of the building based on its residual drift.

A three storey 1/5 scaled building model was examined on shaking table to explore collapse process of the RC framed structure as shown in Figure 2.12. Eight incremental seismic ground motions were applied ranging from 0.08g to 1.1g. Dynamic properties of building model, acceleration and displacement response were determined. The results showed that as the ground motion

acceleration increases and reached to 7th seismic ground motion that is 1.1g, maximum storey drift ratio and residual drift ratio crossed the limit states set by Chinese building design code as shown in Figure 2.12. Study concluded that building model had much greater ductility than the specified value by code (Li et al, 2016).

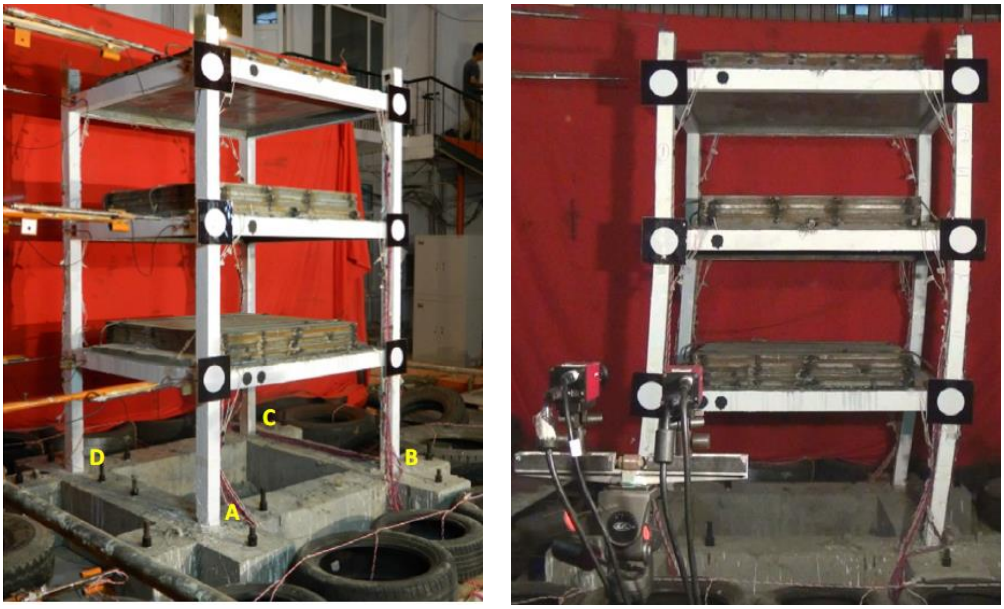

Geometry of RC model **Deformed model after Test 7**

Figure 2.12: Assessment of RC model till structural collapse (Li et al., 2016)

2.5 Methods of Analysis

EN 1998-1 (Section 4) has proposed the methods to analyze and design the building models. The code mentioned four types of methodologies which are:

- Linear static analysis also known as lateral force method or equivalent static analysis (EC8 Clause 4.3.3.1(1), Appendix D)

- Linear dynamic analysis also termed as model response spectrum analysis or linear time history analysis (EC8 Clause 4.3.3.1(2), Appendix D)
- Non-linear static analysis or pushover analysis (POA) (EC8 Clause 4.3.3.1(3), Appendix D)
- Non-linear dynamic analysis also termed as time history analysis (EC8 Clause 4.3.3.1(4), Appendix D)

This research study focuses on nonlinear dynamic assessment of an RC structure. Therefore, out of these four types of methodologies, Time history analysis is selected and discussed below.

2.5.1 Nonlinear dynamic time history analysis

The time history analysis was first introduced in 1970s, which was later considered as an evolution in design procedures for framed structures. Previously, engineers used linear static approaches to analyse the global seismic demand. Linear dynamic approach (response spectrum analysis) also referred to estimate peak response of the structural model. Moreover, nonlinear static analysis (that is Pushover analysis) determined the global displacement demand, which is also termed as target displacement. However, the exact response is quantified by nonlinear dynamic analysis. The response of such type of analysis are reliable and represents the true behaviour of framed structure under seismic ground motions (EC8 Clause 3.2.3.1.1(2), 3.2.3.1.2(4)(a), 4.3.3.4.3(1), and 4.3.3.4.3(3), Appendix D). Nonlinear dynamic analysis shows the time series

of ground motions with an average of 5% damping elastic response spectra. Minimum three artificial or real-time ground motions should be considered. If minimum seven consistent pair of ground motions are used for nonlinear dynamic time history analysis, then the average of their response would be considered otherwise the most unfavourable response would be taken among all the ground motions used FEMA 356 (Clause 3.3.2.2.4).

In order to better understand the nonlinear dynamic behavior of RC structures against multiple excitation, research studies were conducted to derive expressions for the damage features and displacement response.

2.5.1.1 Building response on multiple ground motions

In the past decades, studies reported that the repeated earthquake ground motions had a significant impact on framed structures. A study investigated the behavior of three-dimensional RC structures under multiple earthquakes. The study substantiated that multiple earthquakes lead to accumulating structural damage (Hatzivassiliou & Hatzigeorgiou, 2015). It was observed that damage indexing for multiple sequential ground motions (i-e MAT) were higher than the individual single seismic ground motion (i-e MA1, MA2, MA3, MA4, MA5) as shown in Figure 2.13. It was concluded that 40% degradation of strength or 50% degradation of stiffness caused severe structural damage in the RC buildings (Khoshraftar et al., 2013). It was further determined that strength degradation had more influence on increasing the damage index in comparison with stiffness degradation (Khoshraftar et al., 2013).

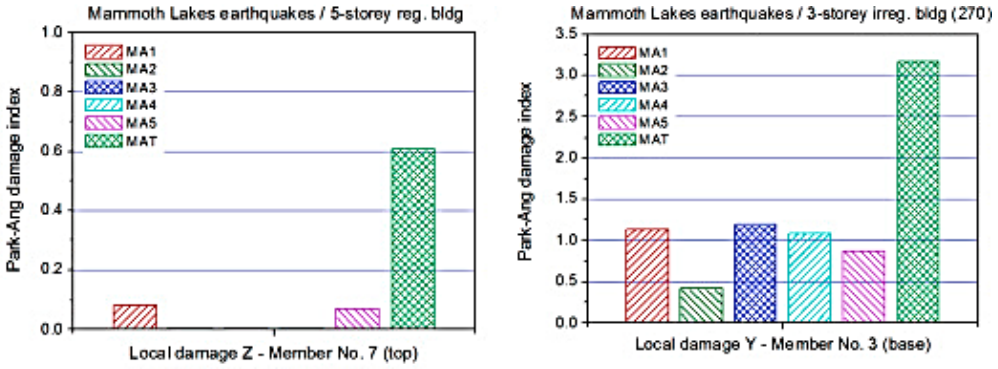

Figure 2.13: Local damage index according to the Park-Ang model (Hatzivassiliou & Hatzigeorgiou, 2015)

Malaysian RC structures has low to moderate seismic impact therefore, a study was conducted to assess the vulnerability of three reinforced concrete public buildings located in Ipoh, Malaysia (Ismail & Adnan, 2016). The buildings were analysed using finite element modelling software IDARC under a variety of earthquake intensities considering low to medium earthquake intensities. Results identified that medium rise building had light damages at an earthquake intensity of 0.15 g. However, high rise building had damages in the range of light damage level to collapse at earthquake intensity of 0.05 g. Another research study on a 3 storey RC frame structure was examined to evaluate the accuracy of POA by comparing with the dynamic time history analysis (THA) during complete collapse of RC building model in shaking table test (Li et al., 2017). Figure 2.14 shows eight sequential ground motion acceleration time histories. The study compared the top displacement, the inter-story drift ratio and the curvature of column ends. They found that the POA tend to underestimate the structural responses when the structure was severely damaged and close to the collapse state. Their study suggested that POA provided

incorrect judgement on the occurrence of collapse. However, THA gave a correct structural response on occurrence of seismic ground motions (Li et al., 2017).

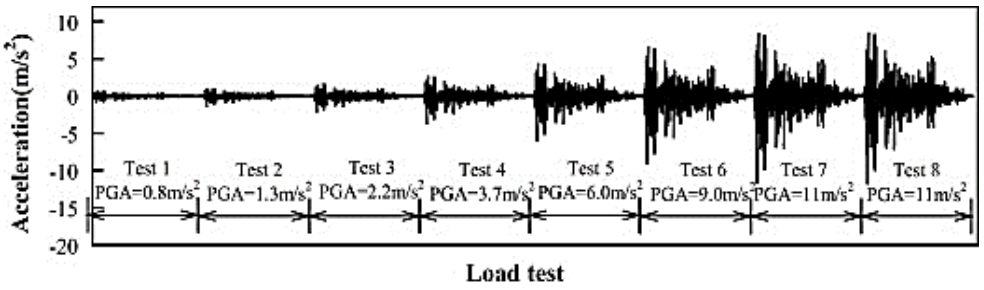

Figure 2.14: Ground motion accelerations from Test 1 to Test 8 (Li et al., 2017)

2.5.1.2 Displacement response and damage limitation

Displacement response is a critical parameter and plays a vital role in earthquake assessment. Therefore, EC8 suggested that Interstorey drift ratio (IDR) act as a verification criterion for damage limitation (EC8 clause 4.4.3.1(1) and 4.4.3.2(1) Appendix D). The limit set on the interstorey drift ratio for no collapse requirement is 1% if there are no non-structural elements attached to the structure. Oyguc et al. (2018) proved that interstorey drifts worked as an effective damage control measure. The study also acknowledged that in some cases, the aftershocks did not increase the residual displacements too. Samanta & Pandey (2018) examined the effects of ground motion duration on the seismic performance of a building. The results for short and long duration of earthquakes in 1st, 5th,10th, and 15th floors were similar. Hence, the maximum story drift ratio was not affected by the duration of ground motion as shown in Figure 2.15. In this study, the residual drift or the permanent deformation of the

building after each seismic event are measured and used to infer the degree of sustained damage to the building.

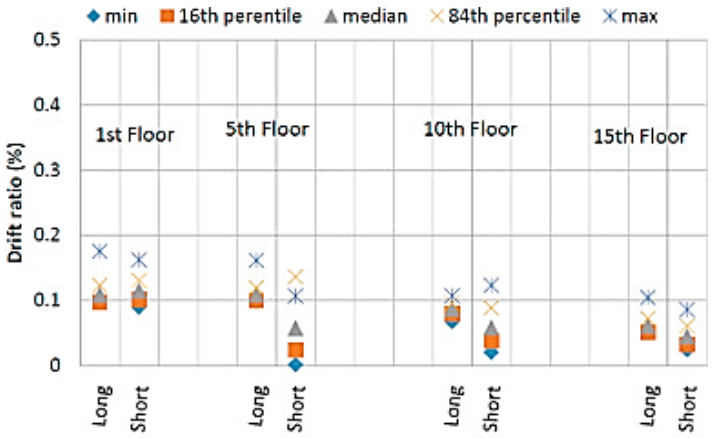

Figure 2.15: Comparison of storey drift ratio for long and short duration ground motion (Samanta & Pandey, 2018)

Another study had described the response of a reinforced concrete SDOF system subjected to different orders of near and far-field records in multiple earthquakes. The performance evaluation was carried out for various first shock damage levels and second shock performance levels. The study highlighted the fact that increment of relative intensity level in the second shock had maximum influence on the residual drift as compared to the first shock (Manafpour & Moghaddam, 2019).

A study of two RC buildings both with regular and irregular height were examined with 48 real seismic sequences from Christchurch, New Zealand earthquakes 2010–2011. Their study found that changing the earthquake direction affected the total drift demands and number of plastic hinges, which caused maximum total residual drifts in the framed structure (Hosseinpour & Abdelnaby, 2017).

A study addressed three storey RC building model which were assessed with 20 ground motions with the magnitude in range of 6.2 to 7.6 M_w and used as single and repeated earthquakes. Their study concluded that the seismic ground motions under single or repeated events did not affect the building model. However, it was found out that higher interstorey drift demand was required in multiple ground motions as compared to single event (Adiyanto et al., 2011).

Three school building models each having two, three and four storey as located in Sabah, Malaysia were examined with seven ground motions for both, single and multiple earthquakes ranging between 0.066g to 0.27g. Study concluded that the action of multiple earthquake had contributed around 55% to 107% higher interstorey drift ratio compared to the single earthquake (Sovester & Adiyanto, 2017).

The studies mentioned above discussed the RC structures under multiple seismic ground motions however, all these studies were limited to low PGAs'. No experiment had been performed on a low-rise RC model with intense PGAs' particularly in Malaysia.

2.6 Similitude Theory

Similitude theory is considered to be valuable tool, which helps to investigate the performance of small scale model on shaking table experimental test (Kim et al., 2009). Similitude theory provides an economical and viable platform to

get full scale model results by performing small scale model test on shaking table (Kim et al., 2009). For full scale model, there are multiple reasons, which negate the idea of examining full scale structure instead of small scale. Lack of experimental facilities such as size of shaking table, and contact sensors capacity were the major concerned. Moreover, a large number of labour is required to construct reinforced concrete structure that makes the testing procedure not economical at all.

A term known as similitude law is defined as a mathematical technique to deduce the theoretical relation of variable describing a physical phenomenon (Stavridis et al., 2010). Similitude law is used to derive equations which can be used for scaling of framed structures. In similitude law, ultimate strength should be identified first before conducting a test on small scaled RC structural model. Similitude law used for material controlled in scaled down RC model showed insufficient results due to occurrence of inelastic state under earthquake motions (Kim et al., 1988). Researcher discovered that similitude law was conservative and inadequate in a way that it could not provide validated results beyond plastic deformation (Harris & Sabnis, 1999; Kim et al., 2004; Kumar et al., 1997). Therefore, Kim et al. (2009) developed multiple equations for 1/5 small scale model to get the full scale model results up to inelastic state. Moreover, Coutinho (2016) indicated that small scaled models can be examined with the help of similitude law, which would validate the prototype model results. Additionally, scaled model should satisfy similitude requirements which are based on dimensional analysis.

2.6.1 Dimensional Analysis

Geometrical scaled models are promoted instead of full scale models to save time as well as money. To have a similitude relationship between the models, special attention is needed while scaling. Therefore, a useful technique has been introduced known as dimension analysis. Dimensional analysis is a tool which is used to simplify the problems by reducing similar relevant variables and produces dimensional homogeneity. It helps in interpolating the experimental data. It also gives us the guideline to check the equation. Physical models have been analyzed through this analysis technique. In case of structural modeling, Length, Mass or Force and Time are the three independent principal scaling factors used for scaled model designing. Dimension analysis tools help to pick the scaled factor and principal dimensions (Rastogi et al., 2015).

In order to have a cost efficient model, dimensional analysis forms a similitude between the prototype and scaled model. To get the behavior of the model similar to prototype, model material properties, fabrication accuracy, loading techniques, measurement methods and interpretation of results should be considered (Rastogi et al., 2015). Dimensional analysis forms non dimensional parameters, which supports in experimenting model physically and numerically. It also adds value in experimental results (Cengel & Cimbala, 2006). Buckingham π Theorem is a method used to create relationship of geometry, loads and material properties amid the model (Rastogi et al., 2015).

Buckingham π Theorem is a general approach for dimensional analysis. It develops dimensionally homogeneous equation involving physical quantities which can be expressed as an equivalent equation involving a set of dimensionless parameters (Andreas et al., 2010). The combination of Buckingham's π Theorem and similitude law, the prototype structure ($\pi_i{}^p$) (full scale) and the scaled model ($\pi_i{}^m$) can be presented in equation (2.16) as (Andreas et al., 2010),

$$\pi_i{}^p = \pi_i{}^m \tag{2.16}$$

Hence, the research prototype design and scaled model design ultimate capacity can be checked through similitude and Buckingham's Pi theorem.

2.7 Signal Processing

Important ground motion parameters can be derived from the acceleration records through a series of data processing approaches. Ground motion parameters and their characteristics are important to seismologists, geologists, and earthquake engineers. Acceleration records can be measured by using accelerograph, seismograph or accelerometer during an earthquake event (Xian, 2017). Figure 2.16 shows the acceleration, velocity, and displacement records of a selected accelerograph station during the 1999 Chi-Chi, Taiwan earthquake. The acceleration records shown were measured in three orthogonal directions. The accelerograph data showed that the earthquake was a transient motion in which the earthquake occurred within a very short duration. The corresponding

velocity and displacement traces computed by using double integration method. It is obvious that the velocity and displacement traces are less spiky than the acceleration trace.

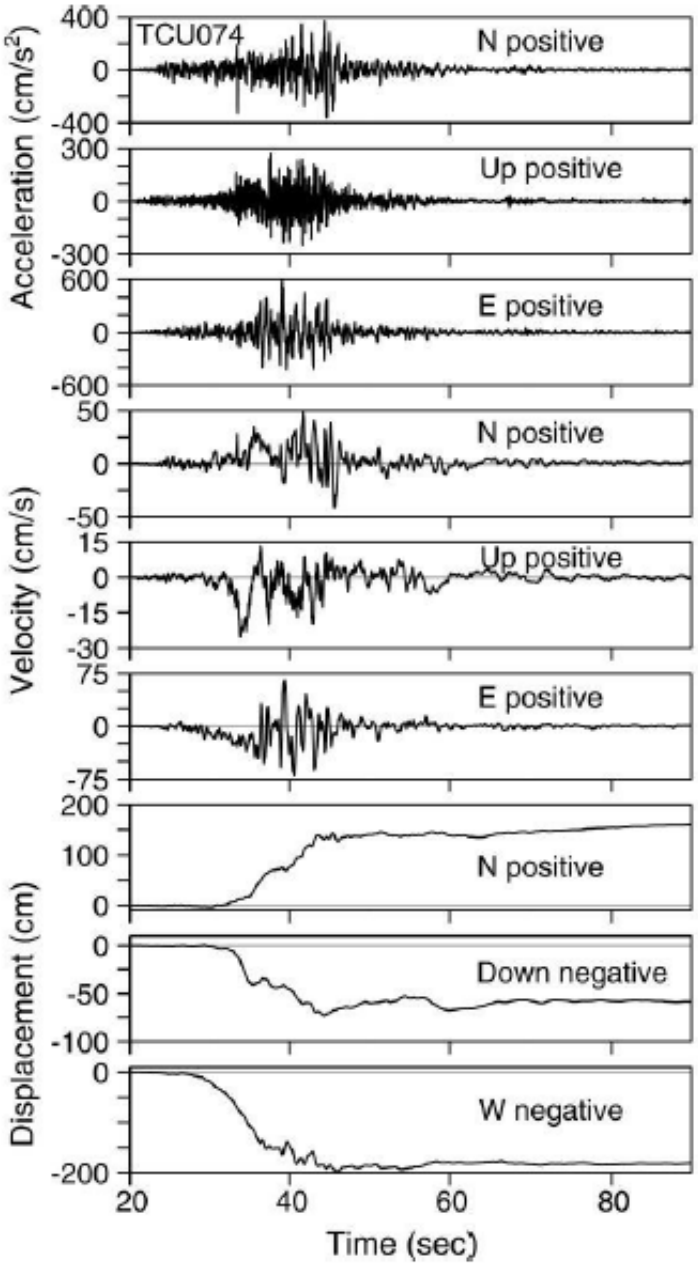

Figure 2.16: Acceleration, Velocity, and Displacement Traces during the 1999 Chi-Chi, Taiwan Earthquake (at station TCU074) (Boore, 2001)

The final displacement in Figure 2.16 is numerically large (i.e. about 2 m) and unphysical (Boore, 2001). Unphysical residual displacement will be encountered if the acceleration record is not corrected or adjusted appropriately. The permanent or residual displacement could also be caused by plastic deformation of near-surface material or elastic deformation of ground as the result of co-seismic slip on the fault (Boore & Bommer, 2005). Under common practices, the interpretation of numerically integrated displacement data from an earthquake event relies upon individual judgement, and hence exposed to numerous uncertainties.

2.7.1 Baseline Correction

The unphysical residual displacement as shown in Figure 2.16 is attributed to the baseline drift and the initial condition in numerical integration. At the end of each shaking motion, the velocity should become zero while certain amount of residual displacement could be expected (Boore & Bommer, 2005). Over the years, numerous adjustment schemes for processing seismic records have been proposed by many researchers worldwide (Boore, 2001; Chiu, 1997a; Iwan et al., 1985; Xian, 2017). Although there are various correction schemes proposed to recover the actual shaking record, it is almost impossible to recover an earthquake record perfectly.

Boore (2001) suggested a simple baseline correction method, which initially required a removal of pre-event mean acceleration records from the entire acceleration record. This process can be regarded as the zeroth-order

baseline correction. Subsequent procedure was to identify the obvious changes in velocity baseline as shown in Figure 2.17. Time instant for that change could be identified and followed by subtracting baseline step changes in the acceleration record. After the acceleration record was baseline adjusted, it could be numerically integrated to obtain the velocity and displacement time-series.

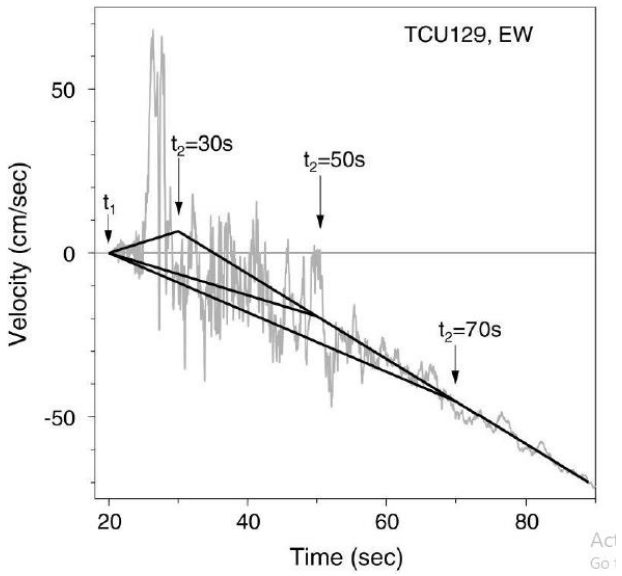

Figure 2.17: Least-Square Fitting of Velocity Record (Boore, 2001)

In Japan, Ohsaki (1995) suggested a well-known baseline correction procedure which was fundamentally based on the assumptions that velocity at the end of shaking would return to zero whilst certain amount of residual displacement could be expected.

In addition, Chiu (1997a) suggested a "stable" three-step algorithm baseline correction scheme for processing digital strong motion data. This method involved least-square fitting in acceleration record, high-pass filtering in acceleration record, and subtracting the initial velocity value. Figure 2.18

shows the acceleration and displacement records using the approach proposed by (Chiu, 1997a).

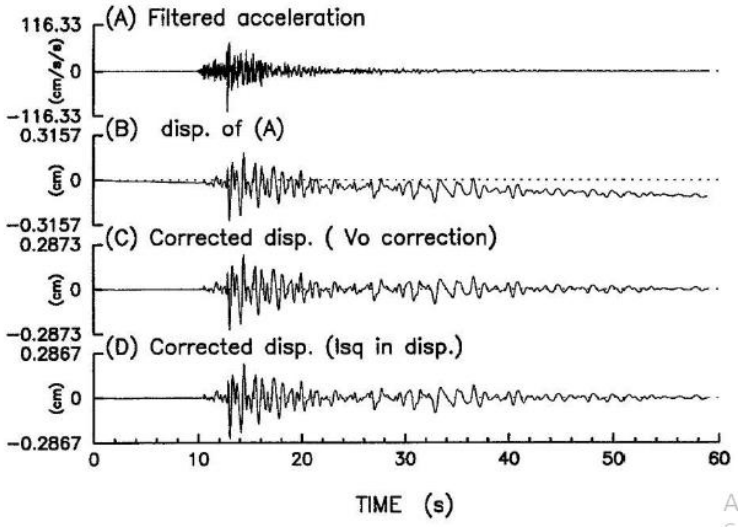

Figure 2.18: Acceleration and Displacement Records using the Stable Baseline Correction (Chiu, 1997a)

It is noteworthy that Boore and Bommer, in their study, find out that baseline correction would not be affected by the choice of baseline correction method (Boore & Bommer, 2005).

2.7.2 Digital Filtering

Low-pass and high-pass digital filtering were useful in removing unwanted noises from the true signal (Boore & Bommer, 2005; Douglas & Boore, 2011). Figure 2.19 shows that the velocity and displacement records were reasonably recovered with the use of the filtering method. However, the unfiltered and filtered acceleration records showed a little discrepancy between each other.

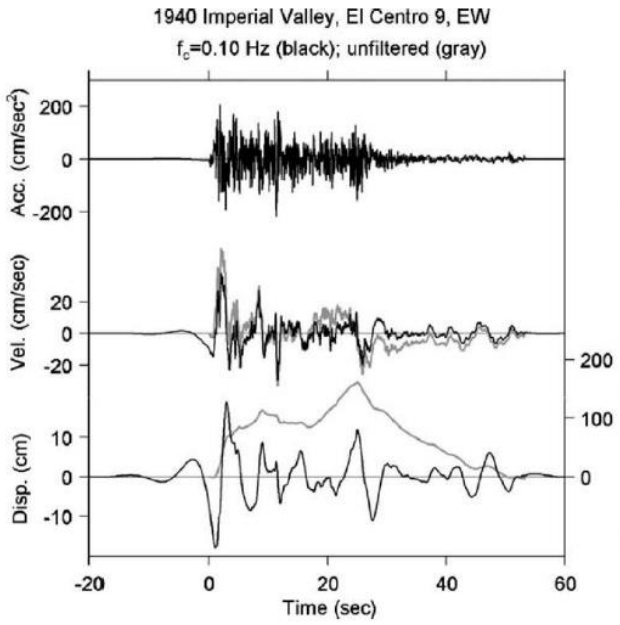

Figure 2.19: Unfiltered and Filtered Acceleration, Velocity, and Displacement Records (Boore & Bommer, 2005)

In general, there were four types of digital filtering models including Butterworth, Ormsby, Elliptical, and Chebychev. The choice of filtering model was found to be less important than the selected cut-off frequencies (Boore & Bommer, 2005). The authors outlined several criteria for selecting the cut-off frequencies in the high-pass filtering. One of the most common criteria was that the corner frequencies should be selected in accordance with the signal-to-noise ratio in a Fourier Acceleration Spectrum (FAS). The minimum signal-to-noise ratio between the actual signal and the model noise was set at three. Figure 2.20 show a FAS, which consists of unfiltered signal, filtered signals, pre-event mean record (assumed as a model noise), and a model noise proposed by Lee and Trifunac in year 1990 (Xian, 2017). Similarly, Douglas & Boore (2011) reported the criteria in choosing reasonable cut-off frequencies for low-pass

filtering. In addition, digital filtering could be categorized into casual and acasual filtering types.

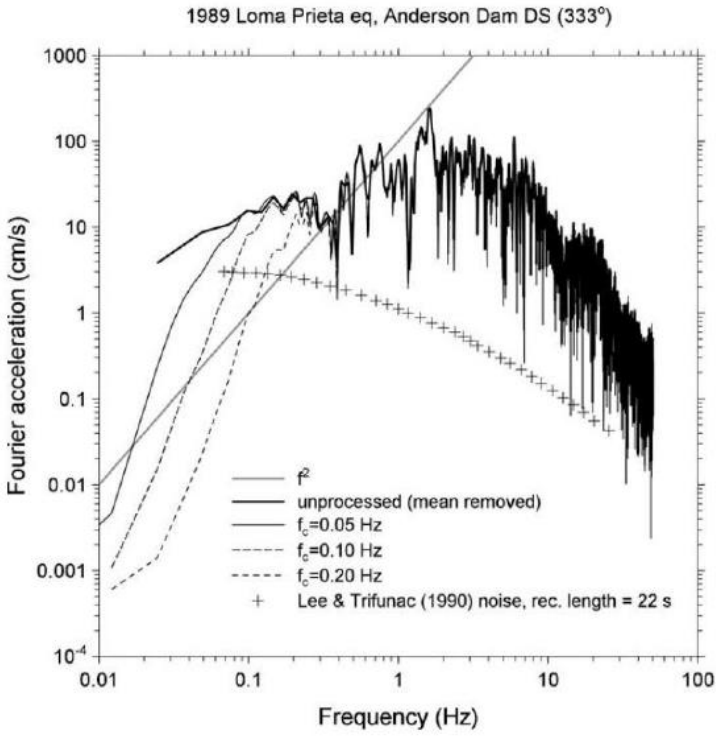

Figure 2.20: Fourier Acceleration Spectrum of Unfiltered and Filtered Acceleration Records (Boore & Bommer, 2005)

The distinguishable feature of acasual filtering is that it would not produce any phase shift in the records. This can be accomplished by adding a line of data with zero amplitude, which is known as pad, before the starting of a record and after the end of the record. The length of pads depends on the filter frequency and filter order (Boore & Bommer, 2005). Boore & Bommer (2005) also opined that the pre-event and post-event records were not often sufficient for the acasual filtering.

Mollova (2007) presented the application of digital filtering using a commercial software, namely SeismoSignal to process an actual earthquake record in Turkey. SeismoSignal is one of the popular commercial software that can be used to process earthquake strong-motion data with the function of graphical user interface. Baseline correction and digital filtering methods are incorporated in the software package. The effects of using various types of digital filtering models (i.e. Chebyshev, Butterworth, Bessel, and Elliptic) were examined in detail. Mollova (2007) examined the influences of filtering types (i.e. Butterworth, Chebyshev, and Bessel) and the order of filtering on the acceleration, velocity, and displacement time series. In addition, the Fourier Amplitude Spectra and the response spectra (with damping characteristics of 5 %) the dynamic event were evaluated.

Hence, Boore (2001) suggested a simple baseline correction method which includes the zeroth-order baseline correction and least-square fitting line prior to numerical integration as it gives best fit to baseline adjustment. Moreover, it is found out that selection of a filtering method is less important than selecting the cut-off frequencies (Boore & Bommer, 2005).

2.8 Summary

History of earthquakes occurred in far-field or near-field were reviewed in this chapter. Malaysia which is located far from ring of fire was considered to be safe from earthquake motions. Aftermath of Indian Ocean earthquake 2004, multiple local earthquakes were reported due to the reactivation of fault lines.

Therefore, Malaysian authorities revised the British Standard code to Eurocode to make RC structures resist against earthquake loads. Moreover, Eurocode particularly EC8 has three ductility classes. However, due to low seismicity in Malaysia, DCL is considered to be viable and preferable as suggested by Eurocode and Malaysian Annex. Linear and nonlinear elastic systems were also the part of study. SDOF and MDOF systems which defined the deformation of structure at single or multiple displacements were reported in this chapter. Usually, RC models which examined on Shaking table follows the equation of MDOF system as it produces the most accurate results. Additionally, out of four analysis methodology, nonlinear time history analysis is the most favourable analysis method due to its precise outcomes. A downscaled model research which was favourable for most of the researcher due to the reason of expensive full-scale specimens and testing facilities. With the study of downscale model many researchers are adopting similitude law with the support of Buckingham theory and defines the important parameters to achieve desired results. The similitude scaling factors for RC model were develop and published in this research. The appropriate signal processing is required to process the acceleration records from an earthquake or a dynamic test. Baseline correction and digital filtering methods are essential to remove the low and high-frequency noises from an actual signal. However, the integrated displacement data from an accelerometer record is often subjected to uncertainties. Therefore, a direct displacement measurement should be used as a reference when processing the measured acceleration records.

From the literature review, it is found out that this study is different and innovative by considering the structural design building code which is based on a single earthquake vibration. Therefore, multiple regional ground motions from near and far field requires to take into account to assess the actual behaviour of local structure. Moreover, it is noteworthy that an earthquake has never occurred in Malaysia with intense sequential ground motions with PGAs' ranging between 0.25 g to 0.82 g. Thus, artificially produced intensive harmonic waves can be produced and used to assess the RC structures in Malaysia with intensive ground motions (0.25g to 0.82g). Lastly, damage limitation set by EC8 for the RC structures under sequential ground motions requires to be validated.

CHAPTER 3

METHODOLOGY

This chapter includes research method adopted in this study. A useful tool Buckingham Pi Theorem is used to scale the model dimensions. A regular two storey reinforced concrete building model is constructed and investigated under a series of nine earthquake motions i.e. five real and four artificial. Signal processing technique is also explained to analysed the recorded data. Lastly, ETABS simulated model is discussed.

3.1 Operational Framework

The main trunk of operational framework of the research is shown in Figure 3.1. The first objective is to evaluate the building response of the two storey small scale RC building model. In order to fulfil the first objective, Buckingham Pi Theorem and similitude theory were applied to the scaled 1:10 model structure. A set of equation was developed based on Buckingham's Pi Theorem and similitude law. The equations were used to support and analyse the full scale structure through the equation of scaling factor S_E. Thereafter, in the structural design phase, the small scale structure was designed manually by using European code 2 and determine the seismic loads according to European code 8. After manually checked the structural design for small scale model, the laboratory work begins with concrete material preparation such as testing of

cylindrical mould. Mix design for concrete grade 30/37 was validated by casting 24 cylindrical moulds and left it for 28days before casting actual components of the framed structure. The strength of moulds was examined through Compression Testing Machine. In order to construct a small scaled low-rise RC building model, a small scale RC column is constructed to validate the scaling factor S_E. Contact sensors such as LVDT and Accelerometer were attached at different locations of the model. The scaled structure was constructed in a conventional construction procedure and then model was placed on shaking table. Artificial ground motions were generated by input parameters frequency and displacement ranging from 0.25g to 0.82g. The harmonic artificially produced ground motions were applied sequentially during shaking table test. The data recorded by contact sensors in each Test was processed through signal processing techniques. Simple quadratic baseline correction and Butterworth low-pass filtering technique was used to eliminate the noise from the recorded data. The response and crack development in scaled model was observed in each seismic excitation.

As the noise removed, the results were obtained to achieve the second objective that is, to determine the critical parameters such as maximum displacement; residual displacement; residual interstorey drift ratio; and acceleration response. All these shaking table results were scale up through scaling factor S_E to obtain the actual values for full scale building model and then compared with finite element analysis software ETABS outcomes and validate it. Therefore, initially all the artificially produced seismic ground motions were added into the simulated software. Thereafter, four real time

ground motions were also used sequentially to assess the building model. Hence, the results from experimental and simulation were discussed and conclude the findings.

Lastly, for third objective, the displacement data recorded by contact sensor LVDT was derived to find interstorey drift ratio and storey drift ratio. These two parameters are used to calculate the damage limitation of the full scaled model. EC8 suggested 1% damage limitation for interstorey drift ratio and 0.5-1% for storey drift ratio.

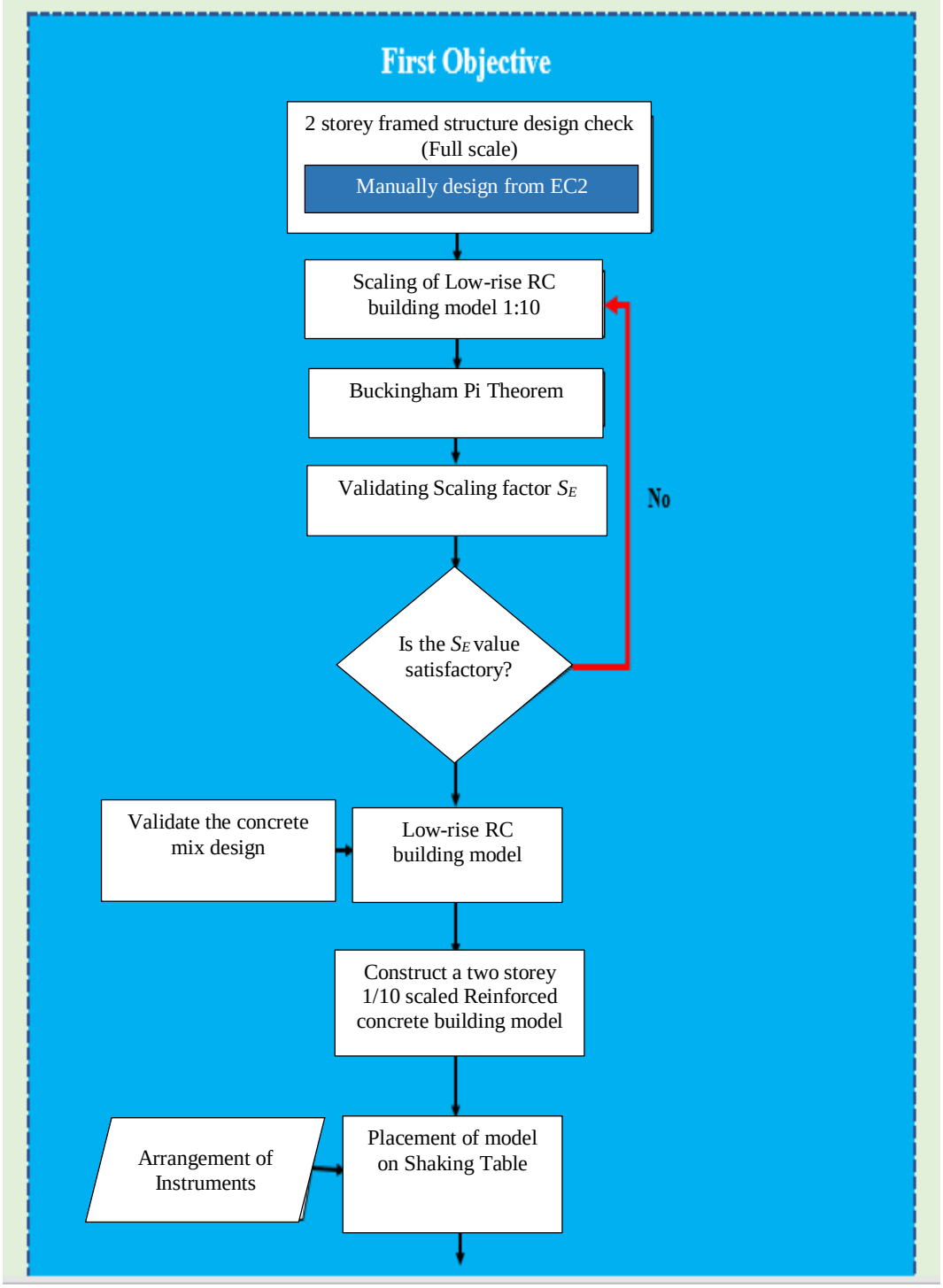

Figure 3.1: Research Study Flowchart

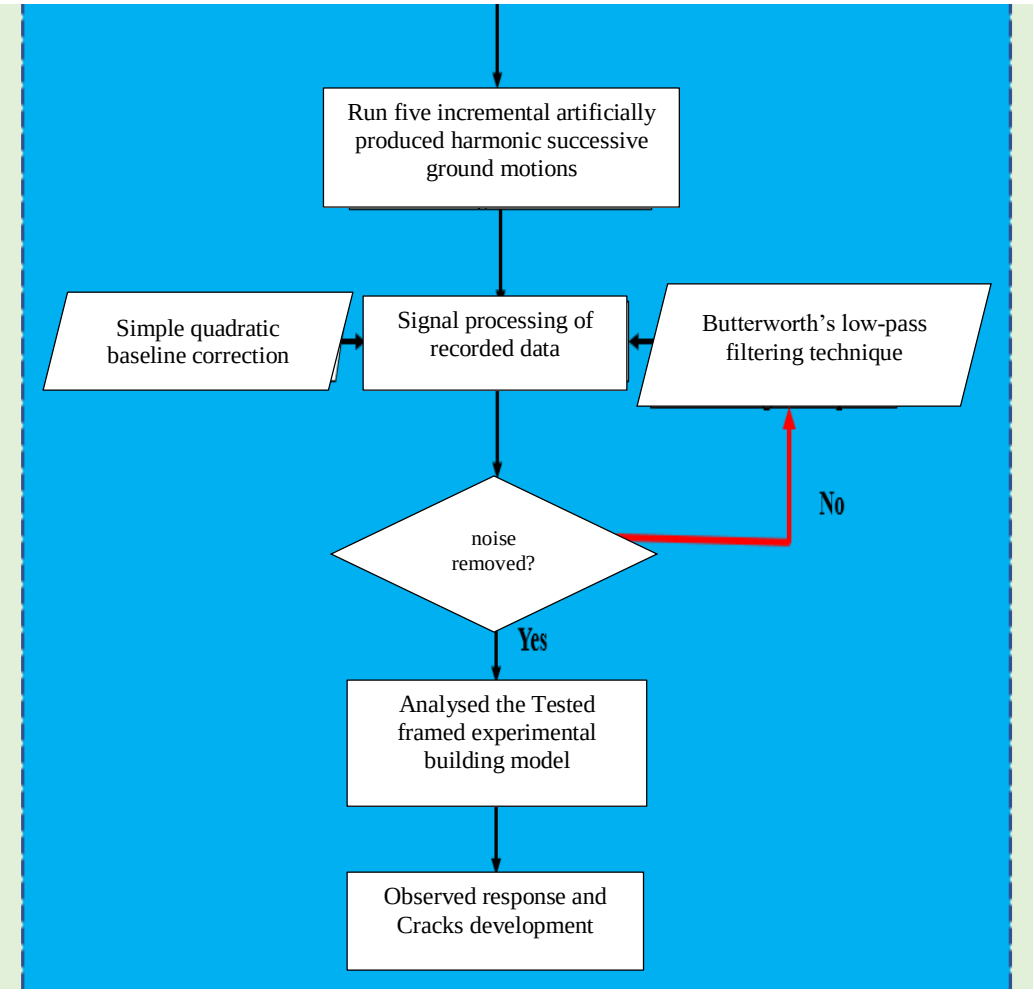

Figure 3.1: **Research Study Flowchart (Continue)**

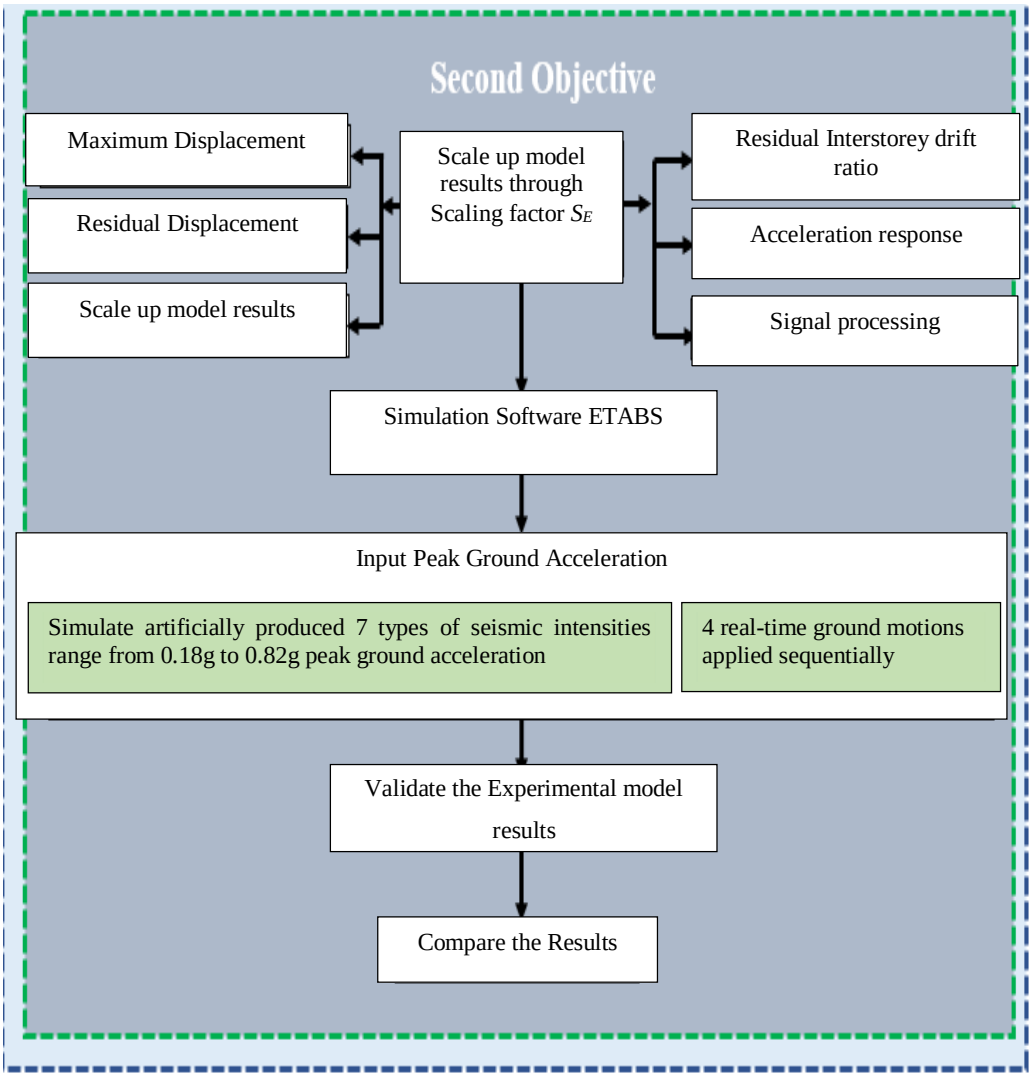

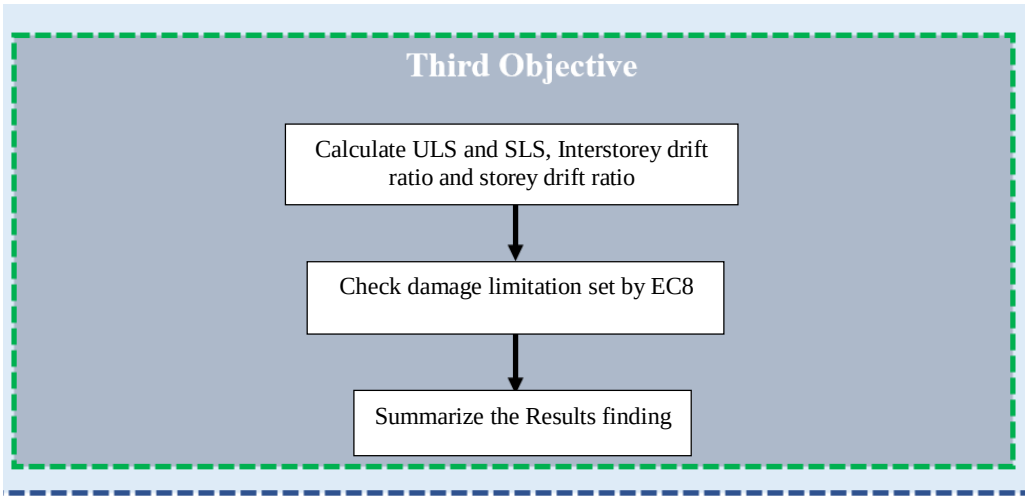

Figure 3.1: **Research Study Flowchart (Continue)**

3.2 Buckingham Pi Theorem

Dimensional analysis is the foundation for Buckingham's Pi theorem. There must be dimensional homogeneity among the variables. Consider a non-dimensional parameter named Pi (π). In a general dimensional analysis problem, Dependent Pi symbolizes as π_1. Remaining Pi's (π's) are independent as they are function of π_1 as shown in equation (3.1).

$$\pi_1 = f(\pi_2, \pi_3, \ldots, \pi_k) \tag{3.1}$$

where, '*k*' is the total number of Pi's.

Independent Pi's of the model (*m*) should have similitude relationship with the corresponding independent Pi's of the prototype model (*p*) as shown in equation (3.2),

$$\pi_{2,m} = \pi_{2,p} \quad , \quad \pi_{3,m} = \pi_{3,p} \quad and \quad \pi_{k,m} = \pi_{k,p} \tag{3.2}$$

Buckingham Pi theorem is a technique which helps to generate these Pi's. Following are the steps followed to find the dimensionless groups (Cengel & Cimbala, 2006).

Step 1: Enlist the parameters stated in the problem and sum up to get the total number '*n*'.

Step 2: Write down the dimensions of parameters '*n*' respectively.

Step 3: Primary dimensions need to be analysed to get the total number of '*j*' values. Solve the equation (3.3) for the expected number of π's equation termed as '*k*'.

$$k = n - j \tag{3.3}$$

Step 4: Select repeating parameters stated as '*j*'.

Step 5: Form '*k*' π's values.

Step 6: Equate the π's equations for both, model and prototype and consequently form each parameter scaling down equation.

3.2.1 Similitude methodology of structural model

Consider a building model having 10 physical parameters (dimensional variables, no dimensional variables, and dimensional constants). So therefore, n = 10. These parameters are shown in functional form as shown in equation (3.4) (Rastogi et al., 2015):

$$\sigma = f(d, t, \rho, E, g, l, V, \Omega, v) \tag{3.4}$$

where,

σ = Stress

d = Displacement

t = Time

ρ = Density

E = Modulus of elasticity

g = Spectral acceleration

l = Length

V = Shear Force

Ω = Frequency

v = Velocity

Following are the Primary dimensions of each 'n' parameters as shown in Table 3.1 (Rastogi et al., 2015).

Table 3.1: Dimensions of Selected Parameters (Rastogi et al., 2015)

Quantities	Dimensions
σ	FL^{-2}
d	L
t	T
ρ	$FT^{2}L^{-4}$
E	FL^{-2}
a	LT^{-2}
g	LT^{-2}
l	L
V	FL^{-2}
Ω	T^{-1}
v	LT^{-1}

In this case, it has been witnessed that total number of variables are 10 and the primary dimensions represent in this problem is three (3). Therefore, the number of dimensionless π groups would be seven (7). Repeating variables selected are *E, ρ* and *l*. Selection of repeating variable is based on geometrical and material properties. Selection also covers that they should not generate a dimensionless group.

Considering these repeating variables (*E, ρ, l*). Multiplying each independent variable (*d, t, g, V, Ω, v*) one by one with the product of repeating variables in order to form Pi's equations. First Pi equation is always formed through dependent variable (σ).

3.2.2 Derivation of Dimensionless groups

The first 'π' is always the dependent 'π' and is formed with the dependent variable 'σ' as shown in equation (3.5),

Dependent π: $$\pi_1 = \sigma E^a \rho^b l^c \quad (3.5)$$

Here, π_1 shows the equation for dependent variable 'σ'. Moreover, *a, b* and *c* are constant exponents that need to be determined. Apply the primary dimensions of Table 3.1 into equation (3.5) and force the π to be dimensionless by setting the exponent of each primary dimension to zero as shown in equation (3.6),

Dimensions of π_1: $$F^0L^0T^0 = \frac{F}{L^2}\left(\frac{F}{L^2}\right)^a \left(\frac{FT^2}{L^4}\right)^b (L)^c \quad (3.6)$$

Since primary dimensions are by definition independent of each other, we equate the exponents of each primary dimension of equation (3.6) independently to solve for exponents *a, b* and *c*.

Force: $$0 = 1 + a + b \quad (3.7)$$

Length: $$0 = -2 - 2a - 4b + c \quad (3.8)$$

Time: $$0 = 2b \quad (3.9)$$

Simultaneously simplify Eq (3.7), (3.8) and (3.9), we get:

$$a = -1$$

$$b = 0$$

$$c = 0$$

Substituting these values in Eq (3.5):

$$\pi_1 = \sigma\, E^{-1}\, \rho^0\, l^0$$

Therefore, π_1 in Eq. (3.10) is represented as,

$$\pi_1 = \frac{\sigma}{E} \tag{3.10}$$

As similarly in Eq. (3.11),

$$\pi_2 = \frac{d}{l} \tag{3.11}$$

where, π_2 shows the equation for independent variable '*d*'. Non dimensional group π_3 is derived with non-repeating variable *'t'* forming a relation with the repeating variables as shown in equation (3.12),

Dependent π_3: $$\pi_3 = t\, E^a \rho^b l^c \tag{3.12}$$

Equate exponents of equation (3.12) independently as shown in equation (3.13), (3.14), (3.15), and (3.16).

Dimensions of π_3: $$F^0L^0T^0 = T\,(\frac{F}{L^2})^a\,(\frac{FT^2}{L^4})^b\; L^c \tag{3.13}$$

Force: $$F = a + b = 0 \tag{3.14}$$

Length: $$L = -2a - 4b + c = 0 \tag{3.15}$$

Time: $$T = 1 + 2b = 0 \tag{3.16}$$

Simultaneously simplify equation (3.14), (3.15) and (3.16),

$$a = \frac{1}{2}$$

$$b = -\frac{1}{2}$$

$$c = -1$$

Substituting these values in equation (3.12),

$$\pi_3 = t\, E^{\frac{1}{2}}\, \rho^{\frac{-1}{2}}\, l^{-1}$$

π_3 is shown in equation (3.17) as,

$$\pi_3 = \frac{t}{l}\sqrt{\frac{E}{\rho}} \tag{3.17}$$

where, π_3 shows the equation for independent variable 't'. Similarly, in the same way, remaining independent variables combine with repeating variables to form independent Pi's as shown in equation (3.18) and (3.19),

$$\{\pi_r\} = \{(\pi_1)_r\,, (\pi_2)_r\,, (\pi_3)_r\,, (\pi_4)_r\,, (\pi_5)_r\,, (\pi_6)_r\,, (\pi_7)_r\} = \{1\} \tag{3.18}$$

Or

$$\{\pi_r\} = \left\{\left(\frac{\sigma}{E}\right)_r,\ \left(\frac{d}{l}\right)_r,\ \left(\frac{t}{l}\sqrt{\frac{E}{\rho}}\right)_r,\ \left(\frac{g\rho l}{E}\right)_r,\ \left(\frac{V}{E}\right)_r,\ \left(\Omega l\sqrt{\frac{\rho}{E}}\right)_r,\ \left(\frac{v\rho l}{E}\right)_r\right\} = \{1\} \tag{3.19}$$

3.2.3 Similitude requirement

The four dimensionless terms derived must be equal for the model and the prototype in order to match the functional relationship between them. The first dimensionless term $\pi_{1model} = \pi_{1prototype}$ i.e.,

$$\frac{\sigma_m}{E_m} = \frac{\sigma_p}{E_p}$$

$$\frac{E_p}{E_m} = \frac{\sigma_p}{\sigma_m}$$

Or

$$\sigma_m = \frac{\sigma_p}{S_E} \tag{3.20}$$

where, $S_E = \frac{E_P}{E_m}$ is the dimensional scaling factor. S_E is the ratio of modulus of elasticity of the prototype to that of the model. From equation (3.20), it follows that the model stress is scale factor *'S_E'* times lesser the stress in the prototype. Similarly for equation (3.21), from the second dimensionless term is represented as,

$$\frac{d_m}{l_m} = \frac{d_p}{l_p}$$

$$\frac{l_p}{l_m} = \frac{d_p}{d_m}$$

Or

$$\frac{l_p}{l_m} = \frac{d_p}{d_m}$$

$$d_m = \frac{d_p}{S} \tag{3.21}$$

where $S = \frac{l_p}{l_m}$ is the dimensional scale factor.

3.2.4 Calculation of scaling factor 'S_E'

From equation (3.20), S_E is derived as shown in equation (3.22),

$$S_E = E_p / E_m \tag{3.22}$$

As we know that $E = F/L^2$, so substitute in equation (3.22) to get equation (3.23) as,

$$S_E = F_p L_m^2 / L_p^2 F_m \tag{3.23}$$

Substitute $F = ma$ in equation (3.23),

$$S_E = (m_p \,.\, a_p \,.\, L_m^2)/(L_p^2 \,.\, m_m \,.\, a_m)$$

Rearrange the values,

$$S_E = (m_p / m_m) \,.\, (a_p/a_m) \,.\, (l_m^2/l_p^2)$$

Input $a_p/a_m = S_a$ and $l_p/l_m = S$ from in equation (3.21), we get equation (3.24),

$$S_E = (m_p / m_m) \,.\, S_a \,.\, (1/S^2) \tag{3.24}$$

Here, equation (3.24) shows the derived equation of S_E to calculate the scaling factor as shown in section 3.3.4.

3.3 Description of structure

RC building of Block N, Universiti Tunku Abdul Rahman (UTAR), Malaysia is selected in this study as shown in Figure 3.2. The prototype full scale model has long spans and multiple number of columns and beams. However, due to the smaller size of shaking table, a part of a building is considered as shown in Figure 3.3. Malaysia has been considered as low seismic zone (Sooria et al., 2012) and Eurocode EC8 suggested to design building model on DCL for low seismicity area. Therefore, a low-rise frame structure is designed on Euro code EC2 (European Standard, 2004a) and EC8 (European Standard, 2004b) for DCL followed by Malaysian National Annex. The Detail calculation of building model is shown in Appendix A.

Figure 3.2: Full scale building model located in Block N, Universiti Tunku Abdul Rahman, Perak, Malaysia

3.3.1 Specimen specifications

The experimental model is scaled to 1/10 through a dimensional analysis tool named Buckingham Pi Theorem as stated in Section 3.2. Framed structure is actually a part of a university building, have 3 bays on X-axis and 1 bay on the Y-axis. The specimen has two storey and rectangular in shape as shown in Figure 3.3. Details of the geometry and reinforcement of this prototype structure are shown in Figure 3.4.

Figure 3.3: Labelled Geometry and Elevation of RC Frame Building Model

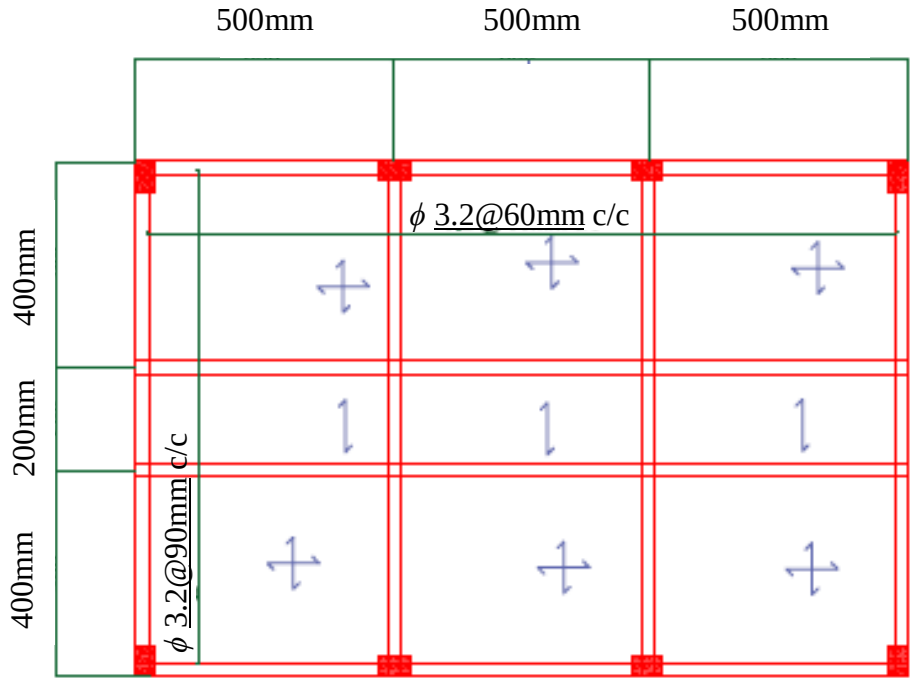

(a) 1st and 2nd Storey Slab Reinforcement and Plan Layout

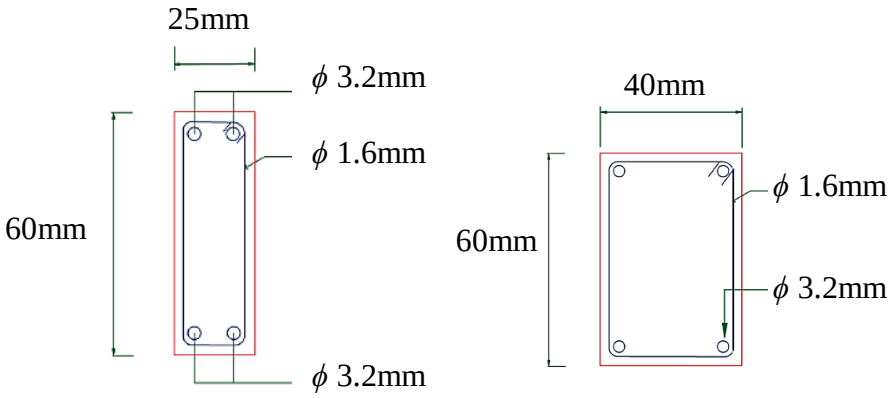

(b) Beam Reinforcement Details **(c) Column Reinforcement Details**

Figure 3.4: Experimental Model Geometry and Reinforcement Details

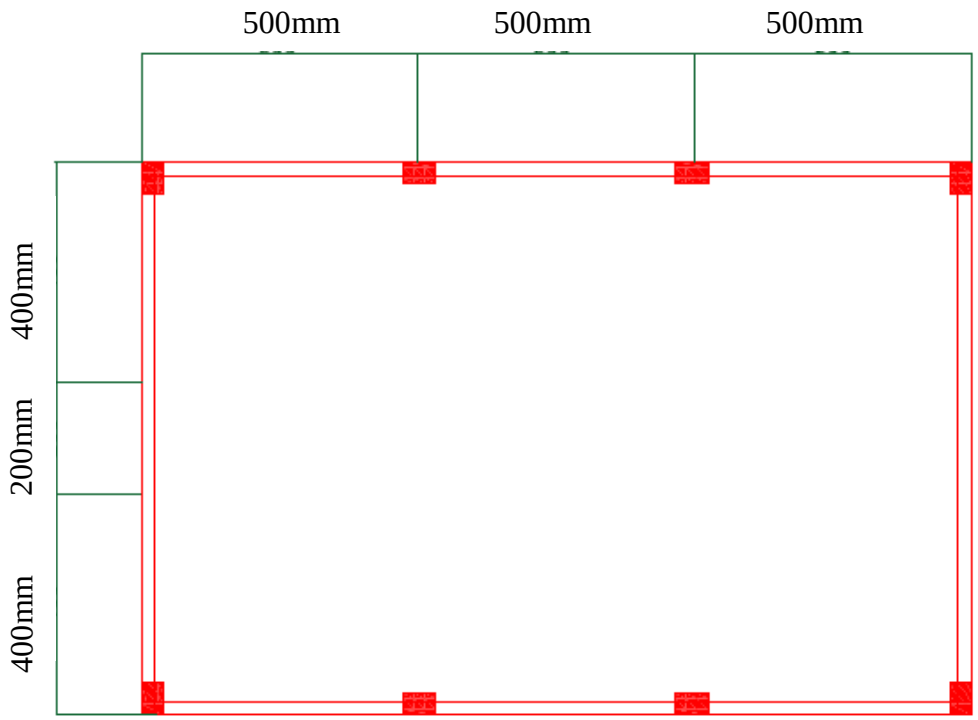

(d) Base Plan Layout

Figure 3.4: Experimental Model Geometry and Reinforcement Details (Continue)

3.3.2 Reinforcement specification

RC model need to analysed and designed manually before constructing the experimental model. Based on the calculation being shown in Appendix A, the diameter used for the reinforcement bars in the downscale model are 1.6mm and 3.2mm. Main reinforcement bars of beams and columns are 3.2mm diameter. Shear rings and ties have a 1.6mm diameter of the bar.

Tensile tests of twelve sample bars with a diameter of 1.6mm and 3.2mm is conducted in Mechanical laboratory of Universiti Tunku Abdul Rahman,

Malaysia as shown in Figure 3.5. The mechanical reinforcement properties are listed in Table 3.2. Reinforcement bar 3.2mm has an average yield stress of 807.95MPa and average modulus of elasticity of 160.56 GPa. Similarly, for 1.6mm bar, average yield stress and modulus of elasticity are 998.95MPa and 144.02GPa respectively. Due to the unavailability of deformed bar in such a small diameter, standard steel was used that is why the modulus of elasticity is lower than 200GPa (a value suggested by EC2 for Class B and C reinforcement). However, the yield strength is higher than the range of 400 to 600MPa as suggested by EC2. This change in parametric values is due to the material property of bar.

Figure 3.5: Laboratory Test of Reinforcement Bar in Universal Testing Machine

Table 3.2: Specifications of Reinforcement Bars (Tensile Strength Test)

Steel bar diameter in mm	Load at yield (KN)	Ultimate load (KN)	Tensile yield stress at yield load (MPa)	Tensile strain at maximum load (mm/mm)	Elastic modulus (GPa)
1.6	1.74	2.06	1023.95	0.06032	155.207
1.6	1.62	2.0	995.06	0.10344	145.509
1.6	1.68	2.01	997.70	0.02548	137.704
1.6	1.65	1.99	987.53	0.02902	138.789
1.6	1.62	1.99	990.53	0.05032	142.902
Average			**998.95**		**144.02**
3.2	5.17	6.55	814.94	0.20349	160.011
3.2	5.10	6.43	799.17	0.16392	154.402
3.2	5.22	6.50	808.15	0.11239	165.437
3.2	5.24	6.49	807.15	0.11013	159.037
3.2	5.11	6.52	810.37	0.22496	163.923
Average			**807.95**		**160.56**

3.3.3 Concrete specification

A compressive strength test is conducted on a cylinder mould with a height of 200mm and diameter 100mm. In order to achieve the concrete strength of 30 N/mm^2 at 28 days, a concrete mix design is used (Franklin et al., 1988; Yip & Marsono, 2016). Preliminary concrete mix design has been validated based on British Standard BS5328: Part 2: 1997. For the quantity of $1m^3$ concrete mix design, the calculated components of a concrete mix is shown in Table 3.3. Here, water/cement ratio is 0.42.

Table 3.3: Components in Concrete Mix Deign for Self Compacting Concrete SCC

Cement (kg/m^3)	Water (kg/m^3)	Fine aggregate (kg/m^3)	Coarse aggregate (kg/m^3)	Density (kg/m^3)	Admixture 1.2% , (kg/m^3)
550.0	233.0	511.0	1086.0	2380.0	6.60

As reported in EC2, the strength class of concrete for RC structures is 30/37 (that is compressive strength of concrete cylinder is 30N/mm^2). Moreover, the mean tensile strength is 2.9 N/mm^2 as shown in Appendix B. Therefore, 16 cylindrical specimens tested for compressive strength and 8 specimen tested for tensile strength of concrete are shown in Table 3.4 and Table 3.5 respectively. Based on the laboratory test as shown in Figure 3.6, the average compressive and tensile strength of concrete is 33.26 N/mm^2 and 12.86 N/mm^2 respectively.

Figure 3.6: Concrete cylindrical Molds Placed in Compression Testing Machine

Table 3.4: Compressive Strength of Concrete for 28days, f_{cu}

Casting date	Weight of Specimen (kg)	Maximum load applied (KN)	Compressive strength , f_{cu} (N/mm^2)
14th February, 2018	3.64	253.6	32.29
14th February, 2018	3.62	239.9	30.55
14th February, 2018	3.64	259.5	33.01
14th February, 2018	3.62	246.8	31.42
8th May, 2018	3.70	256.9	32.71

8th May, 2018	3.62	235.9	30.03
16th May. 2018	3.66	269.7	34.34
16th May. 2018	3.68	291.5	37.12
18th May. 2018	3.66	280.7	35.74
18th May. 2018	3.69	267.0	34.0
20th June, 2018	3.64	237.4	30.23
30th June, 2018	3.50	281.2	35.81
30th June, 2018	3.56	280.3	35.70
30th June, 2018	3.66	285.3	36.33
4th July, 2018	3.66	251.2	31.99
6th July, 2018	3.60	242.2	30.84
Average			**33.26**

Table 3.5: Splitting Tensile Strength of Concrete for 28 days, f_t

Casting date	Weight of Specimen (kg)	Maximum load applied (KN)	Splitting strength, f_t (N/mm^2)
8th May, 2018	3.66	114.5	14.59
8th May, 2018	3.66	84.0	10.70
18th May. 2018	3.64	75.1	9.56
18th May. 2018	3.68	107.2	13.65
20th June, 2018	3.64	108.6	13.83
30th June, 2018	3.54	121.9	15.52
4th July, 2018	3.68	106.7	13.58
6th July, 2018	3.58	89.7	11.42
Average			**12.86**

3.3.4 Theoretical mass of column

As the equation of S_E has been derived in Section 3.2.4, so select one column out of eight columns from the prototype full scale model to get the theoretical mass of each column.

$$\text{Volume of Column} = \text{Length} \times \text{Breadth} \times \text{Height}$$

$$\text{Volume of Column} = 600\text{mm} \times 400\text{mm} \times 7000\text{mm}$$

$$\textbf{\textit{Volume of Column}} = \textbf{\textit{1.68m}}^{\textbf{\textit{3}}}$$

Mass of Prototype (column) = Density of Concrete × Volume of Column

Mass of Prototype (column) = 2500 × 1.68

$$\textbf{\textit{Mass of Prototype (column)}} = \textbf{\textit{4200kg}}$$

So, the theoretical mass of each prototype full scale column is 4200kg.

3.3.4.1 Mass of actual experimental column

The fabrication process of the column is shown in Figure 3.7. To calculate the actual mass of small scaled column, construct a column and get the weight of it.

$$\textbf{\textit{Measured Mass of small scale column}} = \textbf{\textit{4.22kg}}$$

Now, consider the equation (3.24) to calculate S_E,

$$S_E = (4200/4.22) \times 1 \times (1 / 10^2)$$

$$\boldsymbol{S_E} = \textbf{\textit{9.9}}$$

Figure 3.7: Fabrication of small scale column

3.3.4.2 Similitude Relations

Drawing the different similitude relationships and scale factors for dynamic structural model, are shown in Table 3.6. Different parameters have been scaled

down. Dimensional Scale factor *'S'* and *'S_E'* are used to reduce the model scale. Typical scale factor for Slab/beams structures for elastic models is 1:10 (Harris & Sabnis, 1999). Material properties for prototype and scaled model remains similar i.e S_E = 9.9. Table 3.6 shows the reduced model parameters.

Table 3.6: Similitude relation

Parameters	**Dimensions**	**Scale Factor**	
		Equations	**1:10 Scale up Model**
Modulus, *E*	FL^{-2}	S_E	9.9
Stress, σ	FL^{-2}	S_E	9.9
Acceleration, *a*	LT^{-2}	*1*	1
Length, *l*	*L*	*S*	10
Point load, *P*	*F*	$S_E S^2$	$9.9\times(10)^2$
Time, *t*	*T*	$S^{1/2}$	$(10)^{1/2}$
Frequency, Ω	T^{-1}	$S^{-1/2}$	$(10)^{-1/2}$
Velocity, *V*	LT^{-1}	$S^{1/2}$	$(10)^{1/2}$
Mass Density, *p*	$FL^{-4}T^2$	S_E/S	$9.9\times(10)^{-1}$
Moment of Inertia, *I*	L^4	S^4	$(10)^4$
Shear force, *V*	*F*	$S_E S^2$	$9.9\times(10)^2$
Moment, *M*	*FL*	$S_E S^2$	$9.9\times(10)^2$

3.4 Test instruments

In experiment, RC building model are attached with several contact sensors. The contact sensors used in this research study are Accelerometer and LVDT. Moreover, shaking table is a machine on which RC model is examined.

3.4.1 Accelerometers

An accelerometer is an electromechanical device used to measure acceleration forces. Such forces may be static, such as continuous force of gravity or, dynamic to sense movement or vibrations. In order to record the acceleration produced by building model at different storey, 7 accelerometers are attached to the framed specimen. Contact sensor accelerometer is illustrated in Figure 3.8.

Figure 3.8: Accelerometer attached to the building model

3.4.2 Linear Variable Displacement Transformers (LVDT)

A contact sensor LVDT is installed at four locations on the building frame that is at shaking table base, building model base, storey 1, and storey 2. LVDT attached to storey 2 is shown in Figure 3.9. In the shaking table, there is no fixed frame available to adjust the LVDT to record vertical displacement of the test framed specimen.

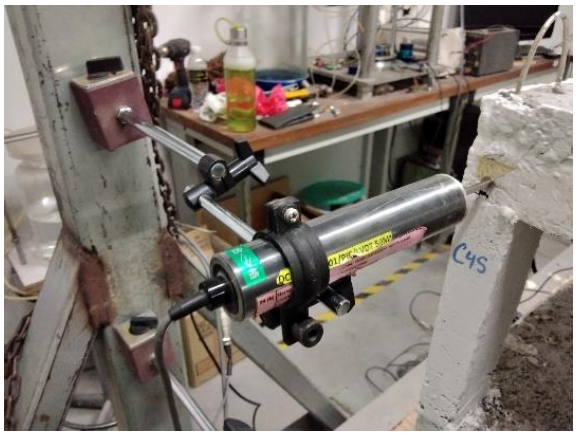

Figure 3.9: LVDT connected with the building model

3.4.3 Shaking table

Figure 3.10 shows the shaking table setup used in the present study. A mega-torque motor was used to produce one-dimensional shaking motion on a level platform (2m by 2m) by generating a mechanical torque repeatedly. The shaking table platform was lifted afloat by supplying an air pressure of 2 bars underneath the table platform to minimize the friction between the base and platform during cyclic horizontal movement. The shaking table was capable of producing frequencies of 0.1 – 20 Hz and horizontal displacements of 0.5-15 mm. The highest achievable peak acceleration was about 0.82g.

Figure 3.10: Shaking Table in UTAR, Malaysia

The physical instruments and contact sensors that are attached at eleven locations in the building frame structure during the test includes Accelerometer and LVDT are shown in Figure 3.11. Out of seven accelerometers, three of them are attached to the shaking table to record the input ‘g’ values as suggested by EC8 (clause 3.2.3.1.2(4) and 3.2.3.1.3, Appendix D). LVDT is placed to record the horizontal displacement at the joints of the beam and column at each story.

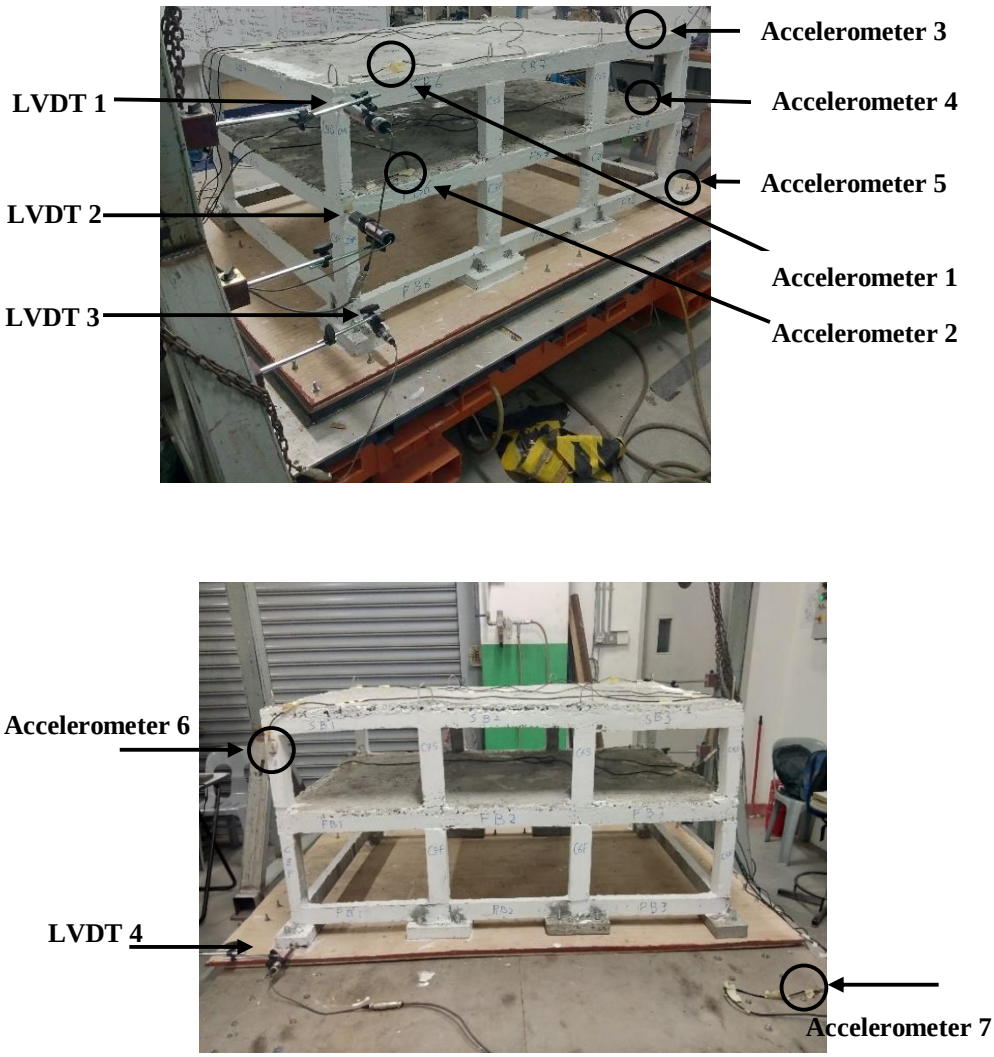

Figure 3.11: Instrumentation Plan

These instruments recorded the time histories of the building frame responses. Furthermore, the shaking table generates the seismic excitation based on input motion (frequency and displacement).

3.5 Dynamic behaviour of building model

The real structures are seldom described by Single degree of freedom (SDOF) system. Due to complexity in deformation particularly structural stiffness and mass, loading characteristics, and response variations, the equation of motion for structural model can describe well in Multiple degree of freedom (MDOF) system as shown in equation (3.25).

$$[M]\{\ddot{y}\} + [C]\{\dot{y}\} + [K]\{y\} = \{p\} - [M]\{\ddot{x_g}\} \tag{3.25}$$

where,

$[M]$ = Mass matrix

$\{y\}$ = Relative displacement vector

$[C]$ = Damping matrix

$[K]$ = Stiffness matrix

'x_g' = Acceleration of ground motion

$\{p\}$ = External force vector.

Furthermore, upper dot notation corresponds to time derivatives, i.e., $\{\dot{y}\}$ and $\{\ddot{y}\}$ correspond to velocity vector and acceleration vector, respectively.

The equation (3.25) is completely satisfying the conditions for elastic behaviour of structure. During the earthquake ground motions, the building model moves towards inelastic range and form a nonlinear relation between restoring forces and deformation. Therefore, Eq. (3.25) need to be replaced for inelastic behaviour. Equation (3.26) represents the equation of motion considering a dynamic nonlinear vibration of an MDOF system with damping excluding the external forces. It can be written as,

$$[M]\{\ddot{y}\} + [C]\{\dot{y}\} + [K]\{y\} = -[M]\{\ddot{x_g}\} \tag{3.26}$$

3.6 Input motion for experimental model

For experimental model, this study focuses on five artificial earthquake motions as listed in Table 3.7. Regarding the artificial ground motion, in UTAR, Malaysia, shaking table performed harmonic motions which were able to simulate desired ‘g’ value and uniform patterns of the signal. Various seismic excitations are determined before performing the test on frame specimen. Afterward, the building model is subjected to multiple excitations where five different artificial harmonic ground motions have been applied sequentially ranging from 0.25g (Test 1) to 0.82g (Test 5). The input ground motions recorded from accelerometer are listed in Table 3.7. Furthermore, the time duration is 15 seconds for all five artificial ground motions.

Table 3.7: Seismic Input of Artificial Seismic Sequence

Test case	Input motion		PGA 'g'(m/s^2)
	Frequency (Hz)	Displacement (mm)	
Test 1	3	1.5	0.25
Test 2	5	0.5	0.30
Test 3	3	2.0	0.36
Test 4	10	0.5	0.64
Test 5	8	0.5	0.82

The PGA values are utilized in increasing order as shown in Figure 3.12(a). It is observed that in Figure 3.12(a), each ground motion (that is Test 1, 2, 3, 4 and 5) has a uniform harmonic wave. Moreover, the acceleration time history and spectrum of ground motion for Test 5 is shown in Figure 3.12(b) and (c). Figure 3.12(c) shows the maximum spectral acceleration of 2.59m/s^2 at 0.1sec.

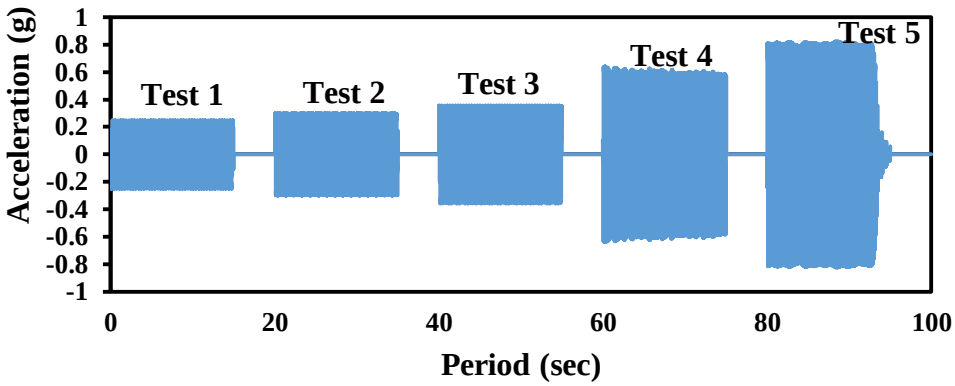

Figure 3.12(a) Input Acceleration Time History from Test 1 to 5

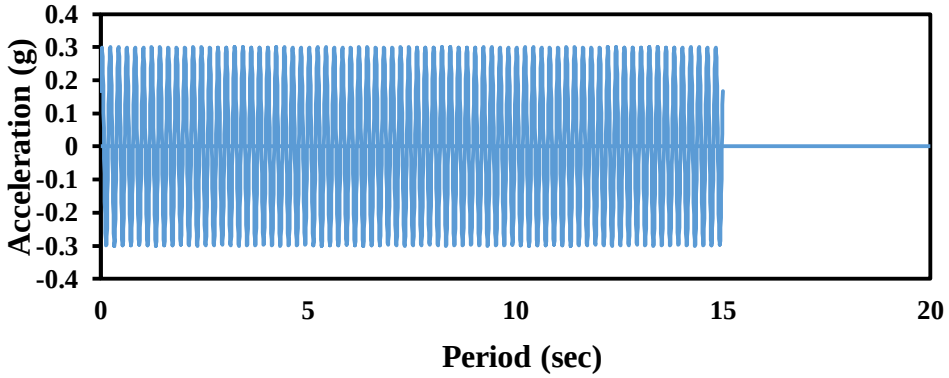

Figure 3.12(b) Input Acceleration Time History of Test 5

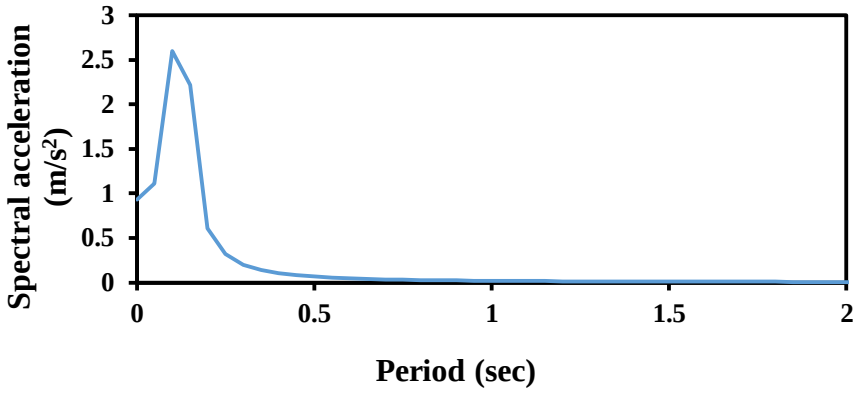

Figure 3.12(c) S_a Spectrum For 5% Damping (Duration Scaled) of Test5

3.7 Signal processing and analysis

The data recorded through accelerometer has a noise effect in each seismic motion signal. Many authors have faced this noise in their study and they have conducted the processing and adjustments in earthquake records such as Boore, (2001); Boore & Bommer (2005); and Chiu (1997b). To recover the correct data, Boore (2001) conducted a study and proposed correction methodologies to improve the actual shaking records. Boore & Bommer (2005) highlighted the effect of noise and proposed to perform baseline correction, where he recommended that a suitable cut off frequency was selected to filter out the noise in the data. Zeroth -order baseline correction was suggested in which a set of mean data recorded in pre-event would be removed from the entire data record in the very beginning stages of signal processing (Boore & Bommer, 2005). The methodology supported to identify the changes in the velocity baseline followed by identification of a change in a particular instant of time and then subtracted the changes in baseline step of the acceleration data record.

Then, the acceleration data baseline had been adjusted and corrected; it would easily integrate to get the numerical values of velocity and displacement. Simple quadratic baseline correction and Butterworth low pass (high-cut) filtering methods are attempted to process the raw acceleration data.

3.7.1 Simple quadratic baseline correction

The original data recorded by the accelerometer is first introduced to correction mythology known as Simple quadratic baseline correction (Seismosoft's Suite of Earthquake Tools, 2018). This correction scheme subtracted the entire acceleration data from a quadratic least-square fitting line prior to numerical integration as shown in equation (3.27), (3.28), and (3.29). Here, SeismoSignal software is used for baseline correction.

$$Acceleration = a_t - (a_0 + a_1 t) \tag{3.27}$$

$$Velocity = v_t - \left(a_0 t + \frac{1}{2} a_1 t^2 \right) \tag{3.28}$$

$$Displacement = D_t - \left(\frac{1}{2} a_0 t^2 + \frac{1}{6} a_1 t^3 \right) \tag{3.29}$$

where,

a_t = Acceleration, m/s^2

v_t = Velocity, m/s

D_t = Displacement, mm

t = Time, sec

a_0, a_1 = Coefficients

Baseline correction has a tendency to eliminate the lower frequencies and considers the higher frequency which is, in fact, a high pass filtering method with an unidentified cut off frequency (Boore & Bommer, 2005).

3.7.2 Butterworth low pass (high-cut) filtering

Filtering technique is used to remove the unwanted frequencies in the signal. Butterworth filtering is a type of filter whose frequency response provides a constant output from direct current up to cut-off frequency and rejects all the signals above that frequency. In experimental model, all the data recorded by accelerometers are filtered based on input frequency as listed in Table 3.7 for each artificial ground motion. Software SeismoSignal is used in filtering the data.

3.8 Seismic Input in ETABS simulated model

After assessing the model on shaking table, the building model is scale up 1:10 (Rastogi et al., 2015; Yip et al., 2018) through scaling factor S_E to get the prototype full scale model. Thereafter, the scaled up model is simulated on a software program known as ETABS with the same structural specification as shown in Figure 3.4 and Figure 3.13.

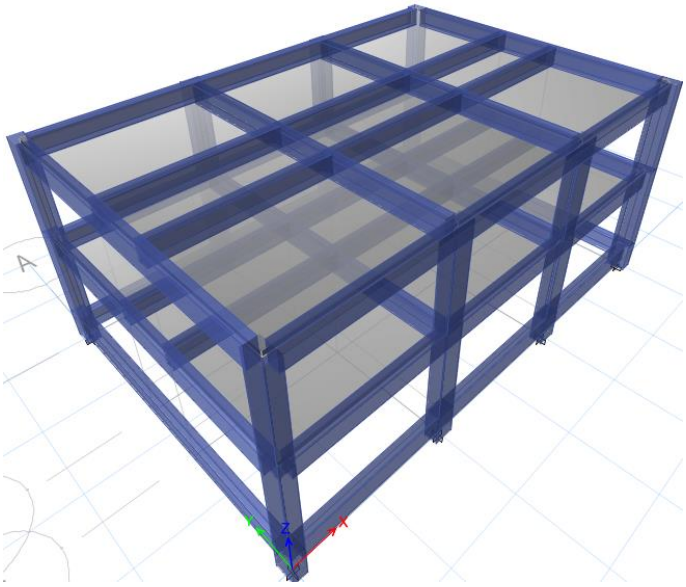

Figure 3.13: Three dimensional view of simulated model

The inputs in simulated model are material properties of steel and concrete, section properties of beam, column and slab, load patterns, and load case for nonlinear time history analysis. Moreover, the same artificial ground motions are defined as the function for time history analysis as listed in Table 3.7. Results of each artificial ground motion in simulated model is validated with accelerations and displacements recorded in shaking table test. Additionally, to examine the simulated model on real time ground motions, Mammoth Lake (1980) earthquake is selected under a series of multiple seismic events. The data is extracted from the Pacific Earthquake Engineering Research Center (PEER, 2019). The sequential seismic events of Mammoth Lake are listed in Table 3.8.

Table 3.8: Seismic Data of Real Ground Motion

Earthquake Event	Station	PGA value (g)	Code name	Date and time
Mammoth Lake (ML)	Long Valley Dam (Upr L Abut)	0.34	ML1	25-05-1980, 4:34pm
		0.14	ML2	25-05-1980, 4:49pm
		0.33	ML3	25-05-1980, 7:44pm
		0.24	ML4	25-05-1980, 8:35pm

Table 3.8 shows the location of station at which PGA was recorded. After the first ground motion ML1, three consecutive ground motions ML2, ML3 and ML4 was observed. The interval between the two real time ground motions are different as shown in Table 3.8. However, 5 sec intervals between oncoming ground motion is selected in simulated model for this study.

3.9 Summary

This chapter began with methodology of dimensional analysis tool Buckingham Pi Theorem, which helps to determine the equations to get full scale model results through the scaling factor S_E. The artificially produced ground motions for shaking table test was briefed. Signal processing was used to remove noise from recorded data through baseline correction and low pass filtering technique. Real-time ground motions used in simulation software ETABS were also discussed in this study.

CHAPTER 4

RESULTS AND DISCUSSION

This chapter presents the results of the research. The section focuses on the observed response of the framed structure, signal processing, scale up model outcomes, maximum displacement, residual displacement, residual interstorey drift ratio, interstorey drift ratio, and acceleration. To calculate the damage limitation, interstorey drift ratio, and storey drift ratio is discussed. Moreover, the building model has passed through multiple sequential seismic excitations (artificial and real-time ground motion). Therefore, the structural behavior in these ground motions have been discussed.

4.1 Observed response and cracks development

In the framed specimen Test 1 and 2, shaking of the building model is observed. However, there are no cracks formed. Particularly intermediate beams and columns has no effect of artificial ground motions. In Test 3, the test model shows the damage. The horizontal, vertical and diagonal cracks are observed at the beam-column joint as well as corner at storey 1 as shown in Figure 4.1. The cracks are formed due to transfer of moments from beam end to column ends. This damage points to the yielding of the beam and column reinforcement.

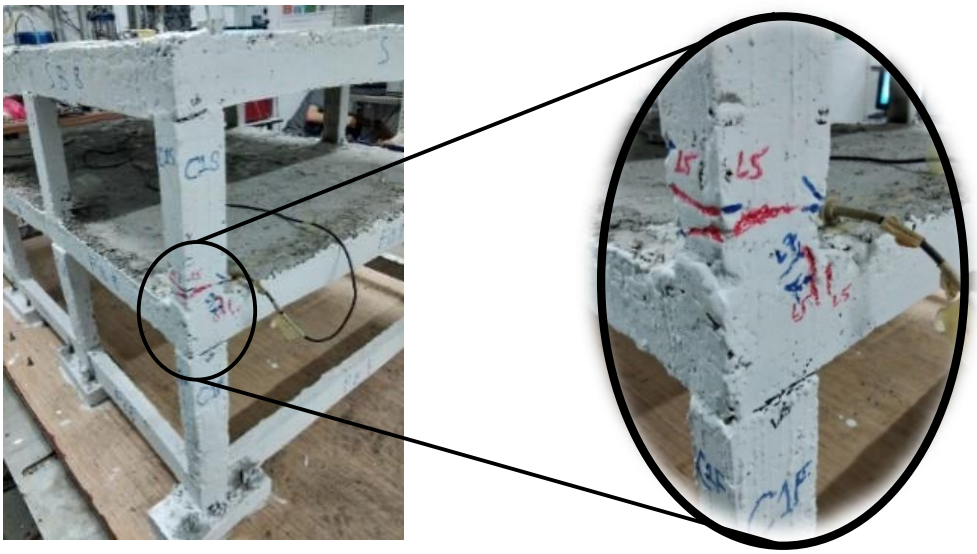

(a)

(b)

Figure 4.1: (a) Flexural horizontal minor cracks at the column in storey 1; (b) Flexural horizontal and vertical cracks at a beam-column joint in storey 1

Moreover, the model is observed to have significant horizontal cracks in the beam-column joint of the roof (storey 2) as shown in Figure 4.2.

Intermediate columns and beams have not shown any significant damage behavior during this artificial ground motion.

Figure 4.2: Flexural horizontal cracks at roof beam column joint

During the Test 4 run, the model has experienced significant cracks at beam-column joint at the base and storey 1 as shown in Figure 4.3 (a) and (b) which was the extension of cracks propagated in Test 3.

Figure 4.3 (a)

Figure 4.3 (b)

At this artificial ground motion, intermediate columns and beams of the framed specimen experience cracks as shown in Figure 4.3 (c) and (d). However, there was no spalling of concrete observed.

Figure 4.3 (c)

Figure 4.3 (d)

Figure 4.3: Significant cracks at (a) base; (b) storey 1; (c) intermediate column and (d) beam-column joint

Lastly, Test 5 has maximum PGA value of 0.82g, which caused the higher frequency of vibration. However, the test specimen sustains and absorb vibrations without any member failure. This seismic sequence further propagates the cracks at inner joints of column and beam as presented in Figure 4.4.

Figure 4.4 (a)

Figure 4.4 (b)

Figure 4.4 (c)

Figure 4.4 (d)

Figure 4.4: (a) Severe flexural crack at periphery beam at base; (b) significant flexural crack at periphery beam at storey 1; (c) flexural crack in the internal beam-beam joint at storey 1; (d) flexural cracks in beam-column joint at storey 2 slab.

Therefore, under successive incremental artificial ground motion, concrete material deterioration starts from storey 1 to the adjacent storey due to the impact of inertial forces in the horizontal direction. The damage concentration in the framed structure is observed to be at the beam-column joints. The damage is less severe especially at the storey 2 as compared to the storey 1. Only concrete cracks and reinforcement internal plasticity is observed. Thus, it is established that the building model with ductility class low (DCL) has a tendency to absorb lower to higher 'g' values and resist the earthquake loading due to the strength of framed structure rather than its ductility.

4.2 Signal processing

After running all the artificially produced seismic motions on shaking table, the data recorded by contact sensors needed to be addressed. In Test 4 and 5, the input frequency is 10Hz and 8Hz, respectively. However, in Figure 4.5, the raw data recorded by the accelerometer shows noise included in the recorded data set. Therefore, it is required to remove unwanted data associated with measured acceleration data.

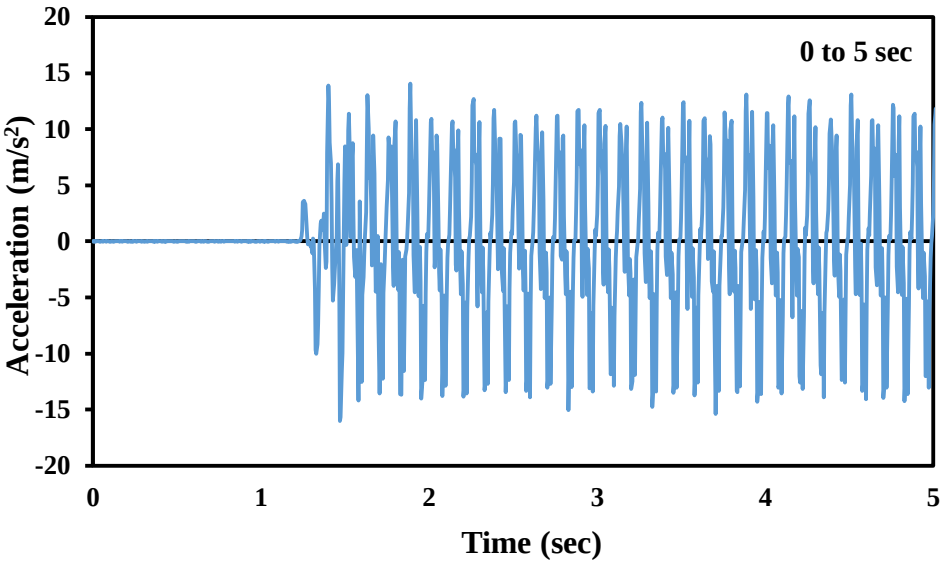

(a)

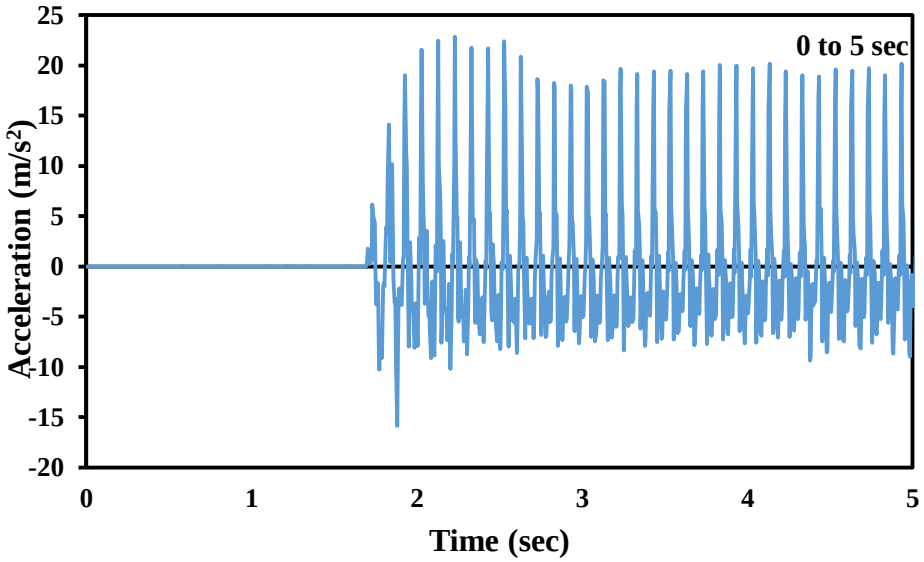

(b)

Figure 4.5: Recorded Acceleration Time Series under Input Frequencies (a) Test 4 (10 Hz), (b) Test 5 (8Hz)

As explained by Berg & Housner (1961), the integration method to obtain numerical data set, acceleration data in Figure 4.5 has integrated to get numeric initial velocity and displacement periodic series by considering the

assumption of initial velocity and displacement conditions respectively. In Figure 4.6 and Figure 4.7, the time series of velocity and displacement has a shift in the baseline. The wave moves toward the negative axis referring to negative direct current bias in the acceleration plot recorded by an accelerometer. Thus, the maximum displacement time series data is required to correct otherwise the end results will be unexpected and inappropriate. Figure 4.7 shows that the maximum displacement recorded at the end of the displacement time series plot is 1100mm that is much higher than actual and input value as listed in Table 3.7.

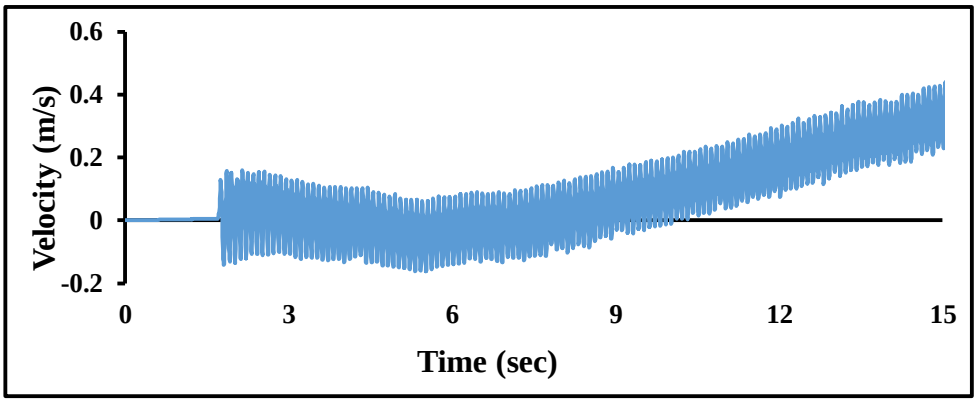

Figure 4.6: Velocity Periodic Plot Extracted from Integrating Acceleration Data Set (Test 4)

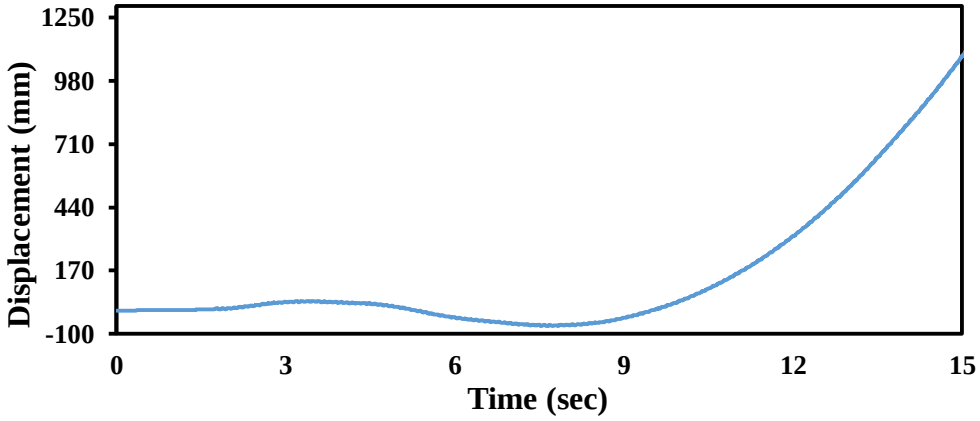

Figure 4.7: Plot of Displacement Time Series through Integrating the Acceleration Data (Test 4)

Therefore, there is a need to correct the data set to remove the wavy nature in displacement time series plot, where due to rotational motion (Graizer, 2006) of building model and low-frequency noises, shifting of baseline occurs.

4.2.1 Baseline Correction

In Figure 4.8, the problem of baseline drift is remediated. However, the data corrected by a simple quadratic baseline still shows the noise in the waveform. Therefore, low-pass filtering technique is selected by considering a realistic cut-off frequency as used by Boore & Bommer (2005).

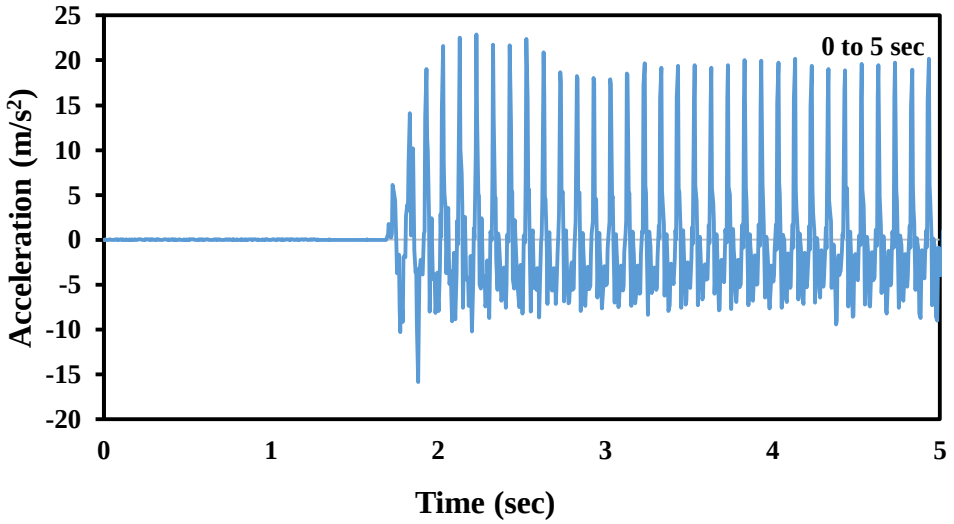

Figure 4.8: Acceleration Records from Accelerometer after Baseline Correction (Test 4)

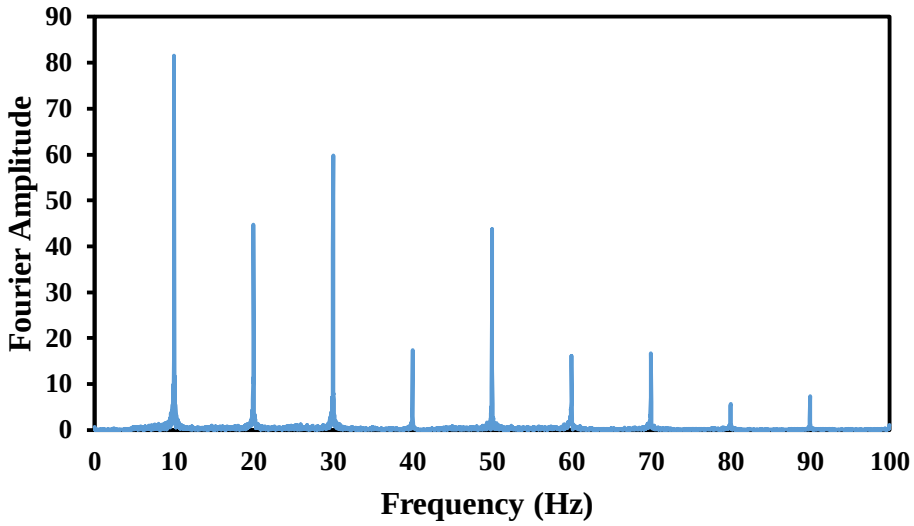

Figure 4.9: Fourier Amplitude after Baseline Correction (Test 4)

4.2.2 Low pass filtering Technique

Baseline correction is determined to be effective in eliminating long-period or low-frequency noise. However, high-frequency noise combines with the signal as shown in Figure 4.9. The input frequency for Test 4 is 10Hz as listed in Table 3.7. The maximum amplitude found at input frequency 10Hz is 81.58 however, Fourier amplitudes are also found on higher frequencies than the input frequency in the signal. Therefore, Fourier amplitude spectrum in Figure 4.9 shows the need to apply filtering in the process of analysing.

Although the shaking frequency is set to 10 Hz for Test 4, frequencies of higher than 10 Hz are still observed in the testing result. Therefore, Butterworth's low-pass (high-cut) filtering technique is used to remove the higher-frequency noise (Boore & Bommer, 2005) as shown in Figure 4.10 and Figure 4.11.

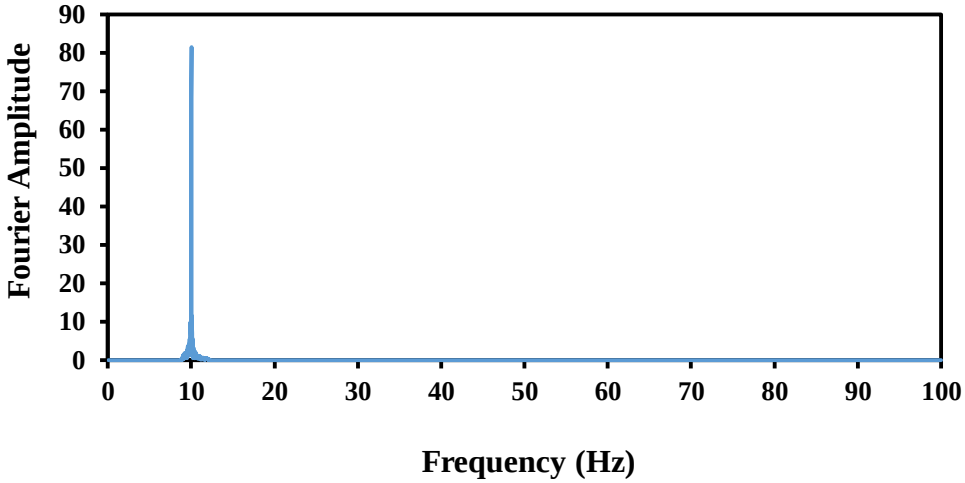

Figure 4.10: Fourier Amplitude after Butterworth Low Pass Filtering (Test 4)

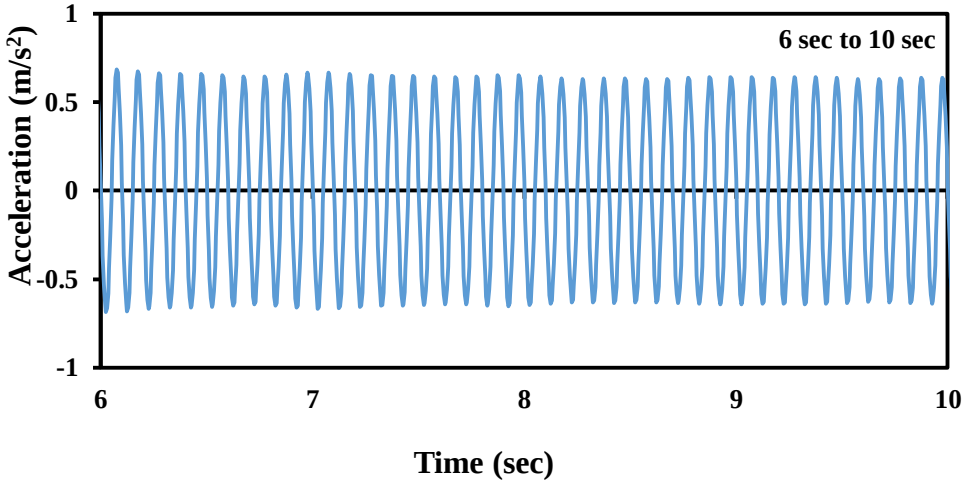

Figure 4.11: Acceleration Records from Accelerometer after Butterworth Low Pass Filtering (Test 4)

Since the acceleration profile obtained upon performing the filtering method shows the best agreement. Thus, Butterworth low pass filtering method is suitable for the signal processing in the present study.

4.3 Scale up model results

The data recorded by contact sensors are scaled up using scaling factor S_E. Table 4.1 shows the results recorded by Accelerometer and LVDT. Additionally, Table 4.1 also shows the scaled up model results which was scaled through scaling S_E, whereas, S_E is already calculated and validated in section 3.2 and 3.3.4. The first three parameters addressed in Table 4.1 are dimensions, material strength and gravitational acceleration. These parameter values are same in each shaking table test and later, scaled through scaling factor S, S_E, and S_a for full scale model. Contact sensor LVDT that was placed on beam-column joints at Storey 1 and 2 as shown in Figure 3.11, has recorded maximum displacement in mm for each ground motion (Test). Here, displacement has a scale factor S to scale up the recorded data for each storey. Shear force has a scaling factor of $S_e S^2$ through which it was determined that full scale model has reached to maximum base shear of 2252.86 KN in Test 5 as calculated in Appendix C. However, storey 1 reaches to maximum shear of 1528.78 KN in Test 4. Similarly, acceleration has scaling factor S_a which is equal to one as shown in Table 4.1. Therefore, the small scale acceleration values multiply by S_a will give the same values for full scale model. The maximum acceleration recorded at base is 0.92g in Test 5. However, storey 1 and 2 has reached to maximum acceleration of 1.38g and 1.58g in Test 4.

The parameter mentioned in Table 4.1 are used to derived other parameters from it, that is residual displacement, residual interstorey drift ratio, serviceability limit state (SLS) and ultimate limit state (ULS), inter storey drift

ratio and storey drift ratio. All these aforementioned parameters influence the scale up model results.

Table 4.1: Scaling up the small scale model results through S_E factor

Parameters	Scale factor	Scaled model (1:10)					Full scale model				
		Test 1	Test 2	Test 3	Test 4	Test 5	Test 1	Test 2	Test 3	Test 4	Test 5
Dimensions	S = 10	0.1					1				
Material Strength	S_e = 9.9	0.1					1				
Gravitational acceleration, a (m/s^2)	S_a = 1.0	9.81					9.81				
Maximum displacement, δ_{max} (mm)	S = 10	Storey 2					Storey 2				
		2.54	6.28	9.10	6.48	7.59	25.38	62.76	90.99	64.76	75.91
		Storey 1					Storey 1				
		1.76	4.47	6.37	3.95	4.45	17.63	44.66	63.72	39.45	44.55
Maximum shear force, V_{max} (KN)	$S_eS^2 = (9.9)(10)^2$	Storey 1					Storey 1				
		0.30	0.40	0.45	1.54	1.26	299.11	398.81	443.12	1528.78	1251.83
		Base					Base				
		0.67	0.84	0.96	1.90	2.28	661.17	832.58	955.02	1885.55	2252.86

		Storey 2					Storey 2				
		0.24	0.35	0.36	1.57	1.26	0.24	0.35	0.36	1.57	1.26
		Storey 1					Storey 1				
Spectral Acceleration ($Sa = mg/m$)= g	$S_eS^2/(S_eS^2/S_a)$ =1	0.27	0.36	0.4	1.38	1.13	0.27	0.36	0.4	1.38	1.13
		Base					Base				
		0.27	0.34	0.39	0.77	0.92	0.27	0.34	0.39	0.77	0.92
		Input PGA values					Input PGA vlaues				
		0.25	0.3	0.36	0.64	0.82	0.25	0.3	0.36	0.64	0.82
Mercalli's scale		Y+					Y+				

4.4 Maximum displacement response

Figure 4.12 (a) and (c) shows the time histories of maximum displacement of storey 1 and 2 for sequential ground motions from test 1 to test 5 on shaking table. Similarly, Figure 4.12 (b) and (d) shows maximum displacement of storey 1 and 2 from ETABS simulation. It is found out that shaking table results are near to the simulated model results from ETABS. The test framed specimen indicates that the building model has a progressive permanent displacement which tends to increase the maximum displacement of each oncoming successive seismic ground motions. In shaking table test, Figure 4.12 (a) and (c) represent that Test 3 (0.34g) has displaced model 63.7mm in storey 1 and 91.0mm in storey 2 as compared with Test 5 (0.82g) having displacements of 44.5mm in storey 1 and 75.9mm in storey 2.

In ETABS simulation, it is observed that Test 3 displaces 52.56mm in storey 1 and 88.84mm in storey 2 as shown in Figure 4.12 (b) and (d). Here, it is noteworthy that in storey 1, displacement of Test 5 (ETABS simulation) in Figure 4.12 (b) i.e. 41.36mm is close to the displacement 44.5mm in Test 5 (shaking table) as shown in Figure 4.12 (a). Similarly, in storey 2, Test 5 has displacement of 71.52mm (ETABS) and 75.9mm (Shaking table) as shown in Figure 4.12 (c) and (d) respectively. Additionally, Figure 4.12 (a), (b), (c) and (d) shows that storey 1 and 2 maximum displacements in Test 3 are approximately three-fold than Test 1. Reason is that, as the PGA increases from Test 1 to Test 3 and so on, the structural stiffness decreases as shown in section 4.1 and cause the structural frame to displace more.

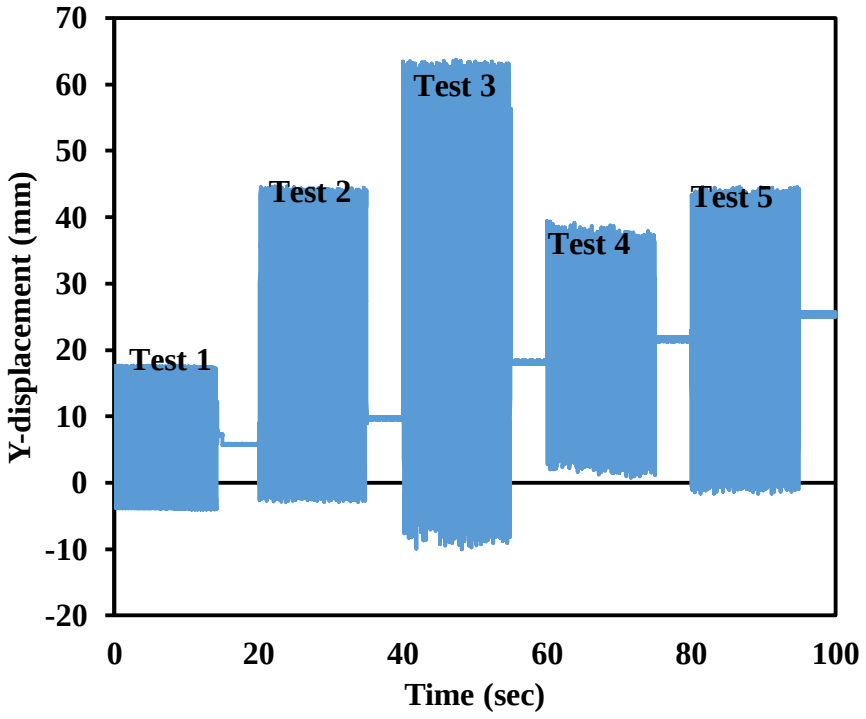

Figure 4.12(a): Time history of Y-axis horizontal displacement (storey 1) under artificial seismic sequence on shaking table

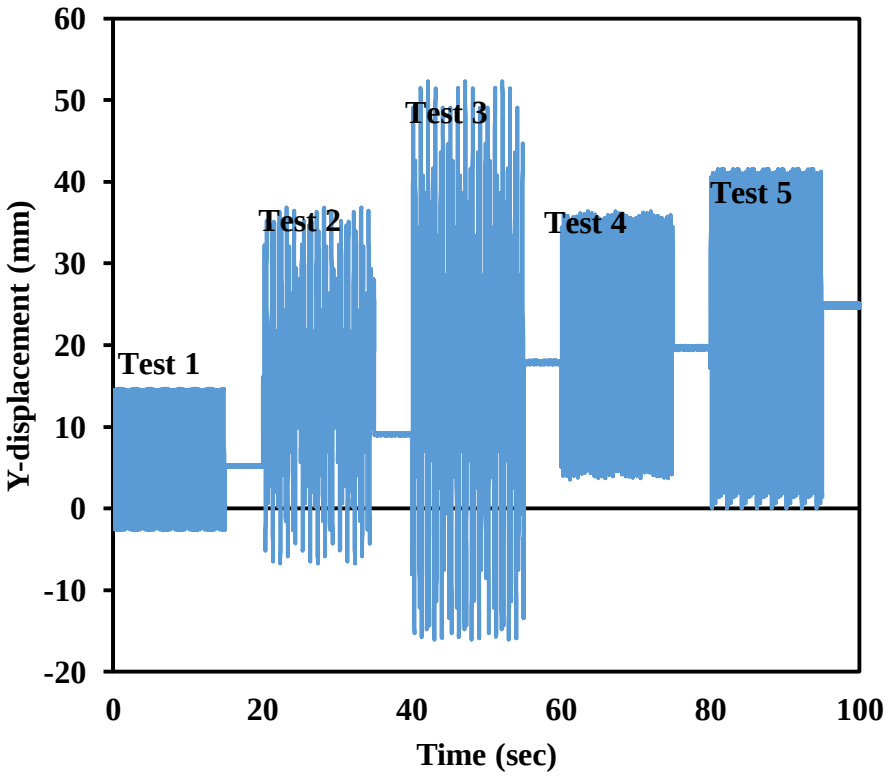

Figure 4.12 (b): Time history of Y-axis horizontal displacement (storey 1) under artificial seismic sequence on ETABS simulation

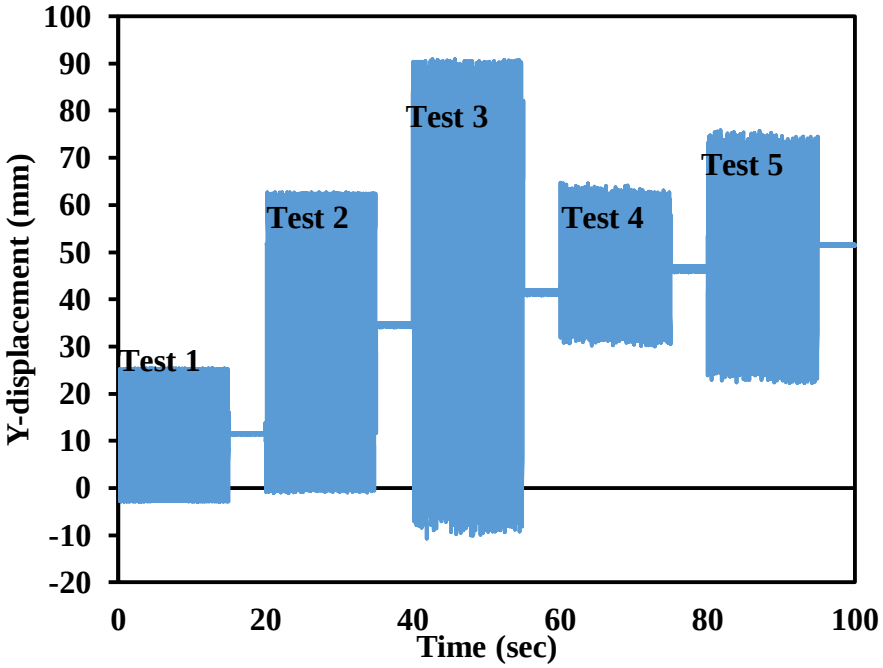

Figure 4.12 (c): Time history of Y-axis horizontal displacement (storey 2) under artificial seismic sequence on shaking table

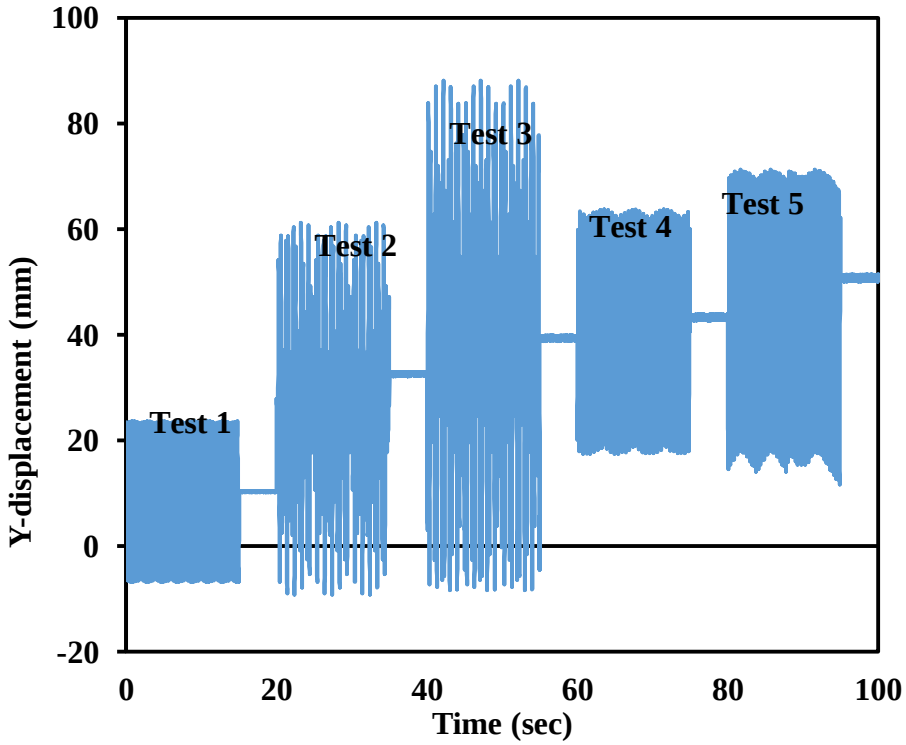

Figure 4.12 (d): Time history of Y-axis horizontal displacement (storey 2) under artificial seismic sequence on ETABS simulation

To assess the building model further, the framed specimen has been examined on real seismic ground motions as shown in Figure 4.13 (a) and (b). In storey 1, ML1 has a maximum displacement 14.8mm (+X-axis) and 10.88mm (-X-axis) as shown in Figure 4.13 (a). The second consecutive ground motion ML2, has a displacement of 0.81mm (+X-axis) and 5.59mm (-X-axis), respectively. ML3 that is the third sequential motion, displaces the model 2.23mm (+X-axis) and 14.49mm (-X-axis). In last ground motion (ML4), model displaces 0.7mm (+X-axis) and 11.33mm (-X-axis), respectively. In storey 2, the maximum displacements of ML1 and ML3 are 21mm (+X-axis) and 30.40mm (-X-axis) as shown in Figure 4.13 (b).

The PGA of ML1 and ML3 are similar that is 0.34g and 0.33g. However, the model displaces maximum 14.49mm (storey 1) and 30.4mm (storey 2) in ML3 representing the maximum displacement in the model as shown in Figure 4.13 (a) and (b). Additionally, surface acceleration and magnitude of an earthquake affects the maximum displacement. Therefore, building model may behave in a different mode in each sequential seismic ground motions. Thus, it can be summarized that results can vary based on the characteristics of framed specimen and successive ground motions.

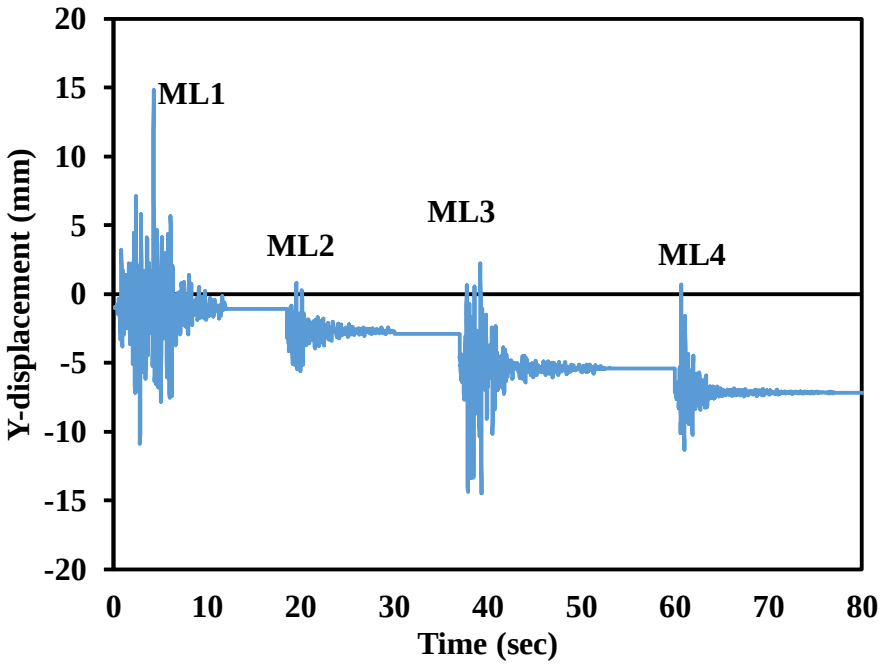

Figure 4.13 (a): Horizontal displacement time histories at storey 1

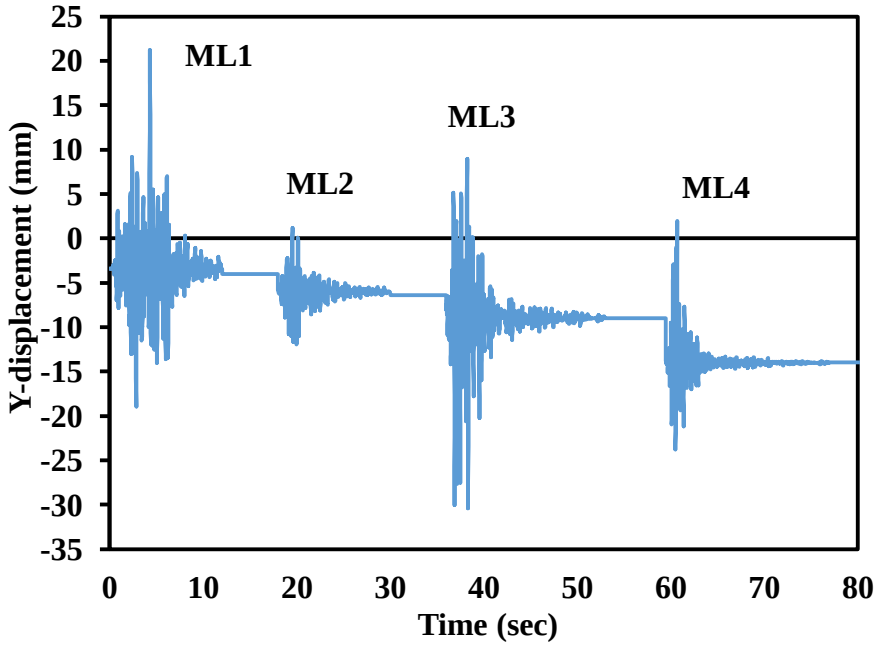

Figure 4.13 (b): Horizontal displacement time histories at storey 2

4.5 Maximum Residual displacement

The sequential ground motion has strongly affected the test specimen and increases the residual displacement in each successive excitation. In Test 1, model displaces permanently 5.76mm and 11.53mm in storey 1 and 2, respectively, as shown in Figure 4.14 (a). It shows that storey 2 displaced twofold than storey 1 in Test 1. Figure 4.14 (b) had similar effects of displacement in Test 1 such as 5.19mm and 10.37mm displacements in storey 1 and 2 which satisfy the results of shaking table and ETABS simulation outcomes. In Test 2, model displaces 34.57mm in storey 2, which is threefold than the displacement found in Test 1 as shown in Figure 4.14 (a). It clearly shows that the residual displacement accumulates with respect to incremental PGAs' in successive ground motions. Most importantly, it has been observed that experimental model does not show any cracks in Test 1 (0.25g) and Test 2 (0.30g) as mentioned earlier in section 4.1 however, it can clearly be seen in Figure 4.14 (a) that Test 1 and 2 have residual displacements of 5.76mm and 9.70mm in storey 1, similarly 11.53mm and 34.57mm in storey 2 which clearly highlights the reinforcement internal plasticity during the shaking table test. Moreover, Figure 4.14 (a) and (b) show that the residual displacement at Test 5 is fivefold than the Test 1 in each storey (i.e. storey 1 and 2) which indicates that multiple ground motions are one of the main cause in strength degradation and make the structure to displace permanently. From Figure 4.14 (a) and (b), it is found out that as the PGAs' increases, the level of residual displacement reaches to maximum 25.35mm (shaking table) and 24.88mm (ETABS) in storey

1 at Test 5. Similarly, 51.52mm (shaking table) and 50.82mm (ETABS) in storey 2 at Test 5 shows the same impact.

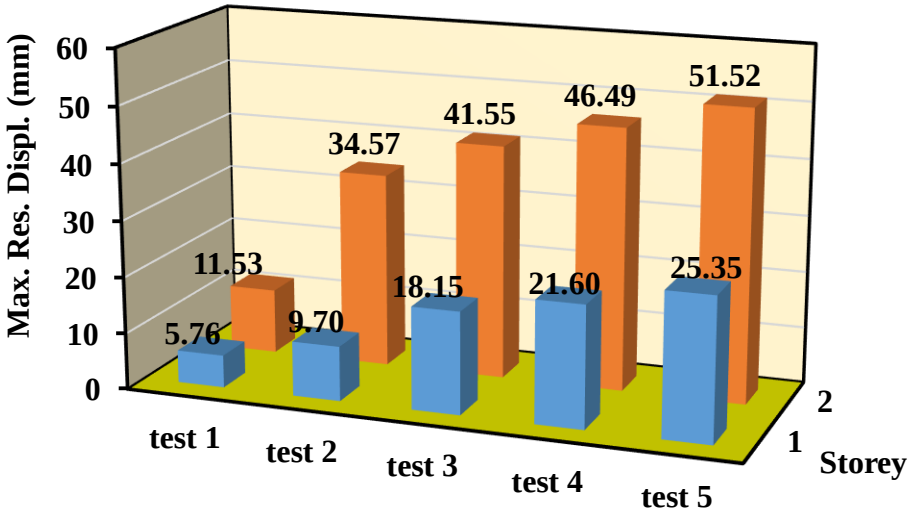

Figure 4.14(a) : Maximum Residual Displacement under successive artificial ground motions (shaking table)

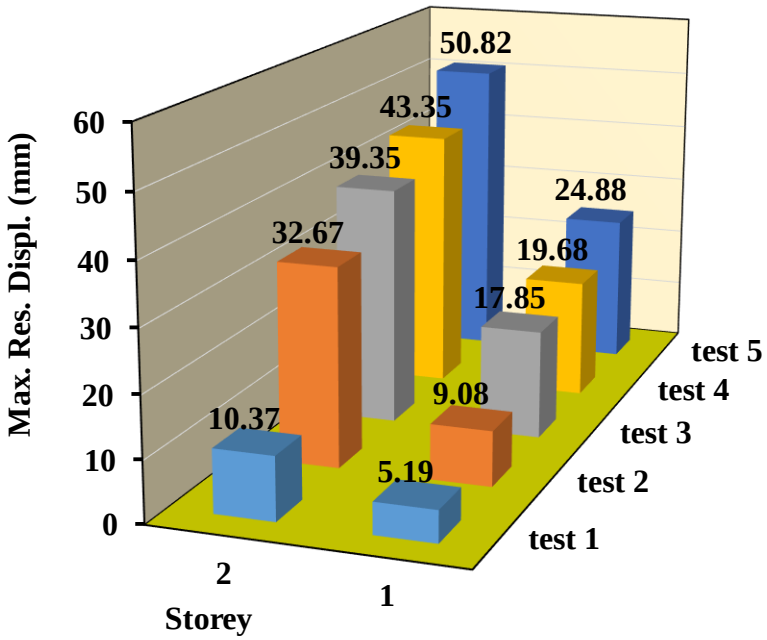

Figure 4.14 (b): Maximum Residual Displacement under successive artificial ground motions (ETABS Simulation)

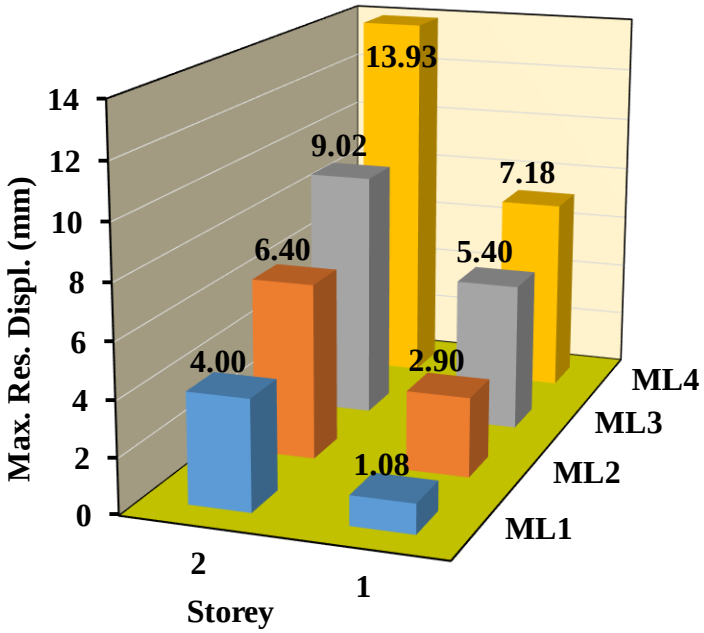

Figure 4.14 (c): Maximum Residual Displacement under Mammoth Lake sequential ground motions (ETABS simulation)

Figure 4.14 (c) showed that ML1 presents the least residual displacement i.e. 1.08mm and 4.0mm at storey 1 and 2 respectively. In Figure 4.14 (c), the sequential excitation ML4 accumulate the displacement threefold in storey 2 and sevenfold in storey 1 as compared to ML1 respectively. Moreover, it can be observed in Figure 4.14 (c) that storey 2 reaches to maximum residual displacement of 13.93mm in the last seismic motion i.e. ML4. It is noteworthy that residual displacement of storey 2 is twofold the storey 1 in ML1 and threefold the storey 1 in ML2 as shown in Figure 4.14 (c). However, in next two consecutive ground motions (ML3 and ML4), the residual displacements are 5.40mm (storey 1) and 9.02mm (storey 2) in ML3, and 7.18mm (storey 1) and 13.93mm (storey 2) in ML4 which shows that the exponentially increment in residual displacements between storey 1 and storey 2 decreases as the number of ground motions increases.

Thus, it is evident and concluded that the first seismic motion affects the stiffness and degrade the strength of the building model which causes the framed structure to displace permanently.

4.6 Residual interstorey drift ratio

The maximum interstorey residual drift for both experimental and simulated model under artificial successive ground motions are shown in Figure 4.15 (a) and (b). The examined structure shows the permanent deformation which remained after each sequential seismic vibration. Multiple earthquake motion accumulates the interstorey residual drift and became maximum in the last excitation (Test 5). It is noteworthy that storey 2 has residual IDR% of 0.83 in Test2, 0.78 in Test 3, 0.83 in Test 4 and 0.87 in Test 5 as shown in Figure 4.15 (a). Similarly, residual IDR percentage from Test 2 to Test 5 are 0.79, 0.72, 0.79, and 0.86 as shown in Figure 4.15 (b). It is observed in Figure 4.15 (a) and (b) that residual IDR% in Test 2 is fourfold than Test 1 in storey 2. Reason is that as the PGA increases from 0.25g (Test 1) to 0.30g (Test 2), the model displaces permanently and causes the structural model to reach to 0.83% (Test 2) from 0.19% (Test 1) as shown in Figure 4.15 (a). Additionally, storey 1 has incremental residual IDR% of 0.14 (Test 1), 0.24 (Test 2), 0.45 (Test 3), 0.54 (Test 4) and 0.63 (Test 5) as shown in Figure 4.15 (a). Similar residual IDR% is observed in Figure 4.15 (b).

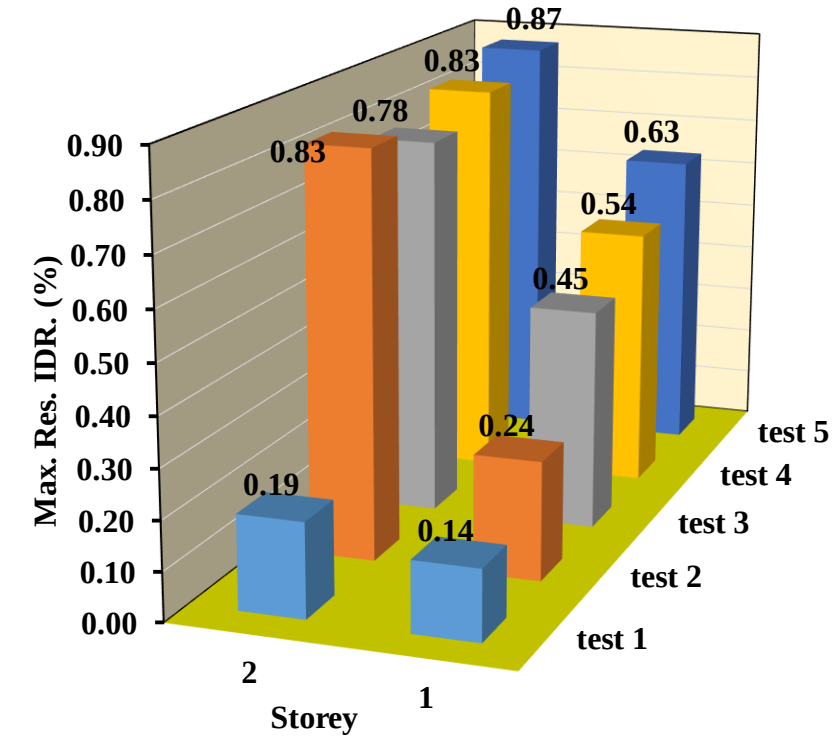

Figure 4.15 (a): Maximum Residual Interstorey Drift Ratio under successive artificial ground motions (shaking table)

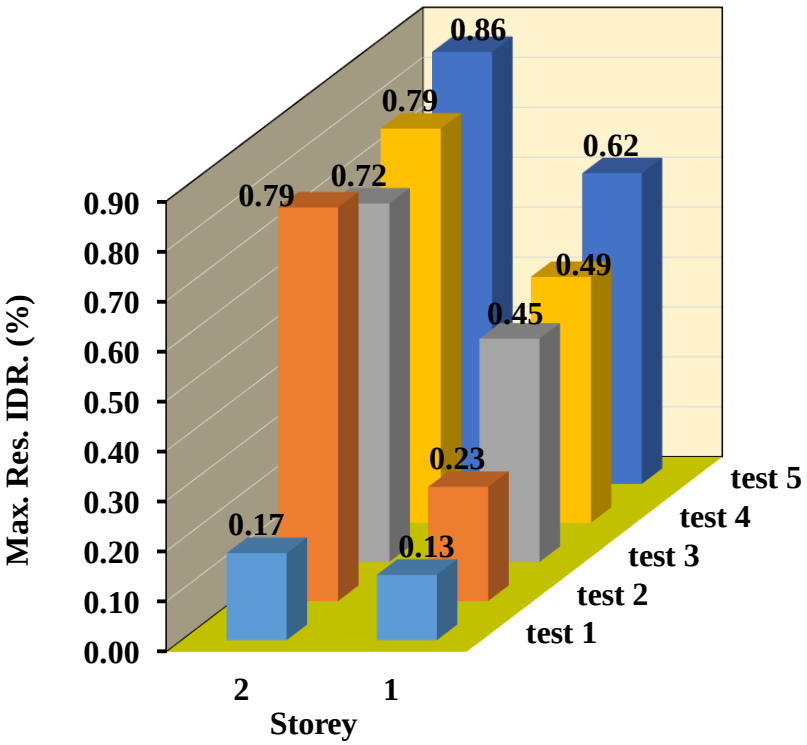

Figure 4.15 (b): Maximum Residual Interstorey Drift Ratio under successive artificial ground motions (ETABS Simulation)

For Mammoth lake ground motions, the effect of sequential motion on structural model is similar as shown in Figure 4.15 (c) which shows that the percentage of residual IDR in storey 1 increases with respect to the seismic sequence. In storey 1, the maximum residual IDR is 0.18% in ML4 as shown in Figure 4.15 (c). However, it can be seen that maximum residual IDR of storey 1 found in Test 2 are 0.23% and 0.24% as shown in Figure 4.15 (a) and (b). It clearly state that Mammoth Lake ML4 cause 0.18% IDR in storey 1 but artificial ground motions in Figure 4.15 (a) and (b) cross it in the second seismic motion (Test 2) which shows that Mammoth Lake ground motions does not affect the model severely as artificial motions did. Furthermore, in Figure 4.15 (c), storey 2 has 0.10% (ML1) and 0.12% (ML2) which concludes that consecutive real ground motions could hardly affect the structural model.

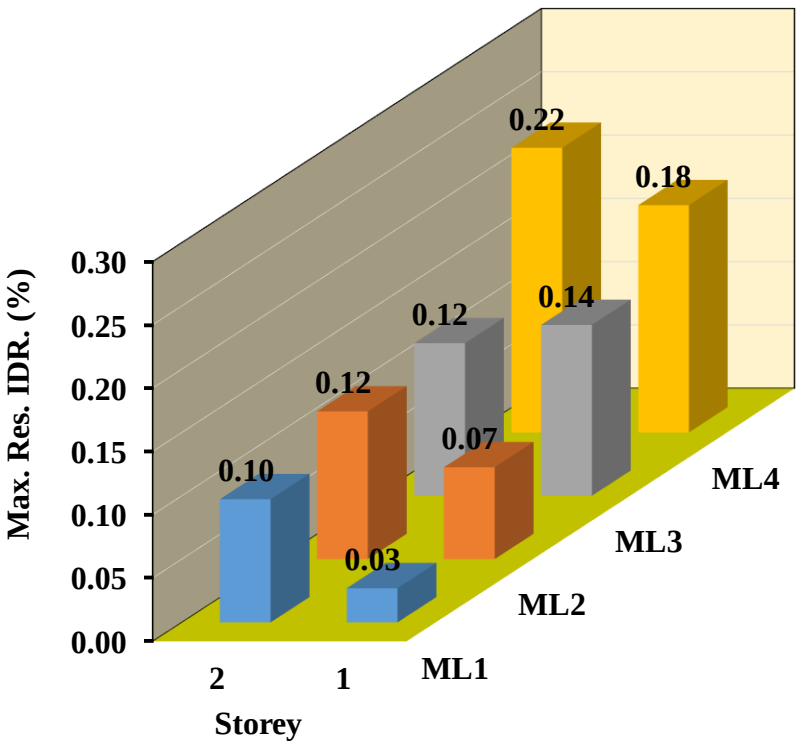

Figure 4.15 (c): Maximum Residual Interstorey Drift Ratio under Mammoth Lake sequential ground motions (ETABS simulation)

4.7 Acceleration response

Figure 4.16 and Figure 4.17 shows the acceleration time histories of 1st and 2nd stories from the Test 1,2 and 3. In test 1 and 2, the concrete material of framed specimen does not reach to its yield point. The maximum acceleration recorded at story 1 in Test 1 and 2 are 2.7m/s^2 and 3.6m/s^2, which shows that as the PGA increases, each storey accelerates. Furthermore, maximum accelerations 2.4m/s^2 and 3.5m/s^2 are recorded at storey 2 in Test 1 and 2, which indicates that model has an increment in acceleration on higher PGA. Furthermore, in Test 3, it is observed in Figure 4.1 that test frame specimen starts to have concrete cracks and approaches to maximum acceleration 4.0m/s^2 and 3.6m/s^2 at storey 1 and 2 as shown in Figure 4.16 and Figure 4.17. It shows that seismic waves do not transfer completely to storey 2 and vibrates storey 1 more.

It is noticeable that in each test, the acceleration had higher values at storey 1 as compared to storey 2 because storey 1 had loaded with a weight of storey 2, which is 111.9 kg as shown in Appendix C. However, there was no storey load above storey 2 which makes the storey 1 critical. Moreover, the seismic waves produced by shaking table are not properly transferred from storey 1 to storey 2 which cause the framed structure to accelerate more at storey 1.

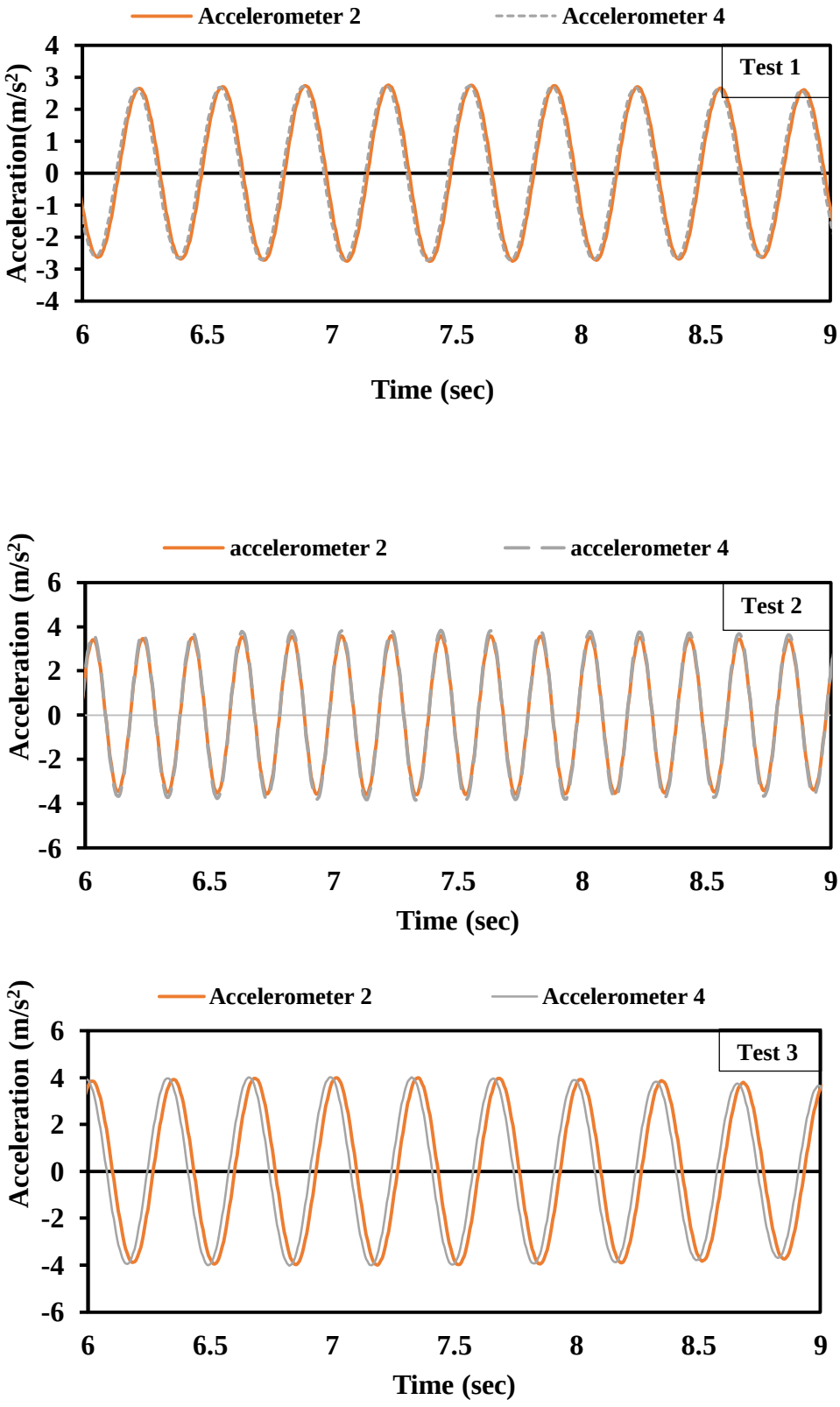

Figure 4.16: Acceleration time histories at 1st story in Test 1, 2 and 3

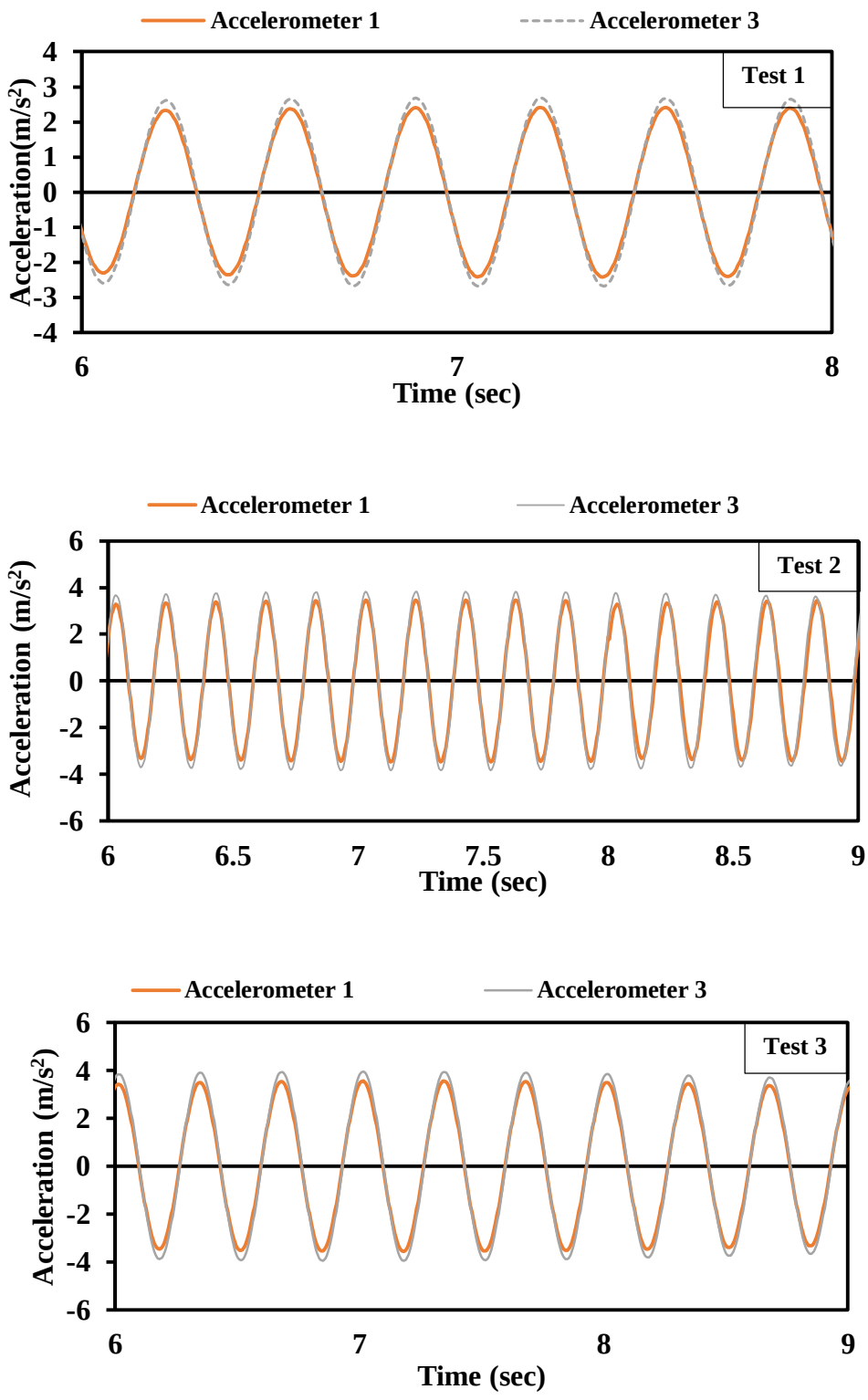

Figure 4.17: Acceleration time histories at 2nd stories in Test 1, 2 and 3

Thereafter, the damage developed progressively in main shocks from Test 4 to 5. In Test 4, it is observed in Figure 4.18 (c) that the building model base is accelerated to 7.7m/s^2 which causes the storey 2 to accelerate 15.7m/s^2 as shown in Figure 4.18 (a). It is observed that the framed specimen got damaged due to high value of 'g'. Similarly, in Test 5, the test model accelerated at 12.6m/s^2 from storey 2 as shown in Figure 4.18 (a) and extend the cracks in framed model. Figure 4.18 (b) shows that Test 4 and Test 5 are accelerated with 13.8m/s^2 and 11.3m/s^2 in storey 1 which is lesser than the acceleration recorded at storey 2 in Figure 4.18 (a). However, from Test 1 to Test 3, storey 1 has accelerated more than storey 2 as shown in Figure 4.16 and Figure 4.17. Thus, as the ground motion acceleration increases, the seismic vibrations start to transfer seismic waves from storey 1 to storey 2. In this way, model maintain its performance without making storey 1 critical.

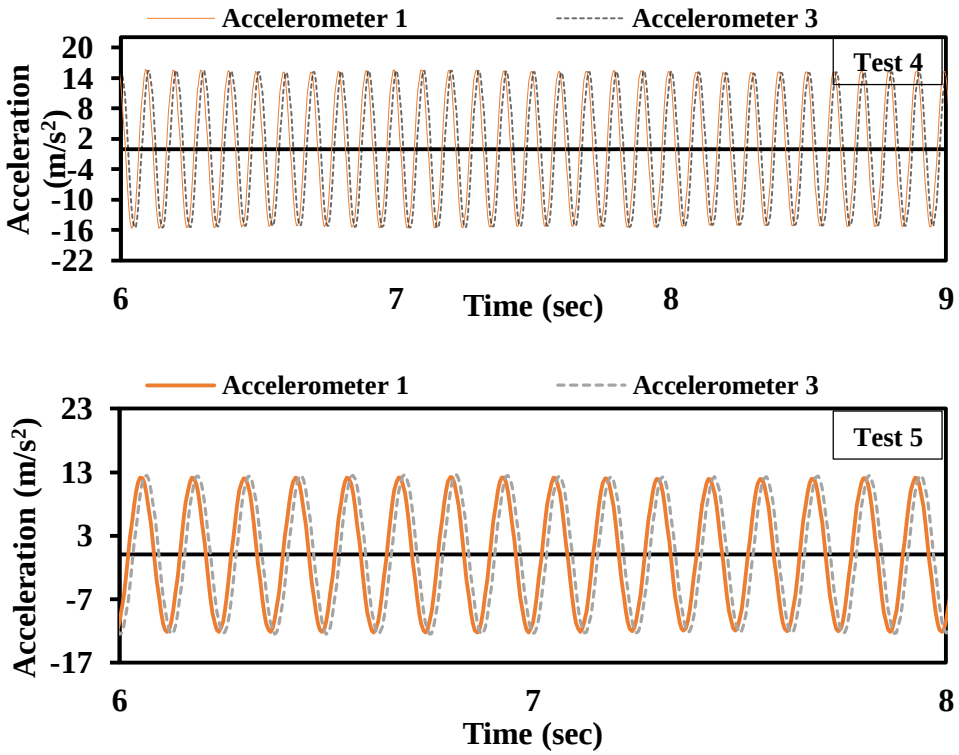

Figure 4.18 (a): Acceleration time histories of storey 2 in Test 4 and 5

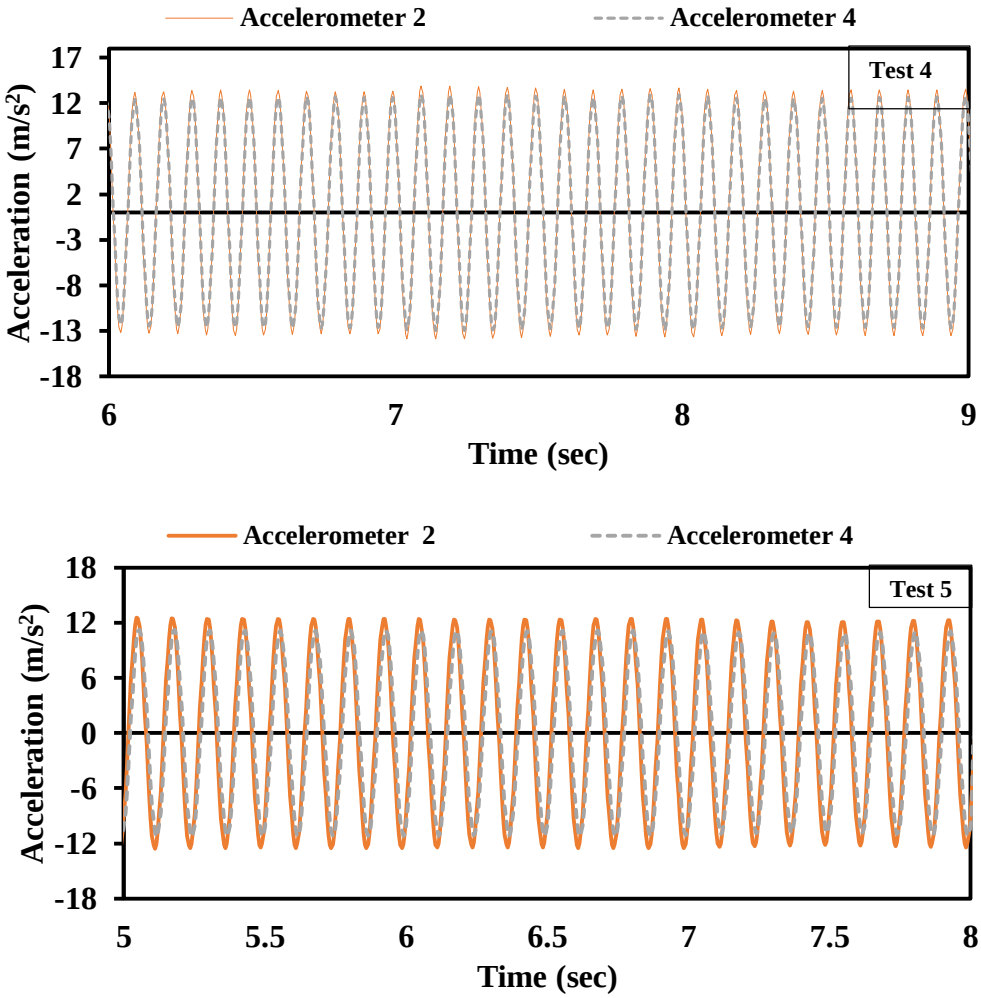

Figure 4.18 (b): Acceleration time histories of Storey 1 in Test 4 and 5

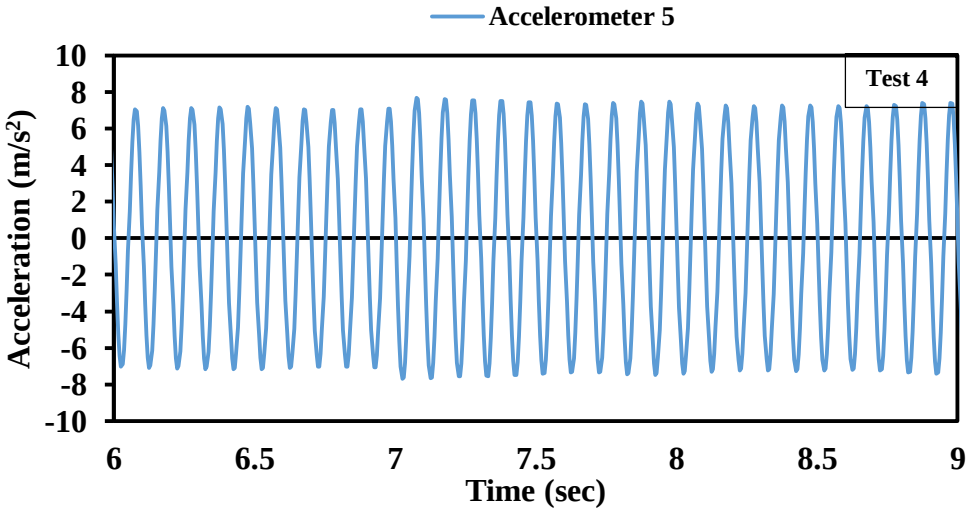

Figure 4.18 (c): Acceleration time histories of Base in Test 4 and 5

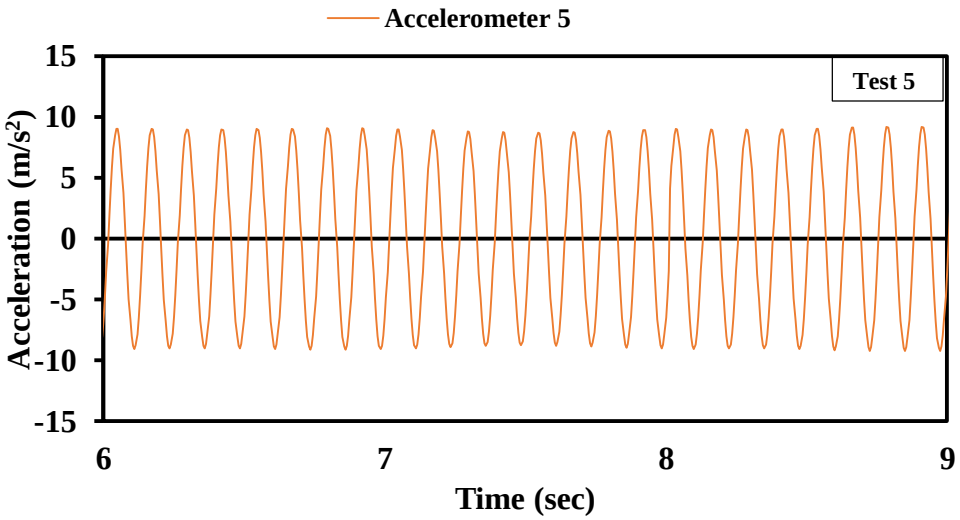

Figure 4.18 (c): Acceleration time histories of Base in Test 4 and 5 (Continue)

Five sequential ground motions have been applied ranging from 0.25 to 0.82g. It has been concluded that low-rise model with lower PGA values can cause the model to accelerate more in storey 1 in correlation with storey 2 due to the weight of storey 2 on storey 1. Load of storey 2 makes the storey 1 critical as if the ground motion waves do not reach to storey 2 and vibrates the storey 1 more.

4.8 SLS and ULS

Annex A1.4.3 of BS EN 1990-1 defines the deflections to be considered at the serviceability limit state (SLS). According to Eurocode, for SLS, horizontal deflection for low-rise frame structure is $\frac{\text{Height (mm)}}{300}$ for both 'u' and 'u_i'. Here, 'u' is the overall horizontal displacement over the building height 'H' and 'u_i' is the horizontal displacement over a storey height 'H_i' as shown in Figure 4.19.

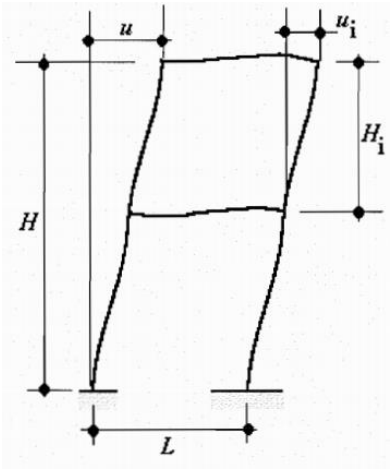

Figure 4.19: Illustration of horizontal displacements (Eurocode 0, 1990)

Here, for full scale model,

H = 7000mm

H_i = 3000mm

So, horizontal deflection calculated for SLS in this study is 23.33mm (overall displacement 'u' over *'H'*) and 10mm horizontal displacement 'u_i' over a storey height 'H_i'. However, for ultimate limit state (ULS), horizontal displacements were recorded through LVDT for each seismic ground motions. In Figure 4.20 (a), it can clearly be seen that Test 3 (13.0mm and 30.33mm) and Test 5 (10.84mm and 25.30mm) have crossed maximum horizontal deflection of SLS i.e. 10mm and 23.33mm. However, Test 1 (3.63mm and 8.46mm), Test 2 (8.97mm and 20.92mm), and Test 4 (9.25mm and 21.59mm) are still with in SLS range. Similarly, Figure 4.20 (b) shows the similar outcomes. Therefore, in initial two consecutive ground motions (that is Test 1 and Test 2) as shown in Figure 4.20 (a) and (b), model was with in a limit state. As the third consecutive ground motion (that is Test 3) vibrates the building model, the

frame structure went across the limit state. In fourth ground motion (Test 4), frame structure return back to its limit state, which shows that there should be no yielding of members in the model. However, still yielding of model is observed as shown in Figure 4.14 (a) and (b) but in the last maximum PGA (Test 5), the model crosses the serviceability limit again as shown in Figure 4.20 (a) and (b).

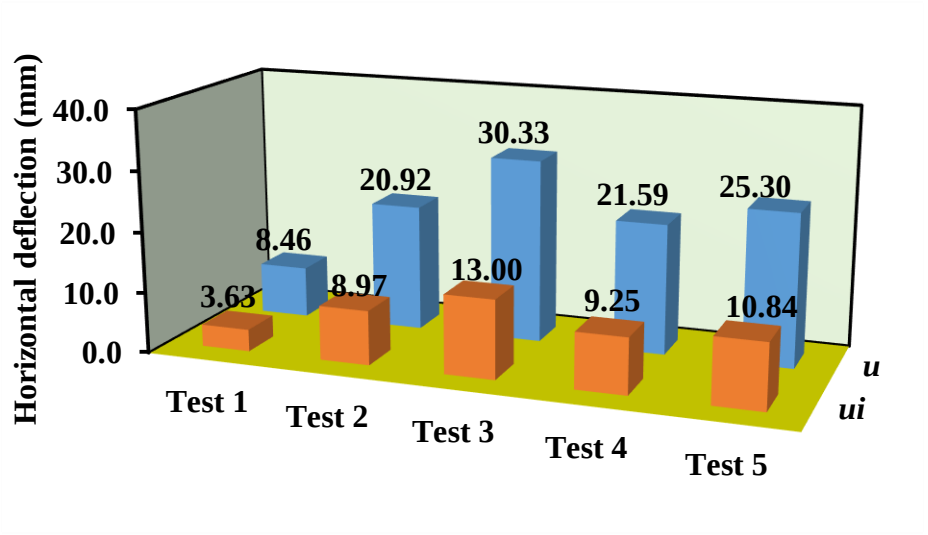

Figure 4.20 (a): Maximum horizontal deflection on successive artificial ground motions (Shaking table)

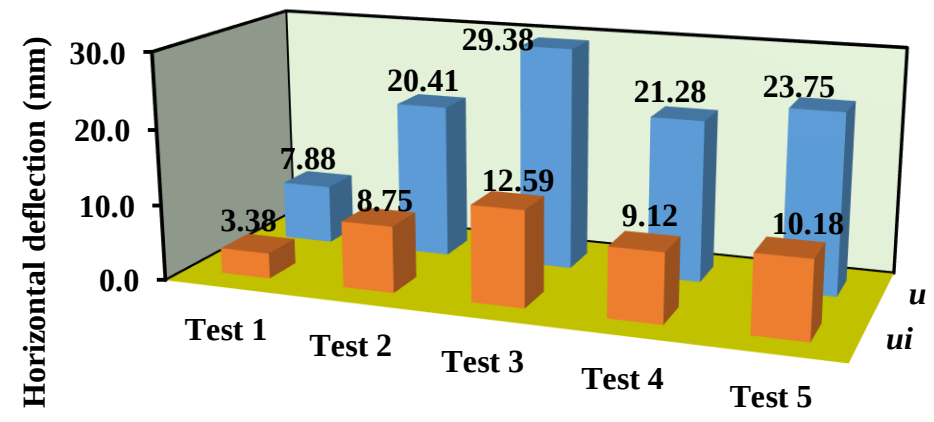

Figure 4.20 (b): Maximum horizontal deflection on successive artificial ground motions (ETABS Simulation)

In real-time ground motion as shown in Figure 4.20 (c), the deflection in each seismic motion keep the model deflections within the SLS range. The maximum deflection found to be 7.08mm which is lower than the limit set by SLS i.e. 23.33mm as shown in Figure 4.20 (c). It is noteworthy that the deflections are quite small due to the lower PGAs' applied in each ground motion.

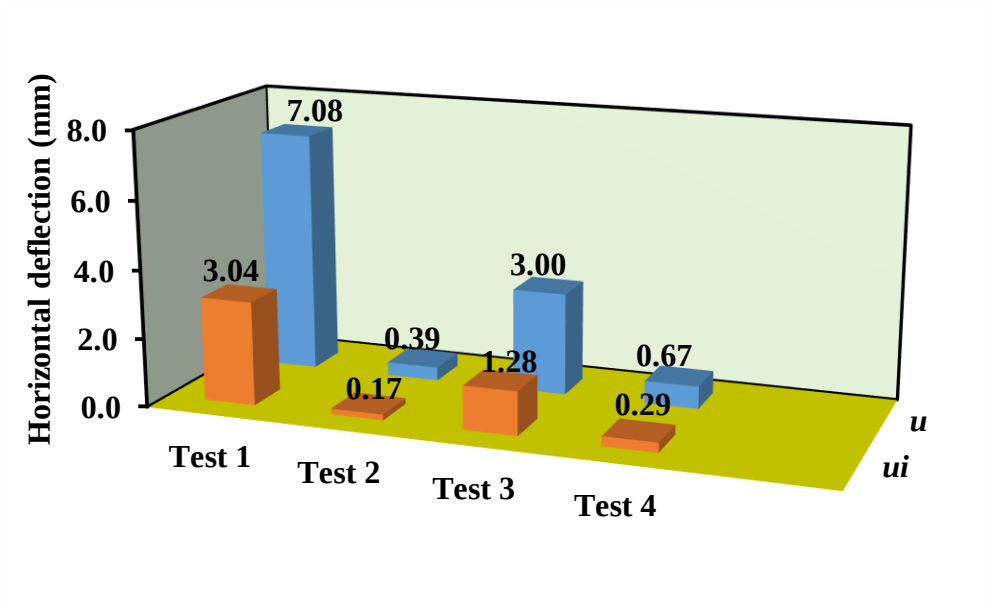

Figure 4.20 (c): Maximum horizontal deflection on Mammoth Lake sequential ground motions (ETABS simulation)

Thus, it is evident that building model crosses the SLS limit in Test 3 and Test 5 as shown in Figure 4.20 (a) and (b). Therefore, it is concluded that multiple ground motion effects the serviceability limit of the building model and cause the model to yield its member in oncoming ground motions. Crossing of serviceability limit leads the model to reach to ultimate limit and later cause the structure to fail. It is required to keep the model deflection with in SLS.

4.9 Interstorey drift ratio and verification of damage limitation

Interstorey drift ratio (IDR) is one of the most critical parameters in structural analysis and design. Interstorey drift ratio (IDR) helps to check the structural damage limitations with respect to EC8. Figure 4.21 (a) and (b) show the maximum interstorey drift ratio followed by sequential ground motions from Test 1 to Test 5.

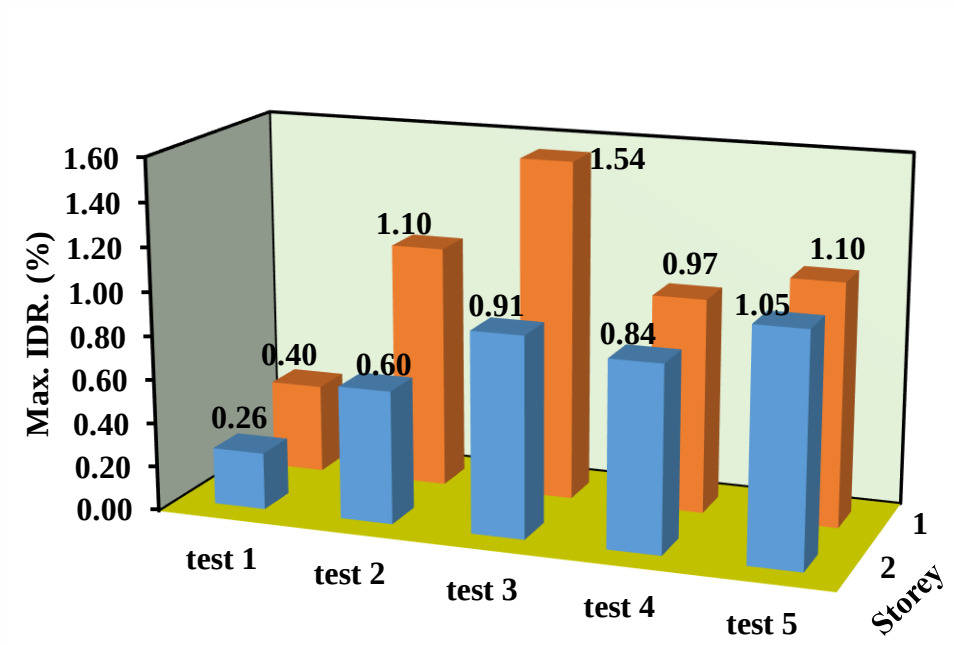

Figure 4.21 (a): Maximum Interstorey Drift Ratio under successive artificial ground motions (Shaking table)

In storey 1, it is evident that damage limitation of Test 3 (simulated and experimental outcomes) reached maximum drift 1.56% and 1.54% in successive seismic motions as shown in Figure 4.21 (a) and (b). In both the stories (i.e. storey 1 and 2), Figure 4.21 (a) and (b) clearly shows that succeeding seismic vibration after the very first ground motion lead to higher drift. Additionally,

storey 1 has maximum IDR of 0.40% (Test 1), 1.10% (Test 2), 1.54% (Test 3), 0.97% (Test 4) and 1.10% (Test 5). As compared with storey 2, IDR% of storey 1 is almost twofold in Test 1, 2 and 3 however, Test 4 and 5 IDR % are similar in both stories as shown in Figure 4.21 (a) and (b) which represents the behavior of building model under artificial ground motions. Similar results are observed in, Figure 4.21 (b). Furthermore, Figure 4.21 (a) shows that the storey 1 of the building model placed on shaking table has crossed damage limitation 1% in Test 2. Even though, there is no structural damage observed as mention earlier in section 4.1. It clearly shows that EC8 undermined the damage limit criteria under sequential ground motions.

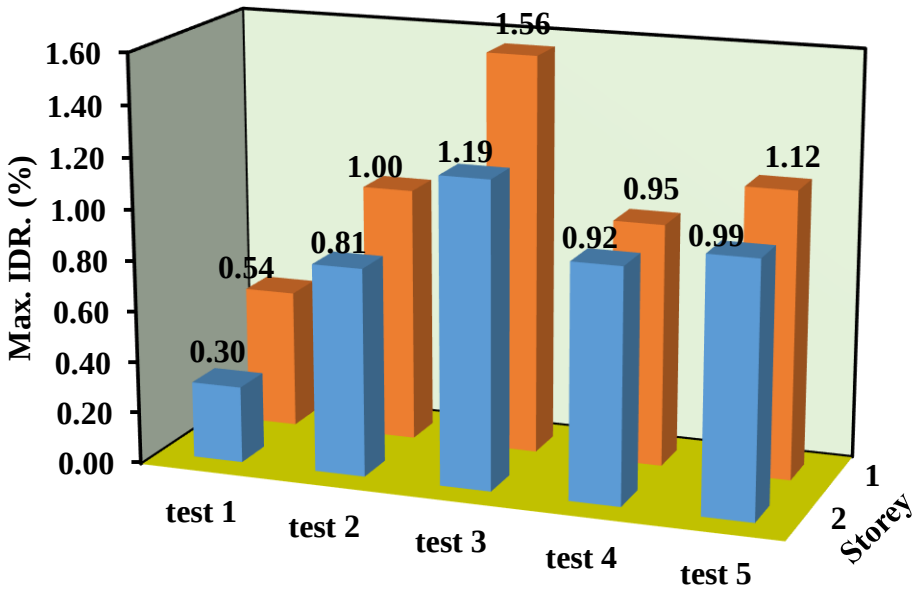

Figure 4.21 (b): Maximum Interstorey Drift Ratio under successive artificial ground motions (ETABS Simulation)

Figure 4.21 (c) show that the real-time sequential seismic vibrations do not illustrate any significant drift effect due to lower PGAs'. However, the building model excites in different modes in oncoming real-time seismic sequence. It is observed that storey 1 and 2 reaches to maximum IDR 0.48% and 0.21% in ML1, which shows that they do not reach to the damage limitation limit i.e. 1%. Hence, no damage is developed. It is noteworthy that ML1 has maximum IDR% as compared to oncoming seismic motions (ML2, ML3 and ML4). Thus, the findings clearly show that successive seismic vibration increase IDR in ML1 and decreases in ML2, ML3, ML4 depending on its ground acceleration values.

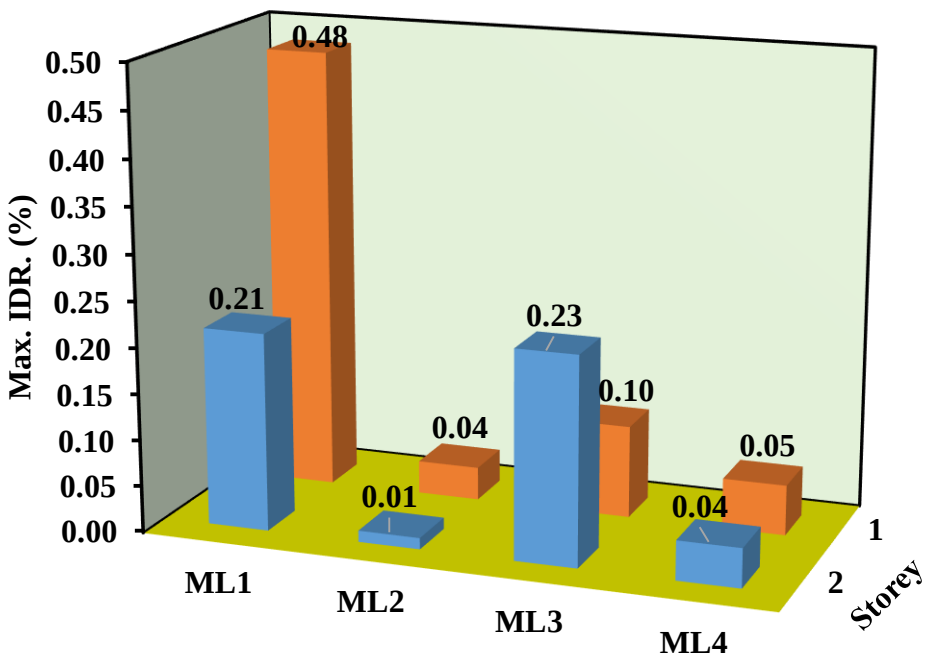

Figure 4.21 (c): Maximum Interstorey Drift Ratio under Mammoth Lake sequential ground motions (ETABS simulation)

4.10 Storey drift ratio and damage limitation

In EC8, damage limitation for storey drift ratio should be less than 0.5-1% (Fardis, 2008). However, it can be observed in Figure 4.22 (a) and (b) that after the very first seismic motion, the consecutive ground motions crossed the lower limit set by EC8 that is 0.5%. Figure 4.22 (a) and (b) shows that Test 3 has maximum storey drift ratio 1.27% and 1.23%. Moreover, Test 5 which is the last seismic excitation on shaking table, indicates the storey drift ratio 1.08% and 1.01% respectively. It is noteworthy that Test 3 and Test 5 have crossed the upper limit 1%, which determines that damage has start to developed from Test 3 onwards as shown in Figure 4.1. Additionally, Test 3 has storey drift ratio 1.27% (shaking table) and 1.23% (ETABS) which is fourfold than Test 1 with a storey drift ratio 0.34% (shaking table) and 0.32% (ETABS) respectively.

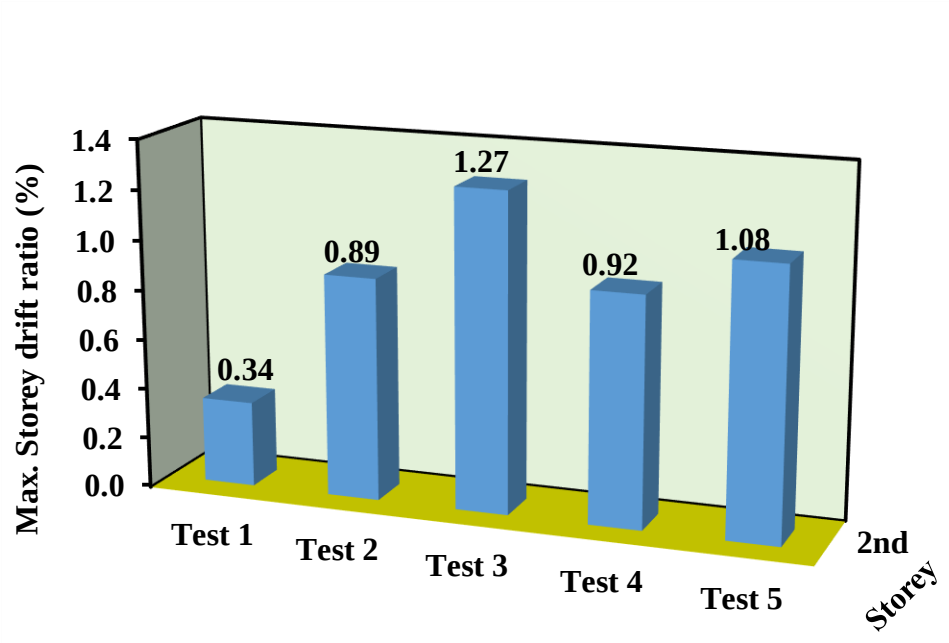

Figure 4.22 (a): Storey drift ratio under sequential ground motions (Shaking table)

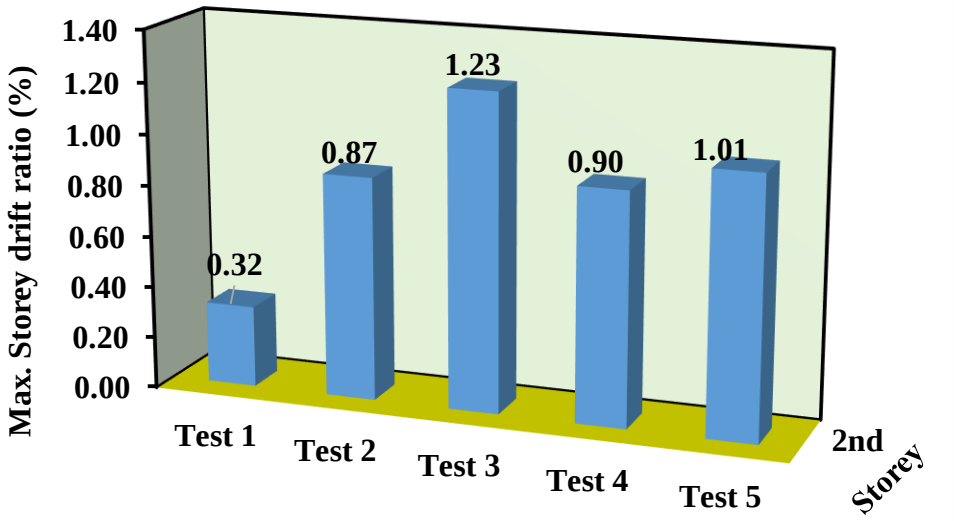

Figure 4.22 (b): Storey drift ratio under sequential ground motions (ETABS Simulation)

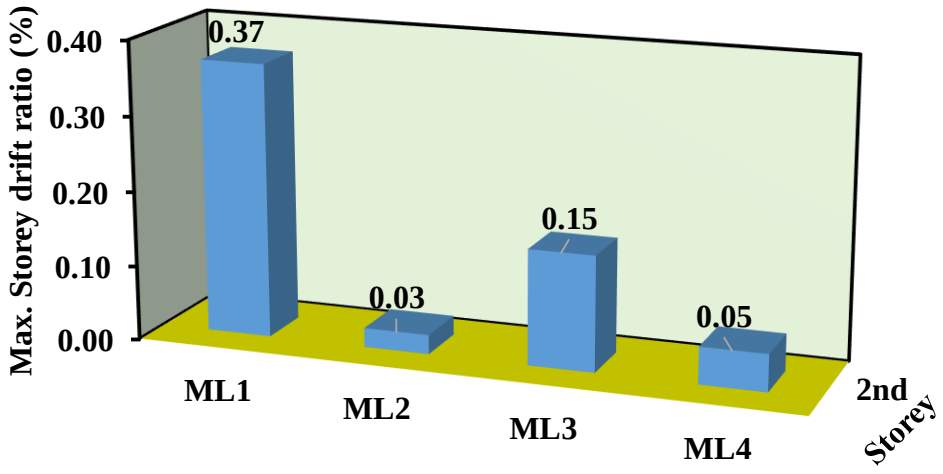

Figure 4.22 (c): Storey drift ratio under Mammoth Lake ground motions (ETABS Simulation)

In real-time ground motions, model has storey drift ratios under the suggested limit by EC8 as shown in Figure 4.22 (c). The maximum storey drift ratio is found in ML1 i.e. 0.37%. However, ML2, ML3 and ML4 are found to be lower than 0.2%. Therefore, model behave well in real-time ground motions.

4.11 Summary

In summary, an RC small scaled model was examined on shaking table through artificially produced five seismic ground motions. These artificial ground motions were applied sequentially to observes the response and crack patterns on building model. During shaking table test, Test 1 and Test 2 did not show any cracks and damages. However, Test 3 showed damage behavior at the beam-column joints at storey 1 and 2. In Test 4, extension of cracks propagated in Test 3 occurred. Significant cracks at beam-column joint at the base and storey 1 were observed. Lastly, in Test 5, seismic sequence further propagated the cracks at inner joints of column and beam. Therefore, development of concrete cracks and reinforcement internal plasticity was observed in artificial ground motions.

Thereafter, running all the artificial ground motions, the data recorded by contact sensor LVDT and accelerometer were scaled up through scaling factor S_E to get the full scale model results. Later, these scale up results were used to calculate the displacement response and acceleration response.

Additionally, full scale model was also simulated in ETABS software to validate the experimental model results. In displacement response, it was

observed that storey 1 and 2 maximum displacements were approximately three-fold in Test 3 then Test 1 (for both simulated and experimental model results). Residual displacement in each test accumulated with respect to incremental PGAs'. Most importantly, residual displacement highlighted the reinforcement internal plasticity from Test 1 onwards during the shaking table test.

In interstorey drift ratio, it was observed that EC8 undermined the damage limit criteria under sequential ground motions. Moreover, succeeding seismic vibration after the very first ground motion lead to higher drift. In residual interstorey drift, it was observed that permanent displacement led to accumulate the residual drift in each ground motion and became maximum in the last excitation.

By considering the serviceability limit state SLS and ultimate limit state ULS, it was observed that building model crossed the serviceability limit in Test 3 and Test 5 during the seismic ground motions. In storey drift ratio, second consecutive ground motion crossed the damage limit set by EC8 and so on.

In ETABS, real-time ground motion that is Mammoth lake was also simulated to observe the behaviour of full scale RC model and calculate the displacement response of it however, due to low PGA of sequential ground motion, results were satisfactory and lie under the limit set by EC8.

In acceleration response during shaking table test, it was observed that storey 1 had higher acceleration as compared to storey 2 in Test 1 and Test 2 however, as the PGA increased in Test 3, the seismic vibrations were transferred completely from storey 1 to storey 2 and so on. The results showed that storey 1 was critical as compared to storey 2 in sequential ground motions.

CHAPTER 5

CONCLUSION

5.1 Overview

To predict the behavior of a building model for sequential ground motion from low to high, Peak Ground Acceleration (PGA) values, a shaking table test had been performed to gather the data of low-rise RC framed building model. Moreover, ETABS simulation had been run to validate the results with shaking table outcome. Additionally, the framed structure also analysed with a real-time sequential ground motion.

The objective is to evaluate the building response on the two storey small scale RC building model placed on a shaking table applying the successive artificial ground motions. The model design was based on Eurocode 8 for DCL. The research objective is achieved by witnessing the structural member behaviour under multiple ground motions during shaking table test. The finding of this objective concludes that the framed model highlighted the structural strength against its ductility, which is justified through the model ability to resist the multiple ground motions in low seismicity region under extreme PGAs' up to 0.82g.

This objective is to determine the displacements response. Thereafter, the scaled up model is examined with real-time sequential ground motions. The research objective is achieved by calculating maximum displacements, residual displacements, residual interstorey drift ratio, SLS and ULS.

In experimental model, Test 3 has maximum displacement three-fold than Test 1 because as the PGA increased from Test 1 (0.25g) to Test 3 (0.36g), the model losses its stiffness (as observed in shaking table test). Incremental PGAs' cause the model to displace thrice (63.7mm and 91.0mm in storey 1 and 2) as compared to the first seismic motion (17.6mm and 25.4mm in storey 1 and 2) which is in line with the study findings. Similar results are observed for sequential ground motions in Hatzivassiliou & Hatzigeorgiou (2015) , and Li et al. (2016) studies, however, they could not analysed the model with intense artificial ground motions. Thus, this study gives the benchmark for displacements in artificially produced sequential ground motion.

Similar results are obtained in simulated model under artificial ground motions. Residual displacement increases in result of sequential ground motions. In experimental model, Test 1 and 2 have residual displacements of 5.76mm and 9.70mm in storey 1. Similarly, 11.53mm and 34.57mm in storey 2 which clearly highlights the reinforcement internal plasticity during the shaking table test. Similar effect is observed in simulated model.

In experimental model, residual interstorey drift ratio leads to accumulate maximum permanent displacement of 0.63% and 0.87% in storey 1 and 2 in last

seismic ground motion (Test 5) respectively. Similar results are observed in simulated model.

In SLS and ULS, Test 3 and Test 5 have crossed maximum horizontal deflection of SLS (that is u = 23.33mm and u_i = 10mm, a limit set by Eurocode). During real-time ground motions, ML4 cause the RC model to displace permanently threefold in storey 2 and sevenfold in storey 1 as compared to ML1 respectively. Moreover, all the deflections during real-time ground motions are within the SLS range therefore, model performed well in each real-time ground motions.

The objective is to calculate the interstorey drift ratio and storey drift ratio for the damage limitation set by EC8 of the prototype reinforced concrete building model. As there was no damage observed in Test 2 during shaking table test, damage limitation of Test 2 (simulated and experimental outcomes) in storey 1 reaches maximum interstorey drift ratio 1.10% and 1.00% in successive seismic motions. Moreover, Test 4 has IDR less than 1% however, cracks and damages has been observed at beam-column joint during shaking table test. The finding of this study shows that storey drift ratio in Test 2 (0.89%) has crossed the lower limit (0.5%) for damage limitation in shaking table test which clearly shows that EC8 underestimated the damage criteria for multiple ground motions.

This study produced a standard assessment database, which could be used for verification of results stating the effects of sequential seismic ground motions on RC framed structures. The policy makers can map the interpretation

of main findings by considering the damage limitation criteria suggested by current study. Additionally, the displacement response under multiple ground motion could be a benchmark for the policy makers to design the frame structure for Malaysia.

5.2 Recommendation for Future Improvement

Some recommendations for RC model future improvement are stated as follows:

i. Adopting the current research methodology on full scale structure to examine the accuracy of the result compare to scaled 1:10 model is required.
ii. The reliability analysis is required for full scaled structure.
iii. Real-time ground motions are required to use in shaking table test for full-scale model considering Malaysian design conditions.
iv. Small scale DCL, DCM and DCH models are suggested to be design on the guidelines of Malaysian Annex and need to be assessed on shaking table.
v. Institution of Engineers Malaysia (IEM) study and validate the damage limitation criteria for medium and high-rise RC structures.
vi. Cost analysis is required for low, medium and high rise building models design on BS code, and Euro code.

REFERENCES

Abas, M. R. C., Musa, R. C., Ahmad, Z., Rahim, I. A., Tongkul, F., Bakar, R. A., … Shuib, M. K. (2017). Active Faults in Peninsular Malaysia with Emphasis on Active Geomorphic Features Of Bukit Tinggi Region. *Malaysian Journal of Geosciences*, *1*(1), 13–26. https://doi.org/10.26480/mjg.01.2017.13.26

Adiyanto, M. I., Faisal, A., and Majid, T. A. (2011). Nonlinear Behaviour of Reinforced Concrete Building under Repeated Earthquake Excitation. *2011 International Conference on Computer and Software Modeling*, *14*(January 2015), 61–65.

Adiyanto, M. I., and Majid, T. A. (2014a). Seismic design of two storey reinforced concrete building in Malaysia with low class ductility. *Journal of Engineering Science and Technology*, *9*(1), 27–46.

Adiyanto, M. I., and Majid, T. A. (2014b). Seismic design of two storey reinforced concrete building in Malaysia with low class ductility. *Journal of Engineering Science and Technology*, *9*(1), 27–46.

Adnan, A., H. Marto, A., and Irsyam, M. (2006). Development of Seismic Hazard Map for Peninsular Malaysia. *Proceeding on Malaysian Science and Technology Congress (MSTC)*.

Ajis, N. A. B. (2012). *Study on The Improvement Code of Practices in Structural Design and Material Specifications*. *Thesis*. Universiti Malaysia Pahang.

Amadio, C., Fragiacomo, M., and Rajgelj, S. (2003). The effects of repeated earthquake ground motions on the non-linear response of SDOF systems. *Earthquake Engineering and Structural Dynamics*, *32*(2), 291–308. https://doi.org/10.1002/eqe.225

Bahadir, F., and Balik, F. S. (2018). Behaviour of 3D RC frames placed at different angles on shaking table. *Journal of the Croatian Association of Civil Engineers*, *70*(3), 171–186. https://doi.org/10.14256/jce.1655.2016

Balendra, T., and Li, Z. (2008). Seismic hazard of Singapore and Malaysia. *Electronic Journal of Structural Engineering*, *8*, 57–63.

Berg, G. V., and Housner, G. W. (1961). Integrated velocity and displacement of strong earthquake ground motion. *Bulletin of the Seismological Society of America*, *51*(2), 175–189.

Boore, D. M. (2001). Effect of baseline corrections on displacements and response spectra for several recordings of the 1999 Chi-Chi , Taiwan , Earthquake. *Bulletin of the Seismological Society of America*, *91*(5), 1199–1211.

Boore, D. M., and Bommer, J. J. (2005). Processing of strong-motion accelerograms : needs , options and consequences. *Soil Dynamics and Earthquake Engineering*, *25*, 93–115. https://doi.org/10.1016/j.soildyn.2004.10.007

British Standard. (1997). Structural use of concrete —Part 1: Code of practice for design and construction. *BS 8110-1: 1997*, (1).

British Standard. (2008). BS NA EN 1998-1 (2004): UK National Annex to Eurocode 8 - Design of structures for earthquake resistance. General rules, seismic actions and rules for buildings.

Cengel Y. A., and Cimbala, J. M. (2006). *Fluid Mechanics Fundamentals and Applications*.

Chiu, H. C. (1997a). Stable baseline correction of digital strong-motion data. *Bulletin of the Seismological Society of America*, *87*(4), 932–944.

Chiu, H. C. (1997b). Stable Baseline Correction of Digital Strong-Motion Data. *Bulletin of the Seismological Society of America*, *87*(4), 932–944.

Coutinho, C. P., Baptista, A. J., and Dias, J. (2016). Reduced scale models based on similitude theory : A review up to 2015. *Engineering Structures*, *119*, 81–94. https://doi.org/10.1016/j.engstruct.2016.04.016

Dai, K., Wang, J., Li, B., and Hong, H. P. (2017). Use of residual drift for post-earthquake damage assessment of RC buildings. *Engineering Structures*, *147*, 242–255. https://doi.org/10.1016/j.engstruct.2017.06.001

Department of Standards Malaysia. (2017). Malaysia National Annex to MS EN 1998-1 : Design of structures for earthquake resistance - Part 1: General rules, seismic actions and rules for buildings.

Douglas, J., and Boore, D. M. (2011). High-frequency filtering of strong-motion records. *Bulletin of Earthquake Engineering*, *9*(2), 395–409. https://doi.org/10.1007/s10518-010-9208-4

Earthquaketrack. (2019). 4.5 magnitude earthquake 70 km from Ranau, Sabah, Malaysia. Retrieved December 27, 2019, from https://earthquaketrack.com/quakes/2019-08-03-15-31-04-utc-4-5-664

Elghazouli, A. Y. (2009). *Seismic Design of Buildings to Eurocode 8*.

EN, O. H. (2019). *Dynamic response of scaled structure with one liquid tuned mass damper*. Bachelors Thesis, Universiti Tunku Abdul Rahman, Malaysia.

Eurocode 0. (1990). *EN 1990 (2002) (English): Eurocode - Basis of structural design* (Vol. 1990).

European Standard. (2004a). Eurocode 2: Design of concrete structures - Part 1-1 : General rules and rules for buildings Eurocode. *EN 1992-1-1*. https://doi.org/10.2514/2.2772

European Standard. (2004b). Eurocode 8 : Design of structures for earthquake resistance —Part 1: General rules, seismic actions and rules for buildings. *BS EN 1998-1:2004*, *3*.

European Standard. (2011). EN 1998-1 (2004) (English): Eurocode 8: Design of structures for earthquake resistance – Part 1: General rules, seismic actions and rules for buildings, *1*(2004).

Faisal, A., Majid, T. A., and Hatzigeorgiou, G. D. (2013). Investigation of story ductility demands of inelastic concrete frames subjected to repeated earthquakes. *Soil Dynamics and Earthquake Engineering*, *44*, 42–53. https://doi.org/10.1016/j.soildyn.2012.08.012

Fardis, M. N. (2008). *Design of buildings for earthquake resistance , according to Eurocode 8-Part 1 (Buildings and concrete buildings)* (Vol. 1).

Fardis, M. N., Eduardo, C., Peter, F., and Alain, P. (2015). *Seismic Design of Concrete Buildings to Eurocode 8 Handbook*.

Franklin, R. E., Erntroy, H. C., and Marsh, B. K. (1988). Design of normal concrete mixes, *2nd editio*.

Gill, J., Shariff, N. S., Omar, K., and Amin, Z. M. (2015). Tectonic Motion of Malaysia: Analysis From Years 2001 To 2013. *ISPRS Annals of Photogrammetry, Remote Sensing and Spatial Information Sciences*, 199–

206. https://doi.org/10.5194/isprsannals-II-2-W2-199-2015
Graizer, V. (2006). Tilts in Strong Ground Motion. *Bulletin of the Seismological Society of America*, *96*(6), 2090–2102. https://doi.org/10.1785/0120060065
Harris, H. G., and Sabnis, G. . (1999). *Structural Modelling and Experimental Techniques* (2nd Editio). CRC Press: Taylor and Francis Group Pennsylvania.
Harris, H., and Sabnis, G. (1999). Structural Modeling and Experimental Techniques.
Hatzigeorgiou, G. D. (2010). Behavior factors for nonlinear structures subjected to multiple near-fault earthquakes. *Computers and Structures*, *88*(5–6), 309–321. https://doi.org/10.1016/j.compstruc.2009.11.006
Hatzigeorgiou, G. D. (2010). Ductility demand spectra for multiple near- and far-fault earthquakes. *Soil Dynamics and Earthquake Engineering*, *30*(4), 170–183. https://doi.org/10.1016/j.soildyn.2009.10.003
Hatzigeorgiou, G. D., and Beskos, D. E. (2009). Inelastic displacement ratios for SDOF structures subjected to repeated earthquakes. *Engineering Structures*, *31*(11), 2744–2755. https://doi.org/10.1016/j.engstruct.2009.07.002
Hatzivassiliou, M., & Hatzigeorgiou, G. D. (2015). Seismic sequence effects on three-dimensional reinforced concrete buildings. *Soil Dynamics and Earthquake Engineering*, *72*(February 2015), 77–88. https://doi.org/10.1016/j.soildyn.2015.02.005
Herayani, N. S., and Adnan, A. (2017). Eastimation of peak ground acceleration of Ranau based on recent eathquake databases. *Malaysian Journal of Geosciences*, *1*(2), 6–9.
Heuisoo, H., Mincheol, P., Sangki, P., Juhyong, K., and Yong, B. (2019). Experimental Verification of Methods for Converting Acceleration Data in High-Rise Buildings into Displacement Data by Shaking Table Test. *Applied Sciences*, *9*(8), 1-25. https://doi.org/10.3390/app9081653
Hosseinpour, F., and Abdelnaby, A. E. (2017). Effect of different aspects of multiple earthquakes on the nonlinear behavior of RC structures. *Soil Dynamics and Earthquake Engineering*, , 706–725. https://doi.org/10.1016/j.soildyn.2016.11.006
Ismail, R., and Adnan, A. A. (2016). Seismic Damage Analysis of Reinforced Concrete Frame of Public Buildings in Ipoh Subjected to Acheh Earthquake Event. *InCIEC 2015*, 149–157. https://link.springer.com/chapter/10.1007/978-981-10-0155-0_15
Iwan, W. D., Moser M. A., and Peng, C. Y. (1985). Some observations on strong-motion earthquake measurement using a digital acceleration. *Bulletin of the Seismological Society of America*, *66*(6), 1271–1302. https://doi.org/10.1785/0120160029
Katsuichiro, G., and Colin A., T. (2012). Effects of aftershocks on peak ductility demand due to strong ground motion records from shallow crustal earthquakes. *Earthquake Engineering and Structural Dynamics*. https://doi.org/10.1002/eqe.2188 Effects
Khoshraftar, A., Abbasnia, R., and Raof, F. F. (2013). The effect of degradation on seismic damage of RC buildings. *Advances in Environmental Biology*, *7*(5), 861–867.

Kim, N., Kwak, Y., and Chang, S. (2004). Pseudodynamic tests on small scale steel models using the modified similitude law. *Proceedings of the 13th World Conference on Earthquake Engineering*, (New York: State University of New York at Buffalo), 1–11.

Kim, N., Lee, J., and Chang, S. (2009). Equivalent multi-phase similitude law for pseudodynamic test on small scale reinforced concrete models. *Engineering Structures*, *31*(4), 834–846. https://doi.org/10.1016/j.engstruct.2008.06.008

Kim, W., Attar, A. E., and White, R. N. (1988). *Small-scale modeling techniques for reinforced concrete structures subjected to seismic loads [Technical Report NCEER-88-0041]*. New York.

Kumar, S., Yoshito, I., Kunihiro, S., and Tsutomu, U. (1997). Pseudodynamic testing of scaled models. *Journal of Structural Engineering*, 524–526. https://doi.org/10.1061/(ASCE)0733-9445(1997)123:4(524)

Latiff, A. H. A., and Khalil, A. E. (2016). Hypocenter Relocation of Earthquakes in Peninsular Malaysia. In *National Geoscience Conference*.

Leyu, C., Chang, C., Arnold, E., Kho, S., Lim, Y., Subramaniam, M., … Goh, H. (1985). *Southeast Asia Association of Seismology*. *Series of Seismology* (Vol. III).

Li, S., Zuo, Z., Zhai, C., and Xie, L. (2017). Comparison of static pushover and dynamic analyses using RC building shaking table experiment. *Engineering Structures*, *136*, 430–440. https://doi.org/10.1016/j.engstruct.2017.01.033

Li, S., Zuo, Z., Zhai, C., Xu, S., and Xie, L. (2016). Shaking table test on the collapse process of a three-story reinforced concrete frame structure. *Engineering Structures*, *118*, 156–166. https://doi.org/10.1016/j.engstruct.2016.03.032

Lim, H. K., Kang, J., Pak, H., Chi, H. S., Lee, Y. G., and Kim, J. (2018). Seismic Response of a Three-Dimensional Asymmetric Multi-Storey Reinforced Concrete Structure. *Applied Sciences*, *8*(4), 479. https://doi.org/10.3390/app8040479

Lu, Y., Hao, H., Carydis, P. G., and Mouzakis, H. (2001). Seismic performance of RC frames designed for three different ductility levels. *Engineering Structures*, *23*(5), 537–547. https://doi.org/10.1016/S0141-0296(00)00058-4

Lye, H., Yean, S., Li, P., Liu, F., Izani, A., and Ling, H. (2009). Simulation of Andaman 2004 tsunami for assessing impact on Malaysia. *Journal of Asian Earth Sciences*, *36*(1), 74–83. https://doi.org/10.1016/j.jseaes.2008.09.008

Majid, T. A., Adiyanto, M. I., and Nazri, F. M. (2014). Nonlinear Response of Low Rise Hospital RC Building in Malaysia Due to Far and Near Field Earthquake. *Journal of Civil Engineering Research*, *4*(3A), 130–134. https://doi.org/10.5923/c.jce.201402.22

Majid, T., Zaini, S. S., Nazri, F. M., Arshad, M. R., and Suhaimi, I. F. M. (2007). Development of Design Response Spectra for Northern Peninsular Malaysia Based on UBC 97 Code. *The Institution of Engineers, Malaysia*, *68*(4), 23–29.

Malaymail. (2015). *Sabah earthquake a 2015 shock for the nation*. Retrieved from https://www.malaymail.com/news/malaysia/2015/12/24/sabah-earthquake-a-2015-shock-for-the-nation/1029201

Manafizad, A. N., Pradhan, B., and Abdullahi, S. (2016). Estimation of Peak Ground Acceleration (PGA) for Peninsular Malaysia using geospatial approach. *IOP Conference Series: Earth and Environmental Science*, *37*. https://doi.org/10.1088/1755-1315/37/1/012069

Manafpour, A. R., and Moghaddam, P. K. (2019). Performance capacity of damaged RC SDOF systems under multiple far- and near-field earthquakes. *Soil Dynamics and Earthquake Engineering*, *116*, 164–173. https://doi.org/10.1016/j.soildyn.2018.09.045

Marto, A., and Kasim, F. (2013). Seismic impact in Peninsular Malaysia Seismic impact in Peninsular Malaysia. *The 5th International Geotechnical Symposium-Incheon*, 237–242. https://doi.org/10.13140/2.1.3094.9129

Megawati, K., Lam, N. T. K., Chandler, A. M., and Pan, T. (2004). Cities without a seismic code I : hazard assessment. *13th World Conference on Earthquake Engineering*, (129).

Mercycorps. (2018). *Quick facts: Indonesia earthquakes, tsunamis and other natural disasters*. Retrieved from https://www.mercycorps.org/articles/quick-facts-indonesia-disasters

MMD. (2016). *Malaysian Meteorological Department Annual Report*.

MMD. (2017). *Meteorological Malaysia Department Annual Report*.

Mollova, G. (2007). Effects of digital filtering in data processing of seismic acceleration records. *Eurasip Journal on Advances in Signal Processing*, 1–9. https://doi.org/10.1155/2007/29502

Moustafa, A., and Takewaki, I. (2011). Response of nonlinear single-degree-of-freedom structures to random acceleration sequences. *Engineering Structures*, *33*(4), 1251–1258. https://doi.org/10.1016/j.engstruct.2011.01.002

Newcomb, K. R., and McCann, W. R. (1987). Seismic history and seismotectonics of the Sunda Arc. *Journal of Geophysical Research*, *92*, 421–439.

Nizamani, Z., Seng, S. K., Nakayama, A., Bin Omar Khan, M. S., and Haider, B. (2018). Seismic Effects on Unsymmetrical Building Spectrum Analysis a Horizontally using Response. *MATEC Web of Conferences 203*, *06014*, 0–8. https://doi.org/https://doi.org/10.1051/matecconf/201820306014

Ohsaki, Y. (1995). New introduction to spectrum analysis of earthquake ground motion, *Japan: Kaj*.

Oyguc, R., Toros, C., and Abdelnaby, A. E. (2018). Seismic behavior of irregular reinforced-concrete structures under multiple earthquake excitations. *Soil Dynamics and Earthquake Engineering*, *104*, 15–32. https://doi.org/10.1016/j.soildyn.2017.10.002

Panagiotakos, T. B., and Fardis, M. N. (2004). Seismic Performance of RC Frames Designed to Eurocode 8 or to the Greek Codes 2000. *Bulletin of Earthquake Engineering*, *2*, 221–259.

PEER. (2019). Retrieved April 10, 2019, from http:www.peer.berkeley.edu/smcat

Petersen, M. D., Dewey, J., Hartzell, S., Mueller, C., Harmsen, S., Frankel, A. D., and Rukstales, K. (2004). Probabilistic seismic hazard analysis for Sumatra , Indonesia and across the Southern Malaysian Peninsula. *Tectonophysics*, *390*, 141–158.

https://doi.org/10.1016/j.tecto.2004.03.026
Qianyi, C. L. (2016). Seismic design guides for low-rise masonry buildings in Malaysia. Bachelors Thesis, Universiti Tunku Abdul Rahman, Malaysia.
Rastogi, G., Moin, K., and Abbas, S. M. (2015). Dimensional Analysis and Development of Similitude Rules for Dynamic Structural Models, *5*(3), 68–72.
Rizwan, M., Ahmad, N., and Khan, A. N. (2018). Seismic Performance of Compliant and Non-Compliant Special Moment- Resisting Reinforced Concrete Frames. *ACI Structural Journal*, *115*, 1063–1073. https://doi.org/10.14359/51702063
Rodrigues, H., and Elawady, M. H. (2019). Ductility considerations in seismic design of reinforced concrete frame buildings according to the Eurocode 8. *Innovative Infrastructure Solutions*, *4*(1). https://doi.org/10.1007/s41062-018-0192-x
Samanta, A., & Pandey, P. (2018). Effects of ground motion modification methods and ground motion duration on seismic performance of a 15-storied building. *Journal of Building Engineering*, *15*, 14–25. https://doi.org/10.1016/j.jobe.2017.11.003
Seismosoft's Suite of Earthquake Tools. (2018). Siesmoapps : Technical Information Sheet.
Sooria, S. Z., Sawada, S., and Goto, H. (2012). Proposal for Seismic Resistant Design in Malaysia : Assessment of Possible Ground Motions in Peninsular Malaysia. *Annuals of Disas. Prev. Res. Inst.*, (55B).
Sovester, H., and Adiyanto, M. I. (2017). Seismic Performance of Reinforced Concrete School Buildings in Sabah. *International Journal of Civil Engineering and Geo-Environmental*.
Stavridis, A., Shing, B., and Conte, J. (2010). *Modeling of Shake- Shake - Table Test Structures*.
Tongkul, F. (2015). The 2015 Ranau Earthquake: Cause and Impact. *Sabah Society Journal*, *32*(April), 1–28.
United States Geological Survey database (USGS). (2016). Retrieved from https://earthquake.usgs.gov/earthquakes/eventpage/us2000k82i/region-info
USGS. (1960). M 9.5 - Bio-Bio, Chile. Retrieved May 14, 2019, from https://earthquake.usgs.gov/earthquakes/eventpage/official19600522191120_30/impact
USGS. (2004). M 9.1 - off the west coast of northern Sumatra. Retrieved May 15, 2019, from https://earthquake.usgs.gov/earthquakes/eventpage/official20041226005853450_30/impact
Xian, L. J. (2017). Experimental Study on Dynamic Behaviour of Tropical Residual Soils in Malaysia. Masters Thesis, Universiti Tunku Abdul Rahman, Malaysia.
Yip, C. C., Marsono, A. K., Wong, J. Y., and Lee, S. C. (2018). Seismic Performance of Scaled IBS Block Column for Static Nonlinear Monotonic Pushover Experimental Analysis. *Jurnal Teknologi*, *1*, 89–106.
Yip, C. C., and Marsono, A. K. (2016). Structural seismic performance of reinforced concrete block system for two storeys safe house. *Jurnal Teknologi*, *2*(78), 83–97.

Yusa, Z. (2018). 5.2 magnitude quake hits Sabah. *Free Malaysia Today*. Retrieved from https://www.freemalaysiatoday.com/category/nation/2018/03/08/5-2-magnitude-quake-hits-sabah/

Zahid, M. Z. A. M., Robert, D., and Shahrin, F. (2013). An evaluation of overstrength factor of seismic designed low rise RC buildings. *Procedia Engineering*, *53*, 48–51. https://doi.org/10.1016/j.proeng.2013.02.008

Zhu, Q., Lu, X., Jiang, H., and Zhao, B. (2005). Shaking Table Test and Numerical Analysis on a Shear Wall High-Rise Structure with Huge Podium.

APPENDICES

Appendix A Structural Design Check

Design of Slab (Eurocode 2)

(i) Check the minimum thickness of the slab:

Assume,
h = 15mm, φ_{bar} = 3.2mm, cover = 2.5mm

Effective depth of slab (d) = Overall depth (h) – half bar diameter (φ_{bar}) – cover

$d = 15 - \frac{3.2}{2} - 2.5$

d = 10.9mm

$A_{s,min} = 0.0013\ bd$

$A_{s,min} = 0.0013\ (1000)\ (10.9)$

$A_{s,min} = 14.17\text{mm}^2$

$\rho = \frac{100A_{s,min}}{bd}$

$\rho = \frac{100\ (14.17)}{(1000)\ (10.9)}$

ρ = 0.13 (from figure 6.3, basic span effective depth ratio = 29)

Allowable basic span effective depth ratio = 1.3 x 29 = 37.7
Allowable basic span effective depth ratio = 1.5 x 29 = 43.5
Span effective depth ratio provided $= \frac{500}{10.9}$
Span effective depth ratio provided = 45.87 (higher than the allowable upper limit, not satisfied)

Assume, h =16mm, φ_{bar} = 3.2mm, cover = 2.5mm

$d = 16 - \frac{3.2}{2} - 2.5$

d = 11.9mm

$A_{s,min} = 0.0013\ bd$

$A_{s,min} = 0.0013\ (1000)\ (11.9)$

$A_{s,min} = 15.47\text{mm}^2$

$\rho = \frac{100A_{s,min}}{bd}$

$\rho = \frac{100\ (15.47)}{(1000)\ (11.9)}$

ρ = 0.13 (from figure 6.3, basic span effective depth ratio = 29)

Allowable basic span effective depth ratio = 1.3 x 29 = 37.7
Allowable basic span effective depth ratio = 1.5 x 29 = 43.5
Span effective depth ratio provided = $\frac{500}{11.9}$
Span effective depth ratio provided = 42.02 (lower than the allowable upper limit, hence satisfied)

Hence, the thickness of Slab selected is 16mm.

(ii) Check the area of reinforcement required:

l_x = 0.4m, l_y = 0.5m
So
$\frac{l_y}{l_x} = \frac{0.5}{0.4} = 1.25 < 2$

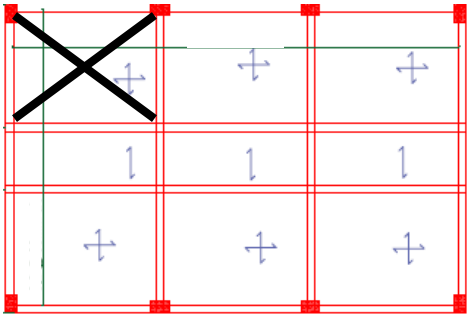

Hence, it is Two-way slab

Permanent load (self-weight) (G_k)
= 0.016 x 25
Permanent load (self-weight) (G_k)
= 0.4 KN/m^2

Live load (Q_k) = 3 KN/m^2
(according to table 6.2 of EC1)

Design load (n) = 1.35 G_k + 1.5 Q_k
Design load (n) = 1.35 (0.4) + 1.5 (3)
Design load (n) = 5.04KN/m^2

- **The slab is considered two adjacent edges discontinuous (from table 8.5 of EC2)**

Positive moment at mid span:

$M_{sx} = \beta_{sx}\, n l_x^2$
M_{sx} = (0.070) (5.04) (0.4)^2
M_{sx} = 0.056 KNm

$M_{sy} = \beta_{sy}\, n l_y^2$
M_{sx} = (0.034) (5.04) (0.6)^2
M_{sx} = 0.062 KNm

Negative moment at continuous edge:

$M_{sx} = \beta_{sx}\, n l_x^2$
M_{sx} = (0.093) (5.04) (0.4)^2
M_{sx} = 0.075 KNm

$M_{sy} = \beta_{sy}\, n l_y^2$
M_{sx} = (0.045) (5.04) (0.6)^2
M_{sx} = 0.082 KNm

For positive moment (X direction):

$k = \frac{M_{sx}}{bd^2 f_{ck}}$

For positive moment (Y direction):

$k = \frac{M_{sy}}{bd^2 f_{ck}}$

$k = \frac{0.056\ (10^6)}{(1000)(11.9^2)(30)}$

$k = 0.013 < 0.167$

No compression reinforcement is required

$z = d\ [\ 0.5 + \sqrt{0.25 - \frac{k}{1.134}}\ ]$

$z = d\ [\ 0.5 + \sqrt{0.25 - \frac{0.013}{1.134}}\ ]$

$z = 0.99\ d > 0.95d$

$A_s = \frac{M_{sx}}{0.87 f_{yk} z}$

$A_s = \frac{0.056\ (10^6)}{0.87\ (316)(0.95 \times 11.9)}$

$A_s = 18.02\ mm^2/m$

$k = \frac{0.062\ (10^6)}{(1000)(11.9^2)(30)}$

$k = 0.015 < 0.167$

No compression reinforcement is required

$z = d\ [\ 0.5 + \sqrt{0.25 - \frac{k}{1.134}}\ ]$

$z = d\ [\ 0.5 + \sqrt{0.25 - \frac{0.015}{1.134}}\ ]$

$z = 0.99\ d > 0.95d$

$A_s = \frac{M_{sx}}{0.87 f_{yk} z}$

$A_s = \frac{0.062\ (10^6)}{0.87\ (316)(0.95 \times 11.9)}$

$A_s = 19.95\ mm^2/m$

<u>For negative moment (X Direction):</u>

$k = \frac{M_{sx}}{bd^2 f_{ck}}$

$k = \frac{0.075\ (10^6)}{(1000)(11.9^2)(30)}$

$k = 0.018 < 0.167$

No compression reinforcement is required

$z = d\ [\ 0.5 + \sqrt{0.25 - \frac{k}{1.134}}\ ]$

$z = d\ [\ 0.5 + \sqrt{0.25 - \frac{0.018}{1.134}}\ ]$

$z = 0.98\ d > 0.95d$

$A_s = \frac{M_{sx}}{0.87 f_{yk} z}$

$A_s = \frac{0.075\ (10^6)}{0.87\ (316)(0.95 \times 11.9)}$

$A_s = 24.13\ mm^2/m$

<u>For negative moment (Y direction):</u>

$k = \frac{M_{sy}}{bd^2 f_{ck}}$

$k = \frac{0.082\ (10^6)}{(1000)(11.9^2)(30)}$

$k = 0.019 < 0.167$

No compression reinforcement is required

$z = d\ [\ 0.5 + \sqrt{0.25 - \frac{k}{1.134}}\ ]$

$z = d\ [\ 0.5 + \sqrt{0.25 - \frac{0.019}{1.134}}\ ]$

$z = 0.98\ d > 0.95d$

$A_s = \frac{M_{sx}}{0.87 f_{yk} z}$

$A_s = \frac{0.082\ (10^6)}{0.87\ (316)(0.95 \times 11.9)}$

$A_s = 26.38\ mm^2/m$

➢ **Slab is considered one long edge discontinuous**

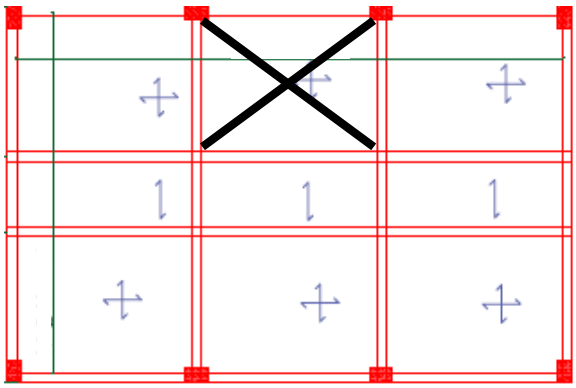

Positive moment at mid span:

$M_{sx} = \beta_{sx}\, nl_x^2$
$M_{sx} = (0.067)\ (5.04)\ (0.4)^2$
$M_{sx} = 0.054$ KNm

$M_{sy} = \beta_{sy}\, nl_y^2$
$M_{sx} = (0.028)\ (5.04)\ (0.6)^2$
$M_{sx} = 0.051$ KNm

Negative moment at continuous edge:

$M_{sx} = \beta_{sx}\, nl_x^2$
$M_{sx} = (0.089)\ (5.04)\ (0.4)^2$
$M_{sx} = 0.072$ KNm

$M_{sy} = \beta_{sy}\, nl_y^2$
$M_{sx} = (0.037)\ (5.04)\ (0.6)^2$
$M_{sx} = 0.067$ KNm

For positive moment (X direction):

$$k = \frac{M_{sx}}{bd^2 f_{ck}}$$
$$k = \frac{0.056\ (10^6)}{(1000)(11.9^2)(30)}$$
$k = 0.013 < 0.167$
No compression reinforcement is required

$$z = d\ [\ 0.5 + \sqrt{0.25 - \frac{k}{1.134}}\ ]$$
$$z = d\ [\ 0.5 + \sqrt{0.25 - \frac{0.013}{1.134}}\ ]$$
$z = 0.99\ d > 0.95d$

$$A_s = \frac{M_{sx}}{0.87 f_{yk} z}$$
$$A_s = \frac{0.054\ (10^6)}{0.87\ (316)(0.95 \times 11.9)}$$
$A_s = 17.37$ mm^2/m

For positive moment (Y direction):

$$k = \frac{M_{sy}}{bd^2 f_{ck}}$$
$$k = \frac{0.051\ (10^6)}{(1000)(11.9^2)(30)}$$
$k = 0.012 < 0.167$
No compression reinforcement is required

$$z = d\ [\ 0.5 + \sqrt{0.25 - \frac{k}{1.134}}\ ]$$
$$z = d\ [\ 0.5 + \sqrt{0.25 - \frac{0.012}{1.134}}\ ]$$
$z = 0.99\ d > 0.95d$

$$A_s = \frac{M_{sx}}{0.87 f_{yk} z}$$
$$A_s = \frac{0.051\ (10^6)}{0.87\ (316)(0.95 \times 11.9)}$$
$A_s = 16.41$ mm^2/m

For negative moment (X Direction):

$$k = \frac{M_{sx}}{bd^2 f_{ck}}$$

For negative moment (Y direction):

$$k = \frac{M_{sy}}{bd^2 f_{ck}}$$

$k = \frac{0.072\ (10^6)}{(1000)(11.9^2)(30)}$

$k = 0.017 < 0.167$

No compression reinforcement is required

$z = d\ [\ 0.5 + \sqrt{0.25 - \frac{k}{1.134}}\ ]$

$z = d\ [\ 0.5 + \sqrt{0.25 - \frac{0.017}{1.134}}\ ]$

$z = 0.98\ d > 0.95d$

$A_s = \frac{M_{sx}}{0.87 f_{yk} z}$

$A_s = \frac{0.072\ (10^6)}{0.87\ (316)(0.95 \times 11.9)}$

$A_s = 23.17\ mm^2/m$

$k = \frac{0.067\ (10^6)}{(1000)(11.9^2)(30)}$

$k = 0.016 < 0.167$

No compression reinforcement is required

$z = d\ [\ 0.5 + \sqrt{0.25 - \frac{k}{1.134}}\ ]$

$z = d\ [\ 0.5 + \sqrt{0.25 - \frac{0.016}{1.134}}\ ]$

$z = 0.99\ d > 0.95d$

$A_s = \frac{M_{sx}}{0.87 f_{yk} z}$

$A_s = \frac{0.067\ (10^6)}{0.87\ (316)(0.95 \times 11.9)}$

$A_s = 21.56\ mm^2/m$

$l_x = 0.2m$, $l_y = 0.5m$

So,

$\frac{l_y}{l_x} = \frac{0.5}{0.2} = 2.5 > 2$

Hence, it is One-way slab

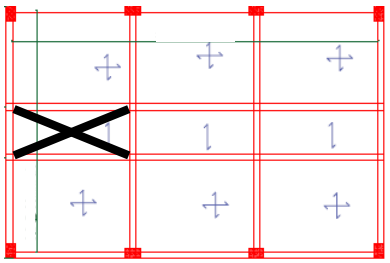

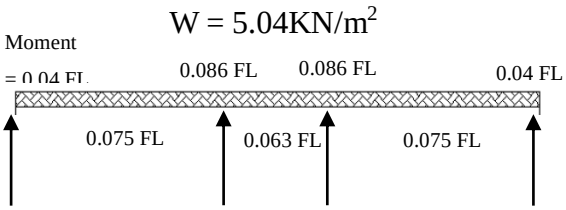

<u>At first interior support:</u>

$M = 0.086\ FL$

$M = 0.86\ (5.04 \times 0.5 \times 0.2)\ (0.5)$

$M = 0.022$ KNm

$k = \frac{M}{bd^2 f_{ck}}$

$k = \frac{0.022\ (10^6)}{(1000)(11.9^2)(30)}$

$k = 0.0052 < 0.167$

No compression reinforcement is required

$z = d\ [\ 0.5 + \sqrt{0.25 - \frac{k}{1.134}}\ ]$

$z = d\ [\ 0.5 + \sqrt{0.25 - \frac{0.0057}{1.134}}\ ]$

<u>Near middle of end span:</u>

$M = 0.075\ FL$

$M = 0.075\ (5.04 \times 0.5 \times 0.2)\ (0.5)$

$M = 0.019$ KNm

$k = \frac{M}{bd^2 f_{ck}}$

$k = \frac{0.019\ (10^6)}{(1000)(11.9^2)(30)}$

$k = 0.004 < 0.167$

No compression reinforcement is required

$z = d\ [\ 0.5 + \sqrt{0.25 - \frac{k}{1.134}}\ ]$

$z = 0.99\,d > 0.95d$

$A_s = \frac{M}{0.87 f_{yk} z}$

$A_s = \frac{0.022\ (10^6)}{0.87\ (316)(0.95 \times 11.9)}$

$A_s = 7.08\ \text{mm}^2/\text{m}$

<u>At interior support and interior span:</u>

$M = 0.063\,FL$

$M = 0.063\ (5.04 \times 0.5 \times 0.2)\ (0.5)$

$M = 0.016$ KNm

$k = \frac{M}{bd^2 f_{ck}}$

$k = \frac{0.016\ (10^6)}{(1000)(11.9^2)(30)}$

$k = 0.004 < 0.167$

No compression reinforcement is required

$z = d\ [\ 0.5 + \sqrt{0.25 - \frac{k}{1.134}}\ ]$

$z = d\ [\ 0.5 + \sqrt{0.25 - \frac{0.004}{1.134}}\ ]$

$z = 0.99\,d > 0.95d$

$A_s = \frac{M}{0.87 f_{yk} z}$

$A_s = \frac{0.016\ (10^6)}{0.87\ (316)(0.95 \times 11.9)}$

$A_s = 5.15\ \text{mm}^2/\text{m}$

$z = d\ [\ 0.5 + \sqrt{0.25 - \frac{0.004}{1.134}}\ ]$

$z = 0.99\,d > 0.95d$

$A_s = \frac{M}{0.87 f_{yk} z}$

$A_s = \frac{0.019\ (10^6)}{0.87\ (316)(0.95 \times 11.9)}$

$A_s = 6.11\ \text{mm}^2/\text{m}$

<u>At outer support:</u>

$M = 0.04\,FL$

$M = 0.04\ (5.04 \times 0.5 \times 0.2)\ (0.5)$

$M = 0.010$ KNm

$k = \frac{M}{bd^2 f_{ck}}$

$k = \frac{0.010\ (10^6)}{(1000)(11.9^2)(30)}$

$k = 0.0024 < 0.167$

No compression reinforcement is required

$z = d\ [\ 0.5 + \sqrt{0.25 - \frac{k}{1.134}}\ ]$

$z = d\ [\ 0.5 + \sqrt{0.25 - \frac{0.0024}{1.134}}\ ]$

$z = 0.99\,d > 0.95d$

$A_s = \frac{M}{0.87 f_{yk} z}$

$A_s = \frac{0.010\ (10^6)}{0.87\ (316)(0.95 \times 11.9)}$

$A_s = 3.22\ \text{mm}^2/\text{m}$

<u>(iii) Minimum Area of Steel:</u>

$A_{s,min} = 0.0013bd$

$A_{s,min} = 0.0013\ (1000)\ (11.9)$

$A_{s,min} = 15.47\ \text{mm}^2/\text{m}$

<u>(iv) Checking:</u>

Highest $A_{s,req} = 26.38\text{mm}^2/\text{m}$

$\frac{100 A_{s,req}}{bd} = \frac{100\ (26.38)}{(1000)(11.9)}$

$\frac{100 A_{s,req}}{bd} = 0.22\%$ (from Figure 6.3, basic span effective depth ratio = 28)

Basic span-effective depth ratio required = (28 + 28 × 0.22) × 1.3 = 44.41
Basic span-effective depth ratio required = (28 + 28 × 0.22) × 1.5 = 51.24

Actual span-effective depth ratio = $\frac{500}{11.9}$
Actual span-effective depth ratio = 42.02 < 44.41 (Acceptable)

Beam Design (Eurocode 2)

(i) For continuous beam A-D:

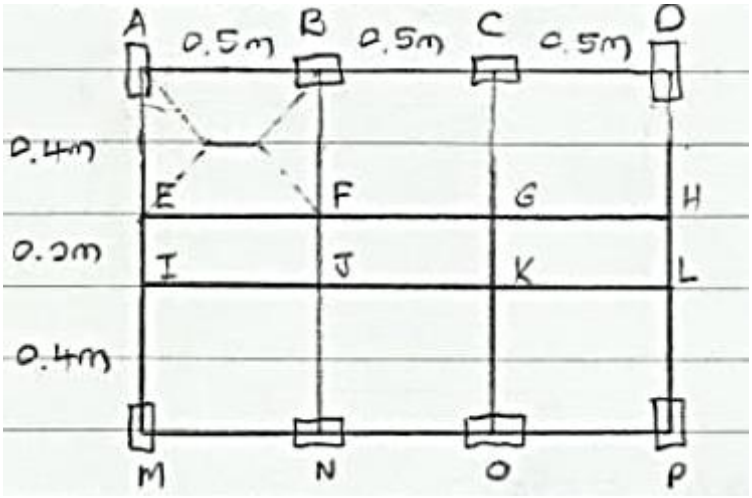

Load at AB = BC = CD
Effective depth of beam = Overall depth – half bar diameter – cover
d = $60 - \frac{3.2}{2} - 5$
d = 53.4mm

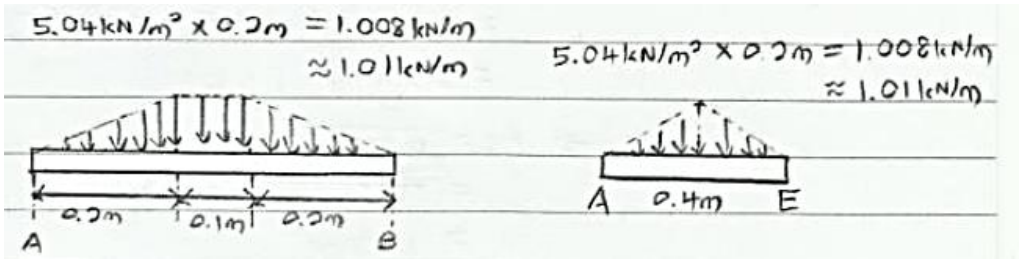

Calculate the total load on AB:
Permanent load (from slab) = $[\frac{1}{2}(1.01)(0.22)](2) + (1.01)(0.1)$
Permanent load (from slab) = 0.3KN

Permanent load (from beam) = $b \times h \times 25$
Permanent load (from beam) = 0.025 × 0.08 × 25
Permanent load (from beam) = 0.0375 KN/m

Variable load = 0

Total load = 1.35 (0.0375) (0.5) + 0.3
Total load = 0.33KN

Mid span of AB and CD end spans – design as T-section:

$M = 0.09\ FL$
$M = 0.09\ (0.33)\ (0.5)$
$M = 0.015$KNm

$b_{eff} = b_w + 2[0.2b' + 0.1 \times 0.85\ L]$
$b_{eff} = 25 + [0.2\ (400 + 40)/2 + 0.1\ (0.85)\ (500)]$
$b_{eff} = 198$mm

$b_w + 2[0.2 \times 0.85\ L] = 25 + 2\ [0.2 \times 0.85\ (500)]$
$= 195$mm

Hence, $b_f = 195$mm

$$k = \frac{M}{bd^2 f_{ck}}$$
$$k = \frac{0.015\ (10^6)}{(195)(53.4^2)(30)}$$
$k = 0.0009 < 0.167$
Hence, No compression reinforcement is required

$$z = d\ [\ 0.5 + \sqrt{0.25 - \frac{k}{1.134}}\ ]$$
$$z = d\ [\ 0.5 + \sqrt{0.25 - \frac{0.0009}{1.134}}\ ]$$
$z = 0.99\ d > 0.95d$

$$A_s = \frac{M}{0.87 f_{yk} z}$$
$$A_s = \frac{0.015\ (10^6)}{0.87\ (316)(0.95 \times 53.4)}$$
$A_s = 1.08$ mm^2/m

Mid span of interior span BC – design as T-section:

$M = 0.07\ FL$
$M = 0.07\ (0.33)\ (0.5)$
$M = 0.012$KNm

$b_{eff} = b_w + 2[0.2b' + 0.1 \times 0.70\ L]$
$b_{eff} = 25 + [0.2\ (400 + 40)/2 + 0.1\ (0.70)\ (500)]$
$b_{eff} = 183$mm

$b_w + 2[0.2 \times 0.70\ L] = 25 + 2\ [0.2 \times 0.70\ (500)]$
$= 165$mm

Hence, $b_f = 165$mm

$$k = \frac{M}{bd^2 f_{ck}}$$
$$k = \frac{0.012\ (10^6)}{(165)(53.4^2)(30)}$$
$k = 0.00085 < 0.167$
Hence, No compression reinforcement is required

$$z = d\ [\ 0.5 + \sqrt{0.25 - \frac{k}{1.134}}\ ]$$
$$z = d\ [\ 0.5 + \sqrt{0.25 - \frac{0.00085}{1.134}}\ ]$$
$z = 0.99\ d > 0.95d$

$$A_s = \frac{M}{0.87 f_{yk} z}$$
$$A_s = \frac{0.012\ (10^6)}{0.87\ (316)(0.95 \times 53.4)}$$
$A_s = 0.86$ mm^2/m

Interior supports – design as a rectangular section
$M = 0.11\ FL$
$M = 0.11\ (0.33)\ (0.5)$
$M = 0.018$KNm

$$k = \frac{M}{bd^2 f_{ck}}$$

$k = \frac{0.018\ (10^6)}{(195)(53.4^2)(30)}$

$k = 0.0053 < 0.167$

Hence, No compression reinforcement is required

$z = d\ [\ 0.5 + \sqrt{0.25 - \frac{k}{1.134}}\ ]$

$z = d\ [\ 0.5 + \sqrt{0.25 - \frac{0.0053}{1.134}}\ ]$

$z = 0.99\ d > 0.95d$

$A_s = \frac{M}{0.87 f_{yk} z}$

$A_s = \frac{0.018\ (10^6)}{0.87\ (316)(0.95 \times 53.4)}$

$A_s = 1.29\ mm^2/m$

Minimum Area of Steel:

$A_{s,min} = 0.0013bd$

$A_{s,min} = 0.0013\ (195)\ (53.4)$

$A_{s,min} = 13.54\ mm^2/m$

Check Deflection:

$I = \frac{bd^3}{12}$

$I = \frac{(165)\ (53.4^3)}{12}$

$I = 2.1 \times 10^6\ mm^4$

$\frac{L}{200} = \frac{500}{200}$

$\frac{L}{200} = 2.5mm$

$\delta_{max} = -\frac{5}{384}\ \frac{wl^3}{EI}$

$\delta_{max} = -\ \frac{5}{384}\ \frac{(0.33)(500^3)(10^3)}{(30000)(2.1 \times 10^6)}$

$\delta_{max} = -\ 0.0085mm < 2.5mm$ (Satisfied)

(ii) For Continuous Beam E-H:

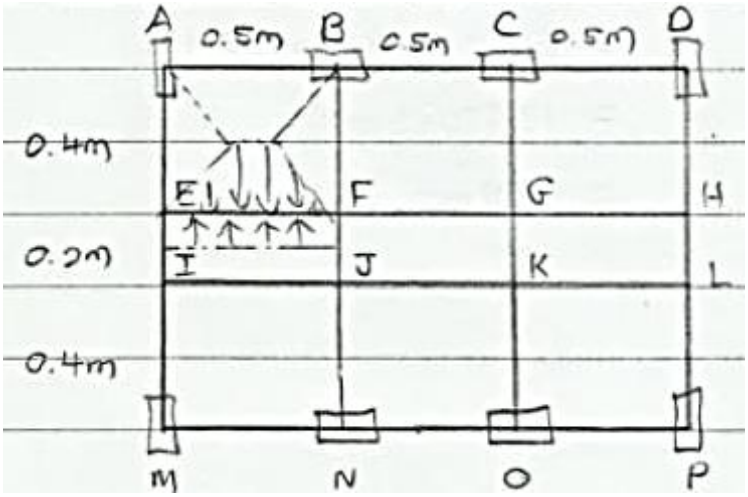

Calculate the total load:

Permanent load (from slab) = $[\frac{1}{2}$ (1.01) (0.22)] (2) + (1.01) (0.1) + (1.01) (0.5)

Permanent load (from slab) = 0.808KN

Permanent load (from beam) = $b \times h \times 25$

Permanent load (from beam) = $0.025 \times 0.08 \times 25$

Permanent load (from beam) = 0.0375 KN/m

Variable load = 0

Total load = 1.35 (0.0375) + 0.808

Total load = 0.86KN

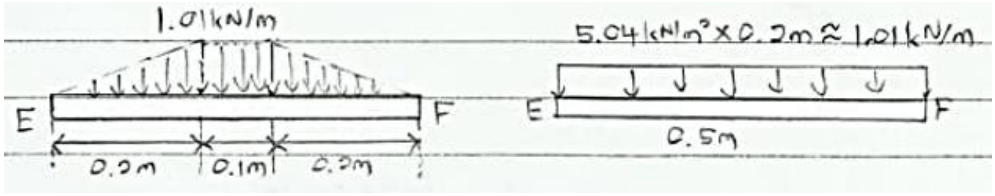

Mid span of EF and GH end spans – design as T-section:

$M = 0.09\ FL$

$M = 0.09$ (0.86) (0.5)

$M = 0.039$KNm

$b_{eff} = b_w + 2[0.2b' + 0.1 \times 0.85\ L]$

$b_{eff} = 25 + [0.2$ (400 + 40)/2 + 0.1 (0.85) (500)]

$b_{eff} = 198$mm

$b_w + 2[0.2 \times 0.85\ L] = 25 + 2$ [0.2 × 0.85 (500)]

Mid span of interior span FG – design as T-section:

$M = 0.07\ FL$

$M = 0.07$ (0.86) (0.5)

$M = 0.03$KNm

$b_{eff} = b_w + 2[0.2b' + 0.1 \times 0.70\ L]$

$b_{eff} = 25 + [0.2$ (400 + 40)/2 + 0.1 (0.70) (500)]

$b_{eff} = 183$mm

$b_w + 2[0.2 \times 0.70\ L] = 25 + 2$ [0.2 × 0.70 (500)]

= 195mm

Hence, b_f = 195mm

$k = \frac{M}{bd^2 f_{ck}}$

$k = \frac{0.039\ (10^6)}{(195)(53.4^2)(30)}$

$k = 0.0023 < 0.167$

Hence, No compression reinforcement is required

$z = d\ [\ 0.5 + \sqrt{0.25 - \frac{k}{1.134}}\ ]$

$z = d\ [\ 0.5 + \sqrt{0.25 - \frac{0.0023}{1.134}}\ ]$

$z = 0.98\ d > 0.95d$

$A_s = \frac{M}{0.87 f_{yk} z}$

$A_s = \frac{0.039\ (10^6)}{0.87\ (316)(0.95 \times 53.4)}$

$A_s = 2.80\ mm^2/m$

= 165mm

Hence, b_f = 165mm

$k = \frac{M}{bd^2 f_{ck}}$

$k = \frac{0.03\ (10^6)}{(165)(53.4^2)(30)}$

$k = 0.0021 < 0.167$

Hence, No compression reinforcement is required

$z = d\ [\ 0.5 + \sqrt{0.25 - \frac{k}{1.134}}\ ]$

$z = d\ [\ 0.5 + \sqrt{0.25 - \frac{0.0021}{1.134}}\ ]$

$z = 0.99\ d > 0.95d$

$A_s = \frac{M}{0.87 f_{yk} z}$

$A_s = \frac{0.03\ (10^6)}{0.87\ (316)(0.95 \times 53.4)}$

$A_s = 2.79\ mm^2/m$

<u>Interior supports – design as a rectangular section</u>

$M = 0.11\ FL$

$M = 0.11\ (0.86)\ (0.5)$

$M = 0.047$KNm

$k = \frac{M}{bd^2 f_{ck}}$

$k = \frac{0.047\ (10^6)}{(40)(53.4^2)(30)}$

$k = 0.014 < 0.167$

Hence, No compression reinforcement is required

$z = d\ [\ 0.5 + \sqrt{0.25 - \frac{k}{1.134}}\ ]$

$z = d\ [\ 0.5 + \sqrt{0.25 - \frac{0.014}{1.134}}\ ]$

$z = 0.99\ d > 0.95d$

$A_s = \frac{M}{0.87 f_{yk} z}$

$A_s = \frac{0.047\ (10^6)}{0.87\ (316)(0.95 \times 53.4)}$

$A_s = 3.37\ mm^2/m$

Check Deflection:

$I = \frac{bd^3}{12}$

$I = \frac{(165)\ (53.4^3)}{12}$

$I = 2.1 \times 10^6\ mm^4$

$\frac{L}{200} = \frac{500}{200}$

$\frac{L}{200} = 2.5mm$

$\delta_{max} = -\frac{5}{384}\ \frac{wl^3}{EI}$

$\delta_{max} = -\ \frac{5}{384}\ \frac{(0.86)(500^3)(10^3)}{(30000)(2.1 \times 10^6)}$

$\delta_{max} = -\ 0.022mm < 2.5mm$ (Satisfied)

For simple supported beam A-M:

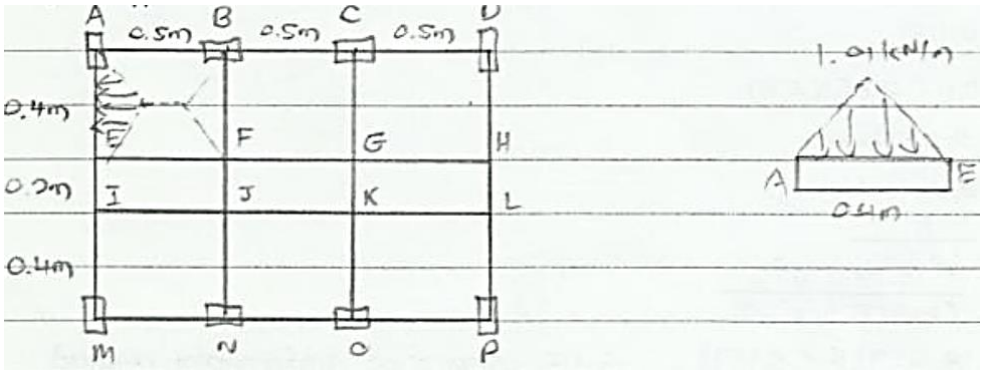

Load on AE = IM

Calculate the total load:

Permanent load (from slab) = $[\frac{1}{2}\ (1.01)\ (0.2)]\ (2)$

Permanent load (from slab) = 0.202KN

Permanent load (from beam) = $b \times h \times 25$

Permanent load (from beam) = $0.025 \times 0.08 \times 25$

Permanent load (from beam) = 0.0375 KN/m

Variable load = 0

Total load = $1.35\ (0.0375)\ (1) + 0.202\ (2) + [\ \frac{(0.86)\ (3)}{2}]\ (2)$

Total load = 3.03KN

$M = \frac{wl}{8}$

$M = \frac{(3.03)(1)}{8}$

$M = 0.38KNm$

$k = \frac{M}{bd^2 f_{ck}}$

$k = \frac{0.38\ (10^6)}{(25)(53.4^2)(30)}$

$k = 0.178 > 0.167$

Hence, compression reinforcement is required

$z' = d\ [\ 0.5 + \sqrt{0.25 - \frac{k\prime}{1.134}}\ ]$

$z' = d\ [\ 0.5 + \sqrt{0.25 - \frac{0.167}{1.134}}\ ]$

$z' = 0.82\ d$

$A_s\ ' = \frac{(k-k')f_{ck}bd^2}{0.87 f_{yk}(d-d')}$

$A_s\ ' = \frac{(0.178-0.167)(30)(25)\ (53.4^2)}{0.87\ (316)(53.4-(1.6+5))}$

$A_s\ ' = 1.83\ mm^2/m$

$A_s = \frac{k' f_{ck} bd^2}{0.87 f_{yk} z'} + A_s\ '$

$A_s = \frac{(0.167)(30)(25)(53.4^2)}{0.87(316)(0.82 \times 53.4)} + 1.83$

$A_s = 31.50\ mm^2$

Check Deflection:

$I = \frac{bd^3}{12}$

$I = \frac{(25)\ (53.4^3)}{12}$

$I = 3.17 \times 10^5\ mm^4$

$\frac{L}{200} = \frac{1000}{200}$

$\frac{L}{200} = 5mm$

$\delta_{max} = -\frac{5}{384}\ \frac{wl^3}{EI}$

$\delta_{max} = -\frac{5}{384}\ \frac{(3.03)(1000^3)(10^3)}{(30000)(3.17 \times 10^5)}$

$\delta_{max} = -4.15mm < 5mm$ (Satisfied)

For simple supported beam B-N:

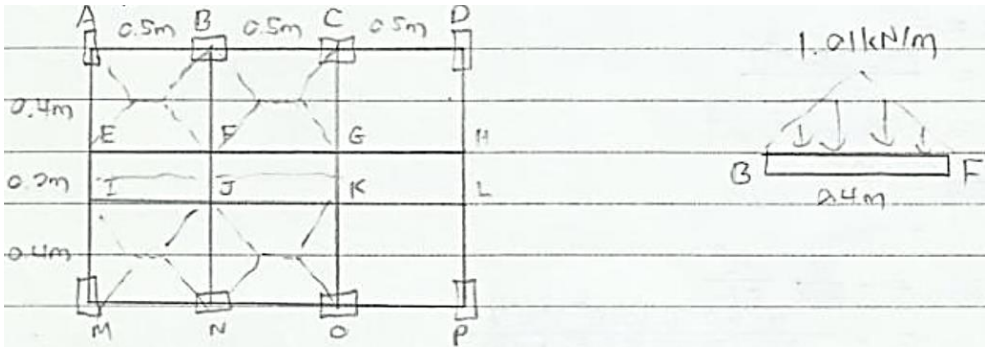

Calculate the total load:

Permanent load (from slab) = $[\frac{1}{2}(1.01)(0.2)](2)$

Permanent load (from slab) = 0.202KN

Permanent load (from beam) = $b \times h \times 25$

Permanent load (from beam) = $0.025 \times 0.08 \times 25$

Permanent load (from beam) = 0.0375 KN/m

Variable load = 0

Total load = 1.35 (0.0375) (1) + 0.202 (4)

Total load = 0.86KN

$$M = \frac{wl}{8}$$

$$M = \frac{(0.86)(1)}{8}$$

M = 0.11KNm

$$k = \frac{M}{bd^2 f_{ck}}$$

$$k = \frac{0.11\ (10^6)}{(25)(53.4^2)(30)}$$

k = 0.051 < 0.167

Hence, no compression reinforcement is required

$$z = d\ [\ 0.5 + \sqrt{0.25 - \frac{k}{1.134}}\ ]$$

$$z = d\ [\ 0.5 + \sqrt{0.25 - \frac{0.051}{1.134}}\ ]$$

z = 0.95 d (= 0.95d)

$$A_s = \frac{M}{0.87 f_{yk} z}$$

$$A_s = \frac{0.11\ (10^6)}{0.87\ (316)(0.95 \times 53.4)}$$

A_s = 7.89 mm^2/m

<u>Check Deflection:</u>

$$I = \frac{bd^3}{12}$$

$$I = \frac{(25)\ (53.4^3)}{12}$$

I = 3.17×10^5 mm^4

$$\frac{L}{200} = \frac{1000}{200}$$

$$\frac{L}{200} = 5\text{mm}$$

$$\delta_{\max} = -\frac{5}{384}\ \frac{wl^3}{EI}$$

$\delta_{max} = -\frac{5}{384}\frac{(0.86)(1000^3)(10^3)}{(30000)(3.17\times10^5)}$

δ_{max} = - 1.18mm < 5mm (Satisfied)

Checking shear:

Beam A-D:

$V = 0.45F$
$V = 0.45\ (0.33)$
$V = 0.15$KN

$V = 0.55F$
$V = 0.55\ (0.33)$
$V = 0.18$KN

$V = 0.6F$
$V = 0.6\ (0.33)$
$V = 0.20$KN

Beam A-M:

$V_1 = V_2 = \frac{w}{2}$
$= \frac{3.03}{2}$
$= 1.52$KN

For Beam A-M:

Choose highest $V = 0.20$KN
$V_{Ed} = V - wd$
$V_{Ed} = 0.20 - (\frac{0.33}{0.5})(\frac{53.4}{1000})$
$V_{Ed} = 0.16$KN

$V_{Rd,max} = 0.124\ b_w d\ (1-\frac{f_{ck}}{250})\ f_{ck}$
$V_{Rd,max} = 0.124\ (25)\ (53.4)\ (1 - \frac{30}{250})(30)(10^{-3})$
$V_{Rd,max} = 4.37\text{KN} > V_{Ed} = 0.16\text{KN}$

$\theta = 22^0$
$\cot\theta = 2.5$

$\frac{A_{sw}}{S} = \frac{V_{Ed}}{0.78 d f_{ykCot\theta}}$
$\frac{A_{sw}}{S} = \frac{0.16\ (10^3)}{0.78\ (53.4)(316)(2.5)}$
$\frac{A_{sw}}{S} = 0.005$

Beam E-H:

$V = 0.45F$
$V = 0.45\ (0.86)$
$V = 0.39$KN

$V = 0.55F$
$V = 0.55\ (0.86)$
$V = 0.47$KN

$V = 0.6F$
$V = 0.6\ (0.86)$
$V = 0.52$KN

Beam E-H:

$V_1 = V_2 = \frac{w}{2}$
$= \frac{0.86}{2}$
$= 0.43$KN

For Beam E-H:

Choose highest $V = 0.52$KN
$V_{Ed} = V - wd$
$V_{Ed} = 0.52 - (\frac{0.86}{0.5})(\frac{53.4}{1000})$
$V_{Ed} = 0.43$KN

$V_{Rd,max} = 0.124\ b_w d\ (1-\frac{f_{ck}}{250})\ f_{ck}$
$V_{Rd,max} = 0.124\ (25)\ (53.4)\ (1 - \frac{30}{250})(30)(10^{-3})$
$V_{Rd,max} = 4.37\text{KN} > V_{Ed} = 0.43\text{KN}$

$\theta = 22^0$
$\cot\theta = 2.5$

$\frac{A_{sw}}{S} = \frac{V_{Ed}}{0.78 d f_{ykCot\theta}}$
$\frac{A_{sw}}{S} = \frac{0.43\ (10^3)}{0.78\ (53.4)(316)(2.5)}$
$\frac{A_{sw}}{S} = 0.013$

$\frac{A_{sw,min}}{S} = \frac{0.05\ (F_{ck})^{0.5} b_w}{f_{yk}}$

$\frac{A_{sw,min}}{S} = \frac{0.05(30)^{0.5}(25)}{316}$

$\frac{A_{sw,min}}{S} = 0.022\ (> \frac{A_{sw,min}}{S} = 0.005)$

Hence, assume S = 80mm

$\frac{A_{sw}}{S} = \frac{2 \times \pi\ r^2}{S}$

$\frac{A_{sw}}{S} = \frac{2 \times \pi\ (\frac{3.2}{2})^2}{80}$

$\frac{A_{sw}}{S} = 0.20$

Hence, 3.2mm @ 80mm c/c

$V_{min} = \frac{A_{sw}}{S} \times 0.78\ d\ f_{yk}\ Cot\ \theta$

$V_{min} = 0.20 \times 0.78\ (53.4)\ (316)\ (2.5)\ (10^{-3})$

$V_{min} = 6.58KN$

$\Delta F_{td} = 0.5 V_{Ed}\ Cot\ \theta$

$\Delta F_{td} = 0.5\ (0.16)\ (2.5)$

$\Delta F_{td} = 0.20KN$

$\frac{A_{sw,min}}{S} = \frac{0.05\ (F_{ck})^{0.5} b_w}{f_{yk}}$

$\frac{A_{sw,min}}{S} = \frac{0.05(30)^{0.5}(25)}{316}$

$\frac{A_{sw,min}}{S} = 0.022\ (> \frac{A_{sw,min}}{S} = 0.013)$

Hence, assume S = 80mm

$\frac{A_{sw}}{S} = \frac{2 \times \pi\ r^2}{S}$

$\frac{A_{sw}}{S} = \frac{2 \times \pi\ (\frac{3.2}{2})^2}{80}$

$\frac{A_{sw}}{S} = 0.20$

Hence, 3.2mm @ 80mm c/c

$\Delta F_{td} = 0.5 V_{Ed}\ Cot\ \theta$

$\Delta F_{td} = 0.5\ (0.43)\ (2.5)$

$\Delta F_{td} = 5.25KN$

<u>For Beam A-M:</u>

Choose highest $V = 1.52KN$

$V_{Ed} = V - wd$

$V_{Ed} = 1.52 - (3.03)\ (\frac{53.4}{1000})$

$V_{Ed} = 1.36KN$

$V_{Rd,max} = 0.124\ b_w d\ (1-\frac{f_{ck}}{250})\ f_{ck}$

$V_{Rd,max} = 0.124\ (25)\ (53.4)\ (1 - \frac{30}{250})(30)(10^{-3})$

$V_{Rd,max} = 4.37KN > V_{Ed} = 1.36KN$

$\theta = 22^0$

$\text{Cot}\ \theta = 2.5$

$\frac{A_{sw}}{S} = \frac{V_{Ed}}{0.78 d f_{ykCot\theta}}$

$\frac{A_{sw}}{S} = \frac{1.36\ (10^3)}{0.78\ (53.4)(316)(2.5)}$

$\frac{A_{sw}}{S} = 0.041$

$\frac{A_{sw,min}}{S} = \frac{0.05\ (F_{ck})^{0.5} b_w}{f_{yk}}$

<u>Beam E-H:</u>

$V = 0.43KN$

$V_{Ed} = V - wd$

$V_{Ed} = 0.43 - (0.86)\ (\frac{53.4}{1000})$

$V_{Ed} = 0.38KN$

$V_{Rd,max} = 0.124\ b_w d\ (1-\frac{f_{ck}}{250})\ f_{ck}$

$V_{Rd,max} = 0.124\ (25)\ (53.4)\ (1 - \frac{30}{250})(30)(10^{-3})$

$V_{Rd,max} = 4.37KN > V_{Ed} = 0.38KN$

$\theta = 22^0$

$\text{Cot}\ \theta = 2.5$

$\frac{A_{sw}}{S} = \frac{V_{Ed}}{0.78 d f_{ykCot\theta}}$

$\frac{A_{sw}}{S} = \frac{0.38\ (10^3)}{0.78\ (53.4)(316)(2.5)}$

$\frac{A_{sw}}{S} = 0.012$

$\frac{A_{sw,min}}{S} = \frac{0.05\ (F_{ck})^{0.5} b_w}{f_{yk}}$

$\frac{A_{sw,min}}{S} = \frac{0.05(30)^{0.5}(25)}{316}$

$\frac{A_{sw,min}}{S} = 0.022$ ($< \frac{A_{sw,min}}{S} = 0.041$)

Although Satisfied but for easier calculations, let it be $\frac{A_{sw}}{S}$ = 0.20. Hence, 3.2mm @ 80mm c/c

$\Delta F_{td} = 0.5 V_{Ed}\ Cot\ \theta$

$\Delta F_{td} = 0.5\ (1.36)\ (2.5)$

$\Delta F_{td} = 1.7$KN

$\frac{A_{sw,min}}{S} = \frac{0.05(30)^{0.5}(25)}{316}$

$\frac{A_{sw,min}}{S} = 0.022$ ($> \frac{A_{sw,min}}{S} = 0.012$)

Let, $\frac{A_{sw}}{S}$ = 0.20, and 3.2mm @ 80mm c/c

$\Delta F_{td} = 0.5 V_{Ed}\ Cot\ \theta$

$\Delta F_{td} = 0.5\ (0.38)\ (2.5)$

$\Delta F_{td} = 0.48$KN

Column Design (Eurocode 2)

Load from 2nd floor:

Permanent load (from slab) = 25 × (0.5 × 0.5) × 0.016

Permanent load (from slab) = 0.1KN

Permanent load (from beam) = [25 × (0.025 × 0.06) × 0.5] (3)

Permanent load (from beam) = 0.06 KN

Live load (from slab) = 3 × (0.5 × 0.5)

Live load (from slab) = 0.75KN

Total load = 1.35 (0.1 + 0.06) + 1.5 (0.75)

Total load = 1.34KN

Load from 1st floor:

Permanent load (from slab) = 25 × (0.5 × 0.5) × 0.016

Permanent load (from slab) = 0.1KN

Permanent load (from beam) = [25 × (0.025 × 0.06) × 0.5] (3)

Permanent load (from beam) = 0.06 KN

Live load (from slab) = 3 × (0.5 × 0.5)

Live load (from slab) = 0.75KN

Total load = 1.35 (0.1 + 0.06) + 1.5 (0.75)

Total load = 1.34KN

Load from Ground floor:

Permanent load (from beam) = [25 × (0.025 × 0.06) × 0.5] (2)

Permanent load (from beam) = 0.04 KN

Total load = 1.35 (0.04)

Total load = 0.05KN

Load from Column:

Total load = 1.35 [(0.04 × 0.06) (25)]
Total load = 0.08KN/m

Axial load on Column B:

From $1^{st} – 2^{nd}$ floor
$N_{1st\text{-}2nd}$ = 1.34 + 0.081 (0.3)
$N_{1st\text{-}2nd}$ = 1.36KN

From Ground - 1^{st} floor
$N_{\text{Ground - }1st}$ = 1.36 + 1.34 + 0.081 (0.3)
$N_{\text{Ground - }1st}$ = 2.72KN

From Footing – Ground floor
N_{Ed} = 2.72 + 0.05 + 0.081 (0.1)
N_{Ed} = 2.78KN

W on each beam:
$F.E.M_{12} = \frac{w_{max} l^2}{12}$
$F.E.M_{12} = [(\frac{1.34}{0.5}) (0.25^2)] / 12$
$F.E.M_{12}$ = 0.014 KNm

$F.E.M_{23} = \frac{w_{max} l^2}{12}$
$F.E.M_{23} = [(\frac{0.215}{0.5}) (0.25^2)] / 12$
$F.E.M_{23}$ = 0.002KNm

Member Stiffness:
$\frac{k_{12}}{2} = \frac{1}{2} \times \frac{bh^3}{12L_{12}}$
$\frac{k_{12}}{2} = \frac{1}{2} \times \frac{(0.025)(0.06^3)}{12\ (0.25)}$
$\frac{k_{12}}{2} = 9 \times 10^{-7}$
$\frac{k_{23}}{2} = 9 \times 10^{-7}$

$k_{col} = \frac{bh^3}{12L_{col}}$
$k_{col} = \frac{(0.04)(0.06^3)}{12\ (0.3)}$
$k_{col} = 2.4 \times 10^{-6}$

$k_{col} = \frac{bh^3}{12L_{col}}$
$k_{col} = \frac{(0.04)(0.06^3)}{12\ (0.1)}$
$k_{col} = 7.2 \times 10^{-6}$

Distribution factor for column (2^{nd} floor) = $\frac{k_{col}}{\sum k}$

Distribution factor for column (2^{nd} floor) = $\frac{24 \times 10^{-6}}{9 \times 10^{-7} + 9 \times 10^{-7} + 2.4 \times 10^{-6}}$

Distribution factor for column (2^{nd} floor) = 0.57

Distribution factor for column (1^{st} floor) = $\frac{24 \times 10^{-6}}{9 \times 10^{-7} + 9 \times 10^{-7} + 2\,(2.4 \times 10^{-6})}$

Distribution factor for column (1^{st} floor) = 0.36

Distribution factor for column (Ground floor) = $\frac{24 \times 10^{-6}}{9 \times 10^{-7} + 9 \times 10^{-7} + 2.4 \times 10^{-6} + 7.2 \times 10^{-6}}$

Distribution factor for column (Ground floor) = 0.21

Column Moment M:

At *2nd* floor:

M_{2nd} = 0.57 (0.014 – 0.002)

M_{2nd} = 0.007KN

At *1st* floor:

M_{1st} = 0.36 (0.014 – 0.002)

M_{1st} =0.004KN

At *Ground* floor:

M_{Ground} = 0.21 (0.014 – 0.002)

M_{Ground} = 0.0025KN

Design M_{Ed} :

Effective height of column = 0.3 – thickness of slab

Effective height of column = 0.3 – 0.016

Effective height of column = 0.28m

M_{Ed} (*2nd* floor) = $M + \frac{N_{Ed}\, h}{400}$

M_{Ed} (*2nd* floor) = $0.007 + \frac{(1.36)(0.28)}{400}$

M_{Ed} (*2nd* floor) = 0.0078KNm

M_{Ed} (*1st* floor) = $0.0043 + \frac{(2.72)(0.28)}{400}$

M_{Ed} (*1st* floor) = 0.0063KNm

M_{Ed} (*Ground* floor) = $0.0025 + \frac{(2.78)(0.28)}{400}$

M_{Ed} (*Ground* floor) = 0.0045KNm

- **Design $\frac{N_{Ed}}{bhf_{ck}}$**

2nd floor:

$\frac{N_{Ed}}{bhf_{ck}} = \frac{(1.36)(10^3)}{(40)(60)(30)}$

$\frac{N_{Ed}}{bhf_{ck}} = 0.019$

$\frac{N_{Ed}}{bhf_{ck}} = \frac{(2.72)(10^3)}{(40)(60)(30)}$

$\frac{N_{Ed}}{bhf_{ck}} = 0.038$

$\frac{N_{Ed}}{bhf_{ck}} = \frac{(2.78)(10^3)}{(40)(60)(30)}$

$\frac{N_{Ed}}{bhf_{ck}} = 0.039$

Design $\frac{M_{Ed}}{bh^2f_{ck}}$

2nd floor:

$\frac{M_{Ed}}{bh^2f_{ck}} = \frac{0.0078\ (10^6)}{(40)(60^2)(30)}$

$\frac{M_{Ed}}{bh^2f_{ck}} = 0.0018$

1st floor:

$\frac{M_{Ed}}{bh^2f_{ck}} = \frac{0.0063\ (10^6)}{(40)(60^2)(30)}$

$\frac{M_{Ed}}{bh^2f_{ck}} = 0.0014$

Ground floor:

$\frac{M_{Ed}}{bh^2f_{ck}} = \frac{0.0045\ (10^6)}{(40)(60^2)(30)}$

$\frac{M_{Ed}}{bh^2f_{ck}} = 0.00104$

Values to small, cannot find. Hence, use $A_{s,min}$

Minimum area of reinforcement:

$A_{s,min} = 0.002\ A_c$

$A_{s,min} = 0.002\ (40 \times 60)$

$A_{s,min} = 4.8mm^2$ ($< A_{s,\ prov} = 8.04mm^2$) Satisfied.

Link:

20 × size of the smallest main bar = 20 × 3.2

20 × size of the smallest main bar = 64mm

Least column dimension = 40mm

Hence, maximum vertical spacing = 40mm c/c

Appendix B Concrete properties

Strength classes for concrete														
f_{ck} (MPa)	12	16	20	25	30	35	40	45	50	55	60	70	80	90
$f_{ck,cube}$ (MPa)	15	20	25	30	37	45	50	55	60	67	75	85	95	105
f_{cm} (MPa)	20	24	28	33	38	43	48	53	58	63	68	78	88	98
f_{ctm} (MPa)	1.6	1.9	2.2	2.6	2.9	3.2	3.5	3.8	4.1	4.2	4.4	4.6	4.8	5.0
E_{cm} (GPa)	27	29	30	31	33	34	35	36	37	38	39	41	42	44

f_{ck} = Concrete cylinder strength
f_{cm} = Mean concrete strength
E_{cm} = Mean value of elastic modulus
$f_{ck,cube}$ = Concrete cube strength
f_{ctm} = Mean concrete tensile strength

Appendix C Mass of Building model

Mass of the complete model

1. Volume of column:

= Length × breath × Height × number of columns
= 0.06 × 0.04 × 0.7 × 8
= 0.01344 m^3

2. Volume of beam

= Length × breath × Height × number of beams
= 0.06 × 0.025 × (1 +1.5) × 10
= 0.0375 m^3

3. volume of slab

= Length × breath × Height × number of slabs
= 1.5 × 1 × 0.016 × 2
= 0.048 m^3

Total volume = 0.09894 m^3

Here,

Mass = Density × Volume

Mass = 2500 × 0.09894

Mass = 247.35 kg

Mass of the Storey 2 on Storey 1

1. Volume of column:

= Length × breath × Height × number of columns
= 0.06 × 0.04 × 0.3 × 8
= 0.00576 m^3

2. Volume of beam

= Length × breath × Height × number of beams
= 0.06 × 0.025 × (1 +1.5) × 4
= 0.015 m^3

3. volume of slab

= Length × breath × Height × number of slabs
= 1.5 × 1 × 0.016 × 1
= 0.024 m^3

Total volume = 0.04476 m^3

Here,

Mass = Density × Volume

Mass = 2500 × 0.04476

Mass = 111.9 kg

For the calculation of shear force, multiply the mass of storey with acceleration attached to it.

Appendix D Clauses of EC8

Clause 1.1.2:

1.1.2 Scope of EN 1998-1

(1) EN 1998-1 applies to the design of buildings and civil engineering works in seismic regions. It is subdivided in 10 Sections, some of which are specifically devoted to the design of buildings.

(2) Section **2** of EN 1998-1 contains the basic performance requirements and compliance criteria applicable to buildings and civil engineering works in seismic regions.

(3) Section **3** of EN 1998-1 gives the rules for the representation of seismic actions and for their combination with other actions. Certain types of structures, dealt with in EN 1998-2 to EN 1998-6, need complementing rules which are given in those Parts.

(4) Section **4** of EN 1998-1 contains general design rules relevant specifically to buildings.

(5) Sections **5** to **9** of EN 1998-1 contain specific rules for various structural materials and elements, relevant specifically to buildings as follows:

Clause 3.2.1 (4):

(4) In cases of low seismicity, reduced or simplified seismic design procedures for certain types or categories of structures may be used.

NOTE The selection of the categories of structures, ground types and seismic zones in a country for which the provisions of low seismicity apply may be found in its National Annex. It is recommended to consider as low seismicity cases either those in which the design ground acceleration on type A ground, a_g, is not greater than 0,08 g (0,78 m/s^2), or those where the product $a_g.S$ is not greater than 0,1 g (0,98 m/s^2). The selection of whether the value of a_g, or that of the product $a_g.S$ will be used in a country to define the threshold for low seismicity cases, may be found in its National Annex.

Clause 4.3.3.1:

4.3.3 Methods of analysis

4.3.3.1 General

(1) Within the scope of Section **4**, the seismic effects and the effects of the other actions included in the seismic design situation may be determined on the basis of the linear-elastic behaviour of the structure.

(2)P The reference method for determining the seismic effects shall be the modal response spectrum analysis, using a linear-elastic model of the structure and the design spectrum given in **3.2.2.5**.

(3) Depending on the structural characteristics of the building one of the following two types of linear-elastic analysis may be used:

a) the "lateral force method of analysis" for buildings meeting the conditions given in **4.3.3.2**;

b) the "modal response spectrum analysis", which is applicable to all types of buildings (see **4.3.3.3**).

(4) As an alternative to a linear method, a non-linear method may also be used, such as:

c) non-linear static (pushover) analysis;

d) non-linear time history (dynamic) analysis,

Clause 3.2.3.1.1 (2):

(2)P When a spatial model of the structure is required, the seismic motion shall consist of three simultaneously acting accelerograms. The same accelerogram may not be used simultaneously along both horizontal directions. Simplifications are possible in accordance with the relevant Parts of EN 1998.

Clause 3.2.3.1.2.4 (a):

(4) The suite of artificial accelerograms should observe the following rules:

a) a minimum of 3 accelerograms should be used;

Clause 4.3.3.4.3:

4.3.3.4.3 Non-linear time-history analysis

(1) The time-dependent response of the structure may be obtained through direct numerical integration of its differential equations of motion, using the accelerograms defined in **3.2.3.1** to represent the ground motions.

(3) If the response is obtained from at least 7 nonlinear time-history analyses with ground motions in accordance with **3.2.3.1**, the average of the response quantities from all of these analyses should be used as the design value of the action effect E_d in the relevant verifications of **4.4.2.2**. Otherwise, the most unfavourable value of the response quantity among the analyses should be used as E_d.

Clause 4.4.3.1:

4.4.3 Damage limitation

4.4.3.1 General

(1) The "damage limitation requirement" is considered to have been satisfied, if, under a seismic action having a larger probability of occurrence than the design seismic action corresponding to the "no-collapse requirement" in accordance with **2.1(1)**P and **3.2.1(3)**, the interstorey drifts are limited in accordance with **4.4.3.2**.

(2) Additional damage limitation verifications might be required in the case of buildings important for civil protection or containing sensitive equipment.

Clause 4.4.3.2:

4.4.3.2 Limitation of interstorey drift

(1) Unless otherwise specified in Sections **5** to **9**, the following limits shall be observed:

a) for buildings having non-structural elements of brittle materials attached to the structure:

$$d_r \nu \leq 0{,}005\, h\,; \tag{4.31}$$

b) for buildings having ductile non-structural elements:

$$d_r \nu \leq 0{,}0075\, h\,; \tag{4.32}$$

c) for buildings having non-structural elements fixed in a way so as not to interfere with structural deformations, or without non-structural elements:

$$d_r \nu \leq 0{,}010\, h \tag{4.33}$$

where

d_r is the design interstorey drift as defined in **4.4.2.2(2)**;

h is the storey height;

ν is the reduction factor which takes into account the lower return period of the seismic action associated with the damage limitation requirement.

(2) The value of the reduction factor ν may also depend on the importance class of the building. Implicit in its use is the assumption that the elastic response spectrum of the seismic action under which the "damage limitation requirement" should be met (see **3.2.2.1(1)**P) has the same shape as the elastic response spectrum of the design seismic action corresponding to the "[AC1]no-collapse requirement[AC1]" in accordance with **2.1(1)**P and **3.2.1(3).**

LIST OF PUBLICATIONS

Haider, S.M.B., Nizamani, Z., and Yip, C.C., 2020. Reliability Assessment of a Two Storey Building Model. *Engineering Structures*. (Under-reviewed)

Haider, S.M.B., Nizamani, Z., and Yip, C.C., 2020. Non-Linear Dynamic Assessment of Low-Rise RC Building designed according to European Norms. *Structural Engineering and Mechanics*. (Accepted)

Haider, S.M.B., Nizamani, Z., and Yip, C.C., 2019. Nonlinear Dynamic Analysis of Two Storey RC Building Model. *International Conference on Sustainable Development Goals (ICSDG 2019)*. (Published)

Haider, S.M.B., Nizamani, Z., and Yip, C.C., 2018. Behavioral Study of Shear Wall with Correlational to Bracing under Seismic Loading. I*nternational Conference on Civil and Environmental Engineering (ICCEE 2018)*. (Published)